NTNU
Norwegian University of
Science and Technology

Dolomite-based Sorbents for High Temperature Carbon dioxide capture.

Moses Mawanga

Chemical Engineering
Submission date: June 2017
Supervisor: De Chen, IKP
Co-supervisor: Kumar Ranjan Rout, IKP

Norwegian University of Science and Technology
Department of Chemical Engineering

"Incomplete results can at best reveal an incomplete picture:
the better the quality of input, the more certain will be the conclusion;

**Perhaps in many experimental systems, the choice of the reaction conditions determines
the conclusions reached**.

It's little wonder that the literature contains so many discordant statements,
and that our progress towards our goal is so slow."

—Robert Cunningham, 2007

Abstract

The impact of doping with inert oxides on the long term performance of dolomite-based sorbents for high temperature CO_2 has been investigated in this work. Arctic dolomite was doped with with various oxides Al_2O_3, ZrO_2, MgO, $CaAl_2O_4$ and effect of the amount of oxide were studied. The unmodified and doped dolomite were subjected to multi cyclic operation with dry conditions in a thermo gravimetric reactor. Experimental results demonstrated that the mixed dopants comprising 3.5%Al (5.5% Al_2O_3) and 2%Zr (1.96% ZrO_2) satisfactorily improved the stability of Arctic dolomite during 120 cycles where as a single oxide dopant only marginally improved the stability of the dolomite. The morphology, thermal gravimetric data, phase composition, Nitrogen adsorption all showed that dolomite when subjected to "dry" conditions is stable when doped with this mixed oxide. Up to 120 cycles of carbonation/desorption were carried out in thermo-gravimetric Analyser. There seemed to exist some kind of synergistic effect caused by the mixed dopants towards improving the stability of dolomite. N_2 adsorption analyses revealed that the best case sorbent had a very small surface area of only 5.4 m^2/g with the pore size distribution increase significantly. By optimizing the pore size distribution upon cyclic explicates the enhanced stability.

Preface

This Master's thesis written in the spring of 2017, marked the successful completion of the international two-year master's program in Chemical Engineering at the Norwegian University of Science and Technology. This completion leads to the award of MSc. in Chemical Engineering.

The final year of this duration was spent as a member of a research group in the Catalysis (KinCat) within the Chemical Engineering Department. This work reported in this thesis was a continuation of the specialization project conducted in fall 2016.

This project was done in part with collaboration with GASSNOVA MBCL project for developing sorbents for high temperature CO_2 capture with the relevance to the Calcium Looping Technology.

Declaration of Compliance

I declare that this is an independent piece of work and that it is in accordance to the examination regulations of the Norwegian University of Science and Technology.

<div align="right">

Trondheim, June 26, 2017.
Moses Mawanga.

</div>

Nomenclature

dol	Dolomite (the starting raw material for doping)
TGA	Thermo gravimetric Analyser
BET	Brunett-Emmett-Teller
BJH	Barret-Joyner-Halenda
SEM	Scanning Electron Microscopy
EDX	Energy-Dispersive X-Ray
GC	Gas Chromatography
XRD	X-Ray Diffraction
XRF	X-Ray Fluorescence
IWI	Incipient wetness impregnation
CaL	Calcium Looping
SSA	Specific Surface Area
CLC	chemical looping combustion
CaL-CLC	calcium looping cycles integrated with chemical looping combustion
CCS	carbon capture and sequestration
FBR	fluidized bed reactor
SESR	sorption-enhanced Steam Reforming
SER-CLC	sorption-enhanced reforming integrated with chemical looping combustion
MBCL	Moving Bed Calcium Looping
PSD	Particle size distribution determined by light scattering
t	time
carb	Carbonation
calc	Calcination
N	Number of cycles in a multi cyclic operation
n_{CaO}	Number of moles with CaO
X_N	Conversion as a function of number of cycles
FWHM	Full width at half maximum of the line profile component
LVol IB	Internal Breadth
NPT	Non-productive time
T_T	Tammann temperature in °C
D(v,0.5)	Volume mean diameter of particles below 50% of the distribution

Contents

List of Figures

List of Tables

Introduction

The capture and storage of Carbon dioxide from power plants that rely on fossil fuel like coal and natural gas has received global attention in recent times. To this cause, tremendous efforts have been devised to mitigate greenhouse gases particularly CO_2 in power generation plants. Among the current industrially relevant Carbon capture and storage (CCS) include amine scrubbing (using MEA and DMEA), adsorption on sold porous sorbents (like Metal Organic Frameworks or other sorbents) and membrane separation (Fennel and Anthony, 2015) and these examples of solutions targeted at curbing the ever-rising anthropogenic CO_2 emissions. However amine scrubbing has a high energy penalty whereas the use of membrane technology for CO_2 is a relatively new technology and is thus not widely applied in industrial setting. On the other side the use CaO-derived solid sorbents for CO_2 is considered a very promising option for mitigating the effects CO_2 release into the atmosphere. This is due to the following reasons;

(i) cheap raw materials; the starting material is cheap and is abundant in many regions of the world; Spain, China, the Arctic among others. Similarly the technology used in the Calcium looping is relatively cheap and is widely used in many other industrial processes.

(ii) Low energy penalty; the use of solid CaO-based sorbents has a low energy penalty associated with heat integration in CaL as compared to penalty incurred when using amine scrubbing for example.

1.1 Dolomite-based sorbents

Dolomite-based sorbents are used to preferentially capture and release concentrated CO_2 through a reversible reaction involving the forward carbonation reaction of Calcium Oxide with the subsequent backward de-carbonation reaction. The most widely studied natural CO_2 sorbents are dolomite ($CaMg(CO_3)_2$) (Mastin et al., 2011; Perejón et al., 2016; Valverde, Sanchez-Jimenez and Perez-Maqueda, 2015) and limestone (Calcite $CaCO_3$) (Manovic and Anthony, 2009; Perejón et al., 2016) and these have shown promising economic advantage for high temperature CO_2 sorption. Nowadays, dolomite is prefered for CO_2 capture over limestone because of the low desorption temperature of around 900 °C as compared to limestone which regenerenates at around 930 °C as claimed by Manovic and Anthony (2009). Some of the pros and con of dolomite are shown below.

Advantages	Disadvantage
- High initial sorption capacity	- Rapid decay of sorption capacity with
- High absorption (capture) and	increasing number of cycles due to
regeneration kinetics	sintering
- Widely available	
- Low cost and availability of natural	
dolomite	

Table 1.1.1: *Pros and cons of using dolomite as a CO₂ sorbent*

Unfortunately, CaO-derived from natural limestone/dolomites suffers from a rapid loss of activity (decay) with increased number of repeated cycles. A very low residual conversion of about 8g-CO_2/100 g-sorbent has been reported after 500 multi cycles as stated by Mastin et al. (2011). Under practical conditions on an industrial scale this would necessitate purging of the spent sorbent material from the CaL system and replacing it with new sorbent from time to time, a process that would mean that unnecessary frequent downtime periods (NPT). It is this this motivation that attempts to improve the characteristics (particularly the stability and kinetics) of CaO-based sorbents have been made by numerous researchers.

It is imperative to note that in order to solve a problem one needs to know atleast two things; how the process occurs and the root cause of the problem and then work around in alleviating this actual problem. In order to solve the stability issue of CaO-based sorbents, an understanding the morphology of CaO-based sorbents before and after deactivation is very vital.

It has been widely reported that thermal sintering that plays an important role in sorbent deactivation owing to the low Tammann temperature of $CaCO_3$ of just 533°C which is comparatively lower than the reaction temperature during the CO_2 capture process.

CO_2 capture by CaO-based sorbents occurs in two different regimes; namely (i) a fast-kinetically controlled reaction and (ii) a slow diffusion controlled regime. In the fast regime, a $CaCO_3$ product layer is formed on the surface of CaO grain which is described by the nucleation and growth $CaCO_3$ product isles on the CaO surface.

1.2 The Carbonation reaction

Naturally-occurring dolomite is predominantly $CaMg(CO_3)_2$ which upon sufficient calcination can yield CaO·MgO according to the reaction below. This single stage reaction occurs at pressure approximately below 0.1 atm.

$$CaMg(CO_3)_2 \longrightarrow CaO + MgO + 2\,CO_2$$

At pressure well above 0.1 atm, the decomposition of dolomite occurs in a two stage reaction as shown in the reactions 1.2 below.

$$CaMg(CO_3)_2 \longrightarrow CaCO_3 + MgO + 2\,CO_2$$
$$CaCO_3 \longrightarrow CaO + CO_2$$
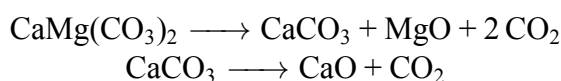
It is widely accepted that the half decomposition reaction 1.2 is not fundamentally affected by CO_2 partial pressure whereas the $CaCO_3$ reaction is shifted towards high tempereture as

the CO_2 partial pressure is increased (Valverde, Perejón, Medina and Perez-Maqueda, 2015). The CaO fraction of the dolomite sorbent can react with CO_2 as per the following reaction;

$$CaO + CO_2 \rightleftharpoons CaCO_3 \qquad \Delta H_{r,298} = \pm 178 \text{ kJ/mol}$$

The reaction is exothermic and thermodynamically feasible. The thermodynamics of the reaction can be deduced from the equation below that relates equilibrium partial pressure to Gibb's free energy of this reaction as stated by Barker (1973):

$$K_a = P_{CO_2} = exp\left[\frac{(-\Delta G^{\theta}_{rxn})T}{RT}\right]$$

where $-\Delta G^{\theta}_{rxn}$ is the Gibb's free energy for the carbonation reaction.
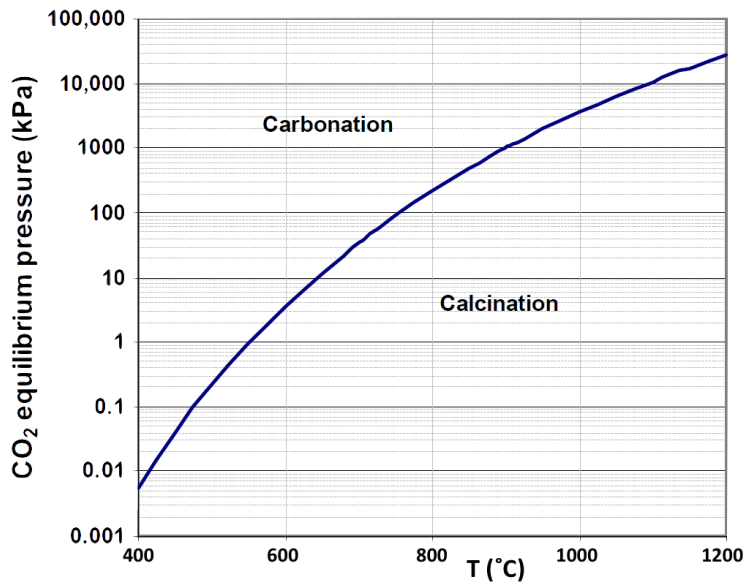
$$log_{10}P(atm) = 7.079 - \frac{8308}{T(K))}$$

Thermodynamics of CaCO₃-CaO system

The carbonation reaction 1.2 occurs when the equilibrium pressure of CO_2 is below the partial pressure of CO_2 surrounding the particles. Since the reaction is of an exothermic nature, it is obvious that carbonation (forward reaction) is favoured by lower temperature and low partial pressure. At this low temperature, the kinetics of the reaction has to be sufficient enough to drive the reaction forward, while the temperature is low enough that the system is below the equilibrium point where CO_2 is absorbed. This concept is well illustrated by the figure above.

Dolomite samples are calcined separately in a static oven at 1000 °C for 3 hours upon which all $CaCO_3$ is expected to be decomposed to CaO. The first carbonation cycle stops at a CaO conversion below unity meaning that a significant amount of CaO does not react to form CaO. This incomplete conversion is believed to be caused by the closure of narrow pores owns to the large difference in the molar volume of the product and reactant (36.9 ml/-mol for $CaCO_3$ and 16.9 ml/min for CaO) respectively (Bhatia and Perlmutter, 1983).

More so, naturally occurring dolomite has a draw back in that its CO_2 capture activity loss dramatically decreases with the number of cycles as observed and reported by Grasa et al.

(2007). This is due to thermal sintering because of the low Tammann temperature of the nascent CaO crystallites. The ***objective*** of this work was therefore to find a rational design of dolomite-based CO_2 sorbents that exhibit a relatively high CO_2 capture capacity while at the same time having good kinetics and multicyclic stability during repeated sorption and desorption stages. In order to achieve this, the attributes of a good sorbent were then defined to be:

1. the active phase of the sorbent (CaO) should be as small as possible preferably in the nano range. The powder particles of the sorbent should finely ground as this increases the surface area for the reaction and enhances the kinetics.

2. It is logical that fusing the CaO having a low Tammann temperature with inert oxide(s) or dopant(s) that has an inherently high Tammann temperature. This kind of approach was prompted by the presence of MgO that naturally exist together with CaO in calcined dolomite. MgO having a higher Tammann temperature compared to CaO has a tendency to stabilize CaO nano particles. Hence other compounds like Al_2O_3, ZnO_2, CeO_2 and Y_2O_3 are thought to have a positive effect towards the stability of CaO.

3. More over the composition of these inert oxides (dopants) should be relatively, preferably below 10% on mass basis so as the preserve the capture capacity of CaO. In fact alkaline metals if used as dopants can enhance the carbonation reaction by creation of an electron vacancy in the CaO lattice.

Table 1.2.1 shows examples of various metal oxides that can be used as dopants in the dolomite-based sorbents with their melting and Tammann temperatures, as adapted from Coutures and Rand (1989*a*,*b*)

Material	Tammann temperature [°C]	Melting point temperature [°C]
Calcite ($CaCO_3$)	533	1330
CaO	1313	2590
MgO	1290	2795±10
Al_2O_3	900	2054
ZrO_2	1218	2710±35
SiO_2	725	1734
CeO_2	1064	2230±50
Y_2O_3	-	2439±12

Table 1.2.1: *Tammann and melting point temperature of various materials*

Infering from the current available literature pertaining CaO as a CO_2 sorbent, all researchers agree that the most potent cause of material deactivation is due to sintering upon exposure to high temperature. Figure 1 adapted by a concept put forward by Johnson (2010) attempts to hypothesize the sintering process of CaO nano crystallites due to coalescence of two or more crystallites along a grain boundary. This coalescence is believed to be more pronounced at temperature greater than the Tammann temperature of $CaCO_3$ (533°C) yet the decarbonation reaction will occur at a temperature higher than this temperature (at approximately 866°C)
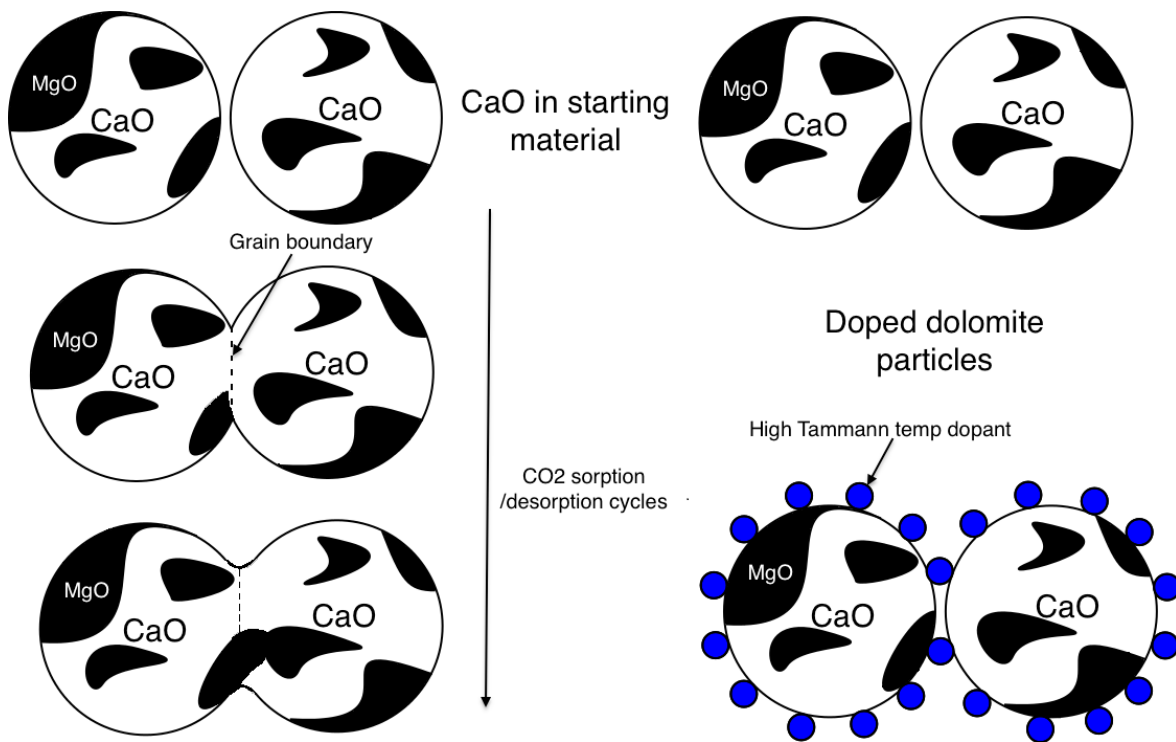
Figure 1: *A hypothesized concept for CaO thermal sintering*

As stated earlier, dolomite has a greater capacity as a Calcium precursor to capture CO_2 under industrially relevant conditions for Calcium looping compared to other Calcium precursors like limestone and hence it is considered to have a high potential as a CO_2 sorbent. The reason behind this phenomena is due to the fact that dolomite unlike limestone contains an equi-molar quantities of Calcium and Magnesium carbonate in form of $CaMg(CO_3)_2$. In fact it the Magnesium content of dolomite which plays a beneficial role in the cyclic CO_2 capture as stabilizer. Upon calcination the resulting MgO, although inert towards carbonation, is believed to aid in the CO_2 capture process because:

- MgO has a high Tammann temperature **??** which aids in stabilizing the CaO particles hence alleviating the loss of activity of CaO.

- Calcium and Magnesium portions in dolomite are mixed at a nanoscale level and this strongly influences the multicyclic CO_2 capture as suggested by Filitz et al. (2012) and Broda et al. (2014).

- Although not fully investigated, Kierzkowska, Poulikakos, Broda and Müller (2013) postulated that the decomposition of Magnesium Carbonate with dolomite to MgO provided an additional surface area in the sorbent, thus favouring the reactivity of the active phase especially in the fast carbonation phase.

This is supported by the fact that post-mortem analysis of spent sorbent after multi-cyclic testing reveals a de-mixing between active CaO phase and the inert MgO phase.

1.3 Goal of research

The goal of this Master's research was therefore to develop stable high temperature sorbents starting with dolomite as the raw material. Such CO_2 sorbents should have the fol-

lowing desirable attributes; high absorption capacity (fairly close to theoretical maximum of 44g-CO_2/100g-sorbent), fast reaction kinetics at low CO_2 partial pressure of below 20 Kpa (20%v/v), low regeneration temperature of around 900 °C, high chemical stability against sintering and high mechanical strength against attrition and degradation especially under a multi-cyclic operation.

Chapter 2

Literature Review

> "The purpose of literature is turn blood into ink."
> —*T.S Eliot*

The following chapter outlines some of the previous work pertaining CO_2 capture using dolomite-based sorbents as well as closely related work performed to produce synthetic sorbents and modification routes of limestones.

2.1 Research on stabilization of Dolomite and improvement of material

Previous research has been conducted on the use of dolomite to capture CO_2 in Sorption enhanced steam reforming as reported by Gil et al. (2015) among many other researchers. However the strongest potential for dolomite has been reported to be used on an industrial scale in CLC plant. Numerous researchers have reported the use of dolomite towards attaining the goals of CCS as outlined below. Manovic and Anthony (2009) tested the CO_2 capture carrying capacity of CaO-based pellet sorbents using limestone and commercially available calcium aluminate cements. The pellets were tested over 30 carbonation and decarbonation cycles in thermogravimetric analyzer. The authors report that these pellet sorbents showed a superior CO_2 capture compared to natural sorbent. This was attributed to the fact that an there was formation of Mayenite ($Ca_{12}Al_{14}O_{33}$) during the multi-cyclic carbonation/desorption which favours performance of CaO doped with alumina compounds. The pellets were also strong for use in a fluidised bed combustion.

Perejón et al. (2016) treated limestone and dolomite with acetic acid to make mixed acetates and observed that although there was no improvement in carbon dioxide capture, the doping with acetates allowed higher calcination efficiency to regenerate CaO at a lower temperature of 930 to 900°C for limestone. If a recarbonation phase is introduced before calcination to reactivate sorbent, a higher residual CO_2 capture was obtained for dolomite derived acetate sorbents. MgO grains in the mixed acetates with a notably reduced segregation promoted solid-state diffusion of ions across the porous structure created after re-carbonation.

Al-Jeboori et al. (2013) used mineral acids to dope limestone to dope Longclife limestone and later subjected the sorbents to repeated multi cycles in a fluidized bed reactor. It was

discerned that a doping concentration of 0.167 mol% of both HBr and HCl significantly improved the long term reactivity of limestone yet HI only marginally improved the reactivity. HNO_3 on the other hand reduced the CO_2 uptake.

Fennell et al. (2007) studied the uptake of CO_2 by CaO, produced by calcining limestone in a fluidized bed reactor in N_2 at 1023 K and found that the carrying capacity in the Nth cycle of carbonation was roughly proportional to the voidage inside pores narrower than ≈150 nm in the calcined CaO before carbonation began. It was thus concluded that the morphological changes, including reduction in the volume of pores narrower than 150 nm within a calcined limestone, are responsible for much of the fall in conversion of carbonation reaction with increasing numbers of cycles. Kierzkowska, Poulikakos, Broda and Müller (2013) reviewed the fundamental aspects of the cyclic carbonation – calcination reactions of CaO such as its reversibility and kinetics and postulated that stabilisation of CaO can be achieved through fusing with a high Tammann temperature support. It was further put forward that the support can be divided into three categories; those that form a mixed oxide with CaO that is, however, inert with respect to the carbonation/calcination (like MgO, Al_2O_3 and ZrO_2) reactions, supports that do not form a mixed oxide with CaO and that do not participate in the CO_2 capture reaction and supports that react with CO_2 (synthetic sorbents). On these ground Kierzkowska, Pacciani and Müller (2013) synthesised CaO-based Al_2O_3-stabilised CO_2 sorbents via co-precipitation and found that the calcium precursor, precipitating base and pH value at which precipitation was performed affected the morphology and chemical composition of the precipitate, and in turn its cyclic CO_2 uptake.

Filitz et al. (2012) suggested that in order to obtain such an excellent CO_2 uptake characteristic it was found to be crucial to mix the Ca^{2+} and Mg^{2+} on a molecular level, that is, within the crystalline lattice. The sorbents which comprised of mixtures of microscopic crystals of $CaCO_3$ and $MgCO_3$, a decay behavior similar to natural limestone was observed. After 15 cycles, the CO_2 uptake of the best sorbent was 0.51 g CO_2/g sorbent exceeding the CO_2 uptake of limestone by almost 100%.

Perhaps the most interesting studies for stabilizing dolomite were those carried by Arstad et al. (2014) and Mastin et al. (2011). Arstad looked at reducing the deactivation and performance loss of dolomite- based CO_2 sorbents using Zr-modified calcined dolomite by investigating the surface area and in-situ IR as well as in-situ XRD, thermogravimetric analyses (TGA) as well as fixed bed reactor studies. The same research group impregnated dolomite with Ti-, Zr- and Al-nano particle suspensions. The samples were tested in 10% dry CO_2 at 600 °C carbonation followed by 850 °C calcination over 60 cycles. The findings gave fundamental information about the deactivation mechanisms taking place during multi cyclic testing of dolomite. Mastin et al. (2011) and Li et al. (2011) independently report that synthesis of CaO/$Ca_{12}Al_{14}O_{33}$ within dolomite or limestone gives better CO_2 capture in which $Ca_{12}Al_{14}O_{33}$ acts a binder. This modification with a pure phase of $Ca_{12}Al_{14}O_{33}$ and $Ca_3Al_2O_6$ solids through a thermal treatment as reported by Li et al. (2011) under controlled conditions leads to a high CO_2 absorption capacity material, with very promising long term stability during sorption/desorption cycles. The table below summarizes some of the work pertaining the stabilization of limestone and dolomite during cyclic CO_2 capture. It is important to note that most of the work reported in this literature review either relates to limestone or synthetic sorbents with the exception of Arstad et al. (2014).

Reference	Modify by	Reactor	Carb.	Calc.	Cycles number	First cycle	Last cycle
Mastin et al.	Al_2O_3 doping	TGA	20% CO_2 780°C	50%CO_2 870°C	150	0.14	0.18
Arstad et al.	0.5% Zr doping	TGA	10% CO_2 600°C	100%N_2 900°C	60	0.33	0.2
Wang et al.	Carbon coating citric acid	FBR	15% CO_2 690°C (15 min)	100% CO_2 870°C	20	0.44	0.35
Pedro et al.	Ball milling	TGA	15% CO_2 in air 650°C (5 min)	70%CO_2 in air 900°C (5 min)	20	0.4[1]	0.3 [2]
Al-Jeboori et al.	limestone HCl HBR	Fl.BR	15% CO_2 - -	- -	150	0.14	0.18
Filitz et al.	nano mixing	TGA	15% CO_2 -	-	150	0.51	-

Table 2.1.1: *Modification routes for CO_2 sorbents and testing conditions used*

Chapter 3

Materials and Methods

3.1 Material Preparation

Arctic dolomite was received from Franzefoss Milkøkalk AS from a quarry in Ballangen in a ground form with a particle size ranging from 2 mm to 2 μm. This was either ground manually in a ceramic mortar or using a Herzog crusher which was later sieved between two sieves with apertures 35 and 45 μm.

The dopant chemicals used during preparation of modified dolomite based sorbents included Zirconyl nitrate $ZrO(NO_3)_2$ in Nitric acid, Zirconium Chloride $ZrCl_4$, Aluminium nitrate nonahydrate $Al(NO_3)_3 \cdot 9H_2O$ and magnesium nitrate hexahydrate $Mg(NO_3)_2 \cdot 6H_2O$ (all obtained from Sigma-Aldrich).

3.1.1 Incipient wetness impregnation

The incipient wetness impregnation (IWI) was used a synthesis route to modify the dolomite samples because it is easy to implement and research suggests that it is a promising route for preparation of high temperature CO_2 sorbent Arstad et al. (2014). In this method, dried material (calcined dolomite in this case) with a pore volume V_{PT} is brought into contact with the precursor solution of approximately the same volume as V_{PT}.

Consequently, the precursor is drawn into the pores of the solid by capillary suction such that there is no excess of solution remains outside the pore space of the solid, hence the name "incipient wetness". The penetration of the liquid phase requires displacement of air from the pores; if the pore radius is very small, the capillary pressure becomes greater than the pressure of the enclosed air such that air will dissolve. In some other situation this may lead to active precursor deposition on the external edge of the solid. The distribution of solute is governed by balance between the diffusion of solute onto the pores and adsorption onto the solid (CaOMgO in this case) (De Jong, 2009). When the precursor adsorbs on to the solid, it's concentration in solution will decrease and as a result diffusion will decrease too as stipulated by Fick's law. Figure 2 illustrates the phenomena of incipient wetness impregnation. (adopted from De Jong (2009))
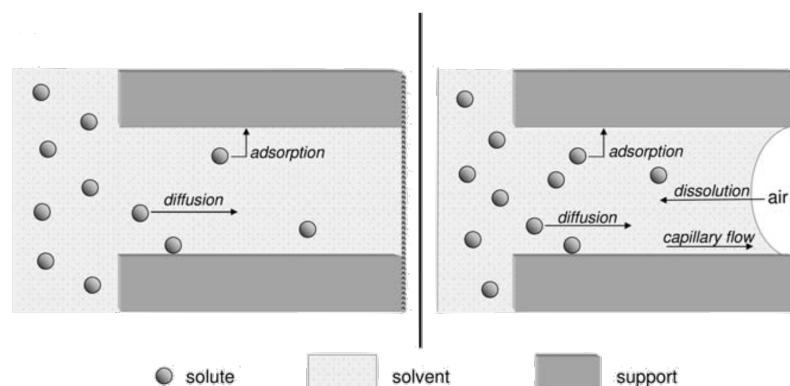
Figure 2: *Incipient wetness impregnation phenomena*

Diffusion can in this case be enhanced by ensuring a high concentration on the immediate exterior of the pellet. In order to effect this technique in the modification of dolomite, 10 g of calcined dolomite were spread onto a flat glass plate (or in a mortar). Appropriate amounts of precursors of either $ZrO(NO_3)_3$, $ZrCl_4$, $Al(NO_3)_3$ and/or $Mg(NO_3)_2$ were weighed and dissolved in approximately 1-2.5 cm^3 of distilled water depending on the quantity of nitrate required to dissolve. The actual amounts of nitrate precursor solids used in this synthesis are shown in appendix. The solution was stirred until it completely dissolved. As large amounts solid nitrates were needed to dissolve in a minimal amount of water (usually 1 ml) sufficient time was allowed for the dissolution. It was observed that less amount of water used during the impregnation method gave the best sorbents. Using a 200 μl pipette, the nitrate precursor solution was slowly added drop-by-drop until all the calcined solid had been rendered humid by the nitrate solution. Care was taken not to have excess solution into the solid. Best results were achieved when the calcined dolomite was as fine as possible with minimal amount of water used. The soggy solid powder was allowed enough time to stand and later dried. Figure 3 illustrates the set-up of tools used in the IWI experiment.

Figure 3: *Set up used for impregnation of dolomite*

Drying by evaporation and Calcination

Impregnated samples were subjected to a heated environment such that solvent is at its boiling point. Water is eliminated from the pores and hence leads to an increase in the ultimate precursor concentration up to saturation and crystallization. The drying was executed in such a way that there was an *egg-shell* distribution of the dopant onto the CaOMgO solid.

The samples were either dried at room temperature overnight or transferred into a preheated high temperature furnace at 50 °C depending on the type of precursor used. After drying the samples were then calcined in air at either 1000 °C for 3 hours. The heating rate during the calcination phase 10°C/minute. The figure below shows the calcination program scheme used to this effect.
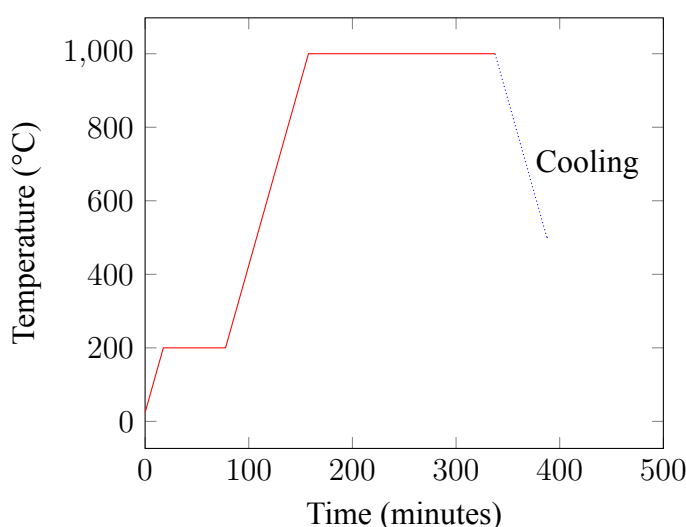
Figure 4: *Calcination temperature program for all sorbents*

3.2 Characterization of Sorbents

The following sub-chapter describes the characterization techniques used for describe the synthesized dolomite-based sorbents; these include particle size analysis, XRF, XRD, SEM, N_2-adsorption and TGA-DSC.

3.2.1 Particle Size Analysis

Dolomite powder samples were analysed for their particle size using the Horiba LA-960 laser particle Size Analyser. In this technique, light from a source interacts with particles dispersed in a solvent (water or isopropanol) and the light scattered by these particles is detected over a wide range if angles by photodiodes. This degree of scattering of this light is used to calculate the particle size distribution of the sample based on the Mie scattering theory (Adapted from Retsch Technology (n.d.)).
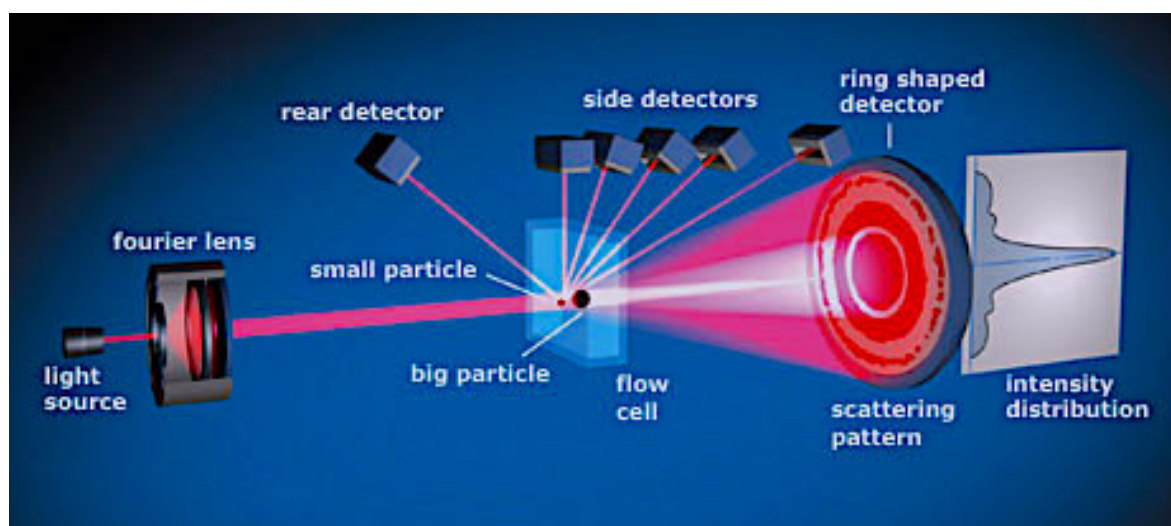
Figure 5: *Light scattering for particle size determination. Laser light interacts with the dolomite particles and is scattered in a manner corresponding to the particle size*

3.2.2 X-Ray Fluorescence

Elemental analysis using this spectroscopic method was performed using Wavelength Dispersive X-Ray Fluorescence (WDXRF) where the sample is illuminated and excited by X-Ray tube from a Palladium (Pd)-source. Sample chemistries are quickly but not destructively determined as characteristic fluorescent X-Rays for each sample. In addition, Compton and Rayleigh scatter from the sample are measured simultaneously by the X-Ray detection system.

Every atoms contains a positively charged nucleus and one or more electrons in the quantum energy state or orbital shells surrounding the nucleus as shown in the figure 6. If an element is heavier than Neon, and contains more orbital shell, the lowest potential energy orbitals will then be K-, L- and M-shells.

When a sample is illuminated/radiated by sufficiently high energy photons generated by sealed isotope Pd-source, electrons from the inner orbital shells (e.g. inner-most orbital shell K) are ejected. The atom instantly fills the electron vacancies as one of the electrons from a higher energy (e.g. L-shell) shell drops to the lower energy state of the ejected electron releasing energy in form of characteristic fluorescent X-Rays.

This movement of an electron from the higher to a lower energy state creates a phenomena called X-Ray Fluorescence. The fluorescent energy released then travels back to Compton window and into the instrument's high resolution detector (Che and Védrine, 2012).
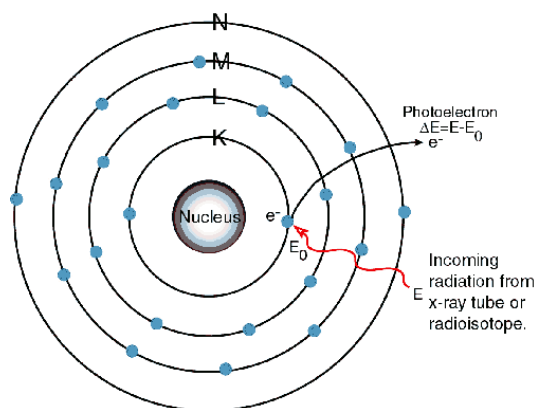
Figure 6: *Concept for the X-Ray Fluorescence*

3.2.3   X-Ray Diffraction

X-Ray Diffraction is a fingerprinting technique used for multiphase quantification and identification of material. The principle is such that when a crystalline solid is exposed to monochromatic X-ray will diffraction by principle of Bragg's law.

A unique powder diffraction pattern arises from the crystal structures of the component phases. The resulting XRD pattern is matched to a reference in order to identify the material present in the sample. Bragg's law is described by the equation 3.2.1 below (Cullity, 1956).
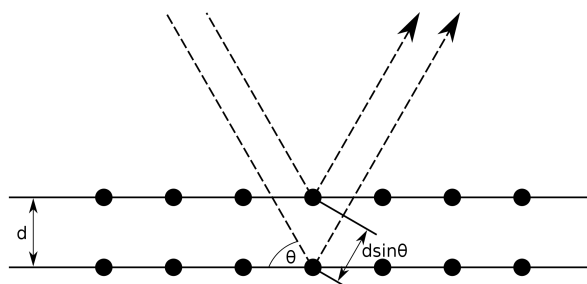
Figure 7: *X-Ray diffraction as per Bragg's law*

$$n\lambda = 2d \cdot Sin\theta \qquad (3.2.1)$$

where *n* is a positive integer, θ is the Bragg (scattering) angle, *d* is the inter plane spacing, λ wavelength of the incident X-Rays.

3.2.4   Nitrogen Adsorption

For determination of surface area

Nitrogen adsorption is used to calculate surface of supports and catalyst, based on N_2 physisorption on material. N_2 is measured at constant temperature of -196°C (77 K). The principle is such that each molecule occupies an area comparable to its cross-sectional area. The

Brunaeur-Emmett-Teller (BET) isotherm is used as an extrapolation to the Langmuir isotherm and is used to describe amount of adsorbed as a function of relative pressure P/P_0 in a mono layer coverage multilayer adsorption (Che and Védrine, 2012).

$$\frac{P}{V(P_0 - P)} = \frac{1}{cV_m} + \frac{(c-1)}{cV_m} \cdot \frac{P}{P_0} \tag{3.2.2}$$

where:
V_m is the volume equivalent to as adsorbed mono layer.
V is the volume adsorbed gas.
c is the constant.
P is the adsorption pressure.
P_0 is the equilibrium pressure of condensed gas.
The BET adsorption is based on the following assumptions:

- Heat of adsorption/ desorption in any layer are equal.

- In the first layer, molecules adsorb on equivalent adsorption sites such that the heat of adsorption for the first layer is constant.

- Heat of adsorption ΔH_{ads} for the second layer and consecutive layer are the same. this heat of adsorption is approximately equal to heat of condensation of the gas.

- The surface is constant during adsorption.

The BET specific surface area calculated in two stages. In the first stage, the physisorption isotherm is transformed to the BET plot form which the mono layer capacity is derived.

Basing on knowledge of N_2 molecular area (16.2 Å) the surface area is calculated by plotting $P/V(P_0-P)$ versus P/P_0 which gives a linear BET plot with slope $(c-1)/cV_m$ and intercept $1/cV_m$.

Note: Although often reported, the surface area measurements from the BET technique are not precisely accurate and thus should be used for relative comparison between adjacent samples. This is because the assumption usually applied in the BET technique of mono layer adsorption for on to a material is always true and the assumption of the close packing of N_2 is not always valid.

For determination of Pore size distributions

The sample is subjected to a relative partial pressure of about 1 and the pore size and volume where determined using the Barett-Joyner-Halenda (BJH) equation or Horwath-Kawazoe estimation (Che and Védrine, 2012). The shape of the adsorption/desorption isotherm can then be deduced from this analysis.

3.2.5   Scanning Electron Microscopy

The scanning Electron Microscopy technique is used to produce images of the sample by scanning a given area of the sample with a focussed beam of electrons. The surface topography of the sample is produced when electrons interact with the atoms of the sample. A primary electron beam directs electrons to the area in focus where high energy back scattered

electrons and secondary electrons are liberated from the sample. It is only the secondary electrons near the surface that escapes hence generating high image resolution at low acceleration voltages.

The sample is typically scanned in a vacuum to alleviate interaction with air or gas molecules that may give erroneous results. By studying the morphology the dolomite samples it can be deduced whether or not the particles are changed in sharp upon treatment with cyclic carbonation-regeneration runs.

3.2.6 Thermal Analysis and Calorimetry

TGA

TGA is used to analyse of the changes in weight of given a sample versus time and temperature in a controlled atmosphere. The temperature program is defined in order to suit the required analysis. TGA is very useful technique for any reaction in which a decrease in mass of the reacting sample is involved for instance in drying, desorption, reduction, degradation in an active atmosphere or where mass is gained wetting, oxidation, adsorption and therefore especially in solid-gas systems. The TGA set-up in the course of this work consisted of a crucible connected to a balance and inserted into a furnace with control over the atmosphere.

Crucibles were of a cylindrical/flat shape made of aluminium oxide Al_2O_3/platinum and had a volume of approximately 50 ml. Al_2O_3 crucibles are the standard choice preferred over platinum crucibles as these do not react with the sample. In addition the set-up had a thermo gravimetric balance which accurately records the weight of the two crucibles during the progress of the reaction experiment. In principle a few milligrams (10-20 mg) of the sample are heated following a defined temperature program and controlled over a chosen atmosphere; the weight is recorded as it varies with time and temperature. Many parameters affect the signal: increasing the mass of the sample raises the reaction temperature, and increasing the scanning rate also raises the temperature. The figure below shows the temperature program followed during thermogravimetric analyses of dolomite.

In order to ensure correct temperature control the TGA-DSC set-up has a combination of thermocouples, capable of working in a temperature range of ambient to 1000°C. Usually, calibration is performed with the melting of standard metallic (e.g Zinc, Nickel or silver) or mineral substances within the crucible.

The TGA is also coupled with DSC which is a temperature-programmed method in which the difference in the heat flow (or thermal power) is measured between a sample and a reference as it varies with time or temperature, in a controlled atmosphere. A TGA-DSC apparatus consists of a pair of crucibles; one crucible is empty and referred to as the *reference* while the other contains the sample to be analysed. Both crucibles are enclosed in a heating vessel, with control over the atmosphere.

Differential Scanning Calorimetry

In the DSC method of analysis, the differences in the energetic behaviour between the sample and the reference material is measured as a function of temperature. The sample and the reference material are heated in a contolled gas environment. DSC can then be used to

measure both the enthalpy and in principle the rates of reaction as well as reaction mechanisms. It is imperative to note that during this work, both TGA and DSC were performed in the thermogravimetric analyser instrument simultaneously as adopted from Che and Védrine (2012).
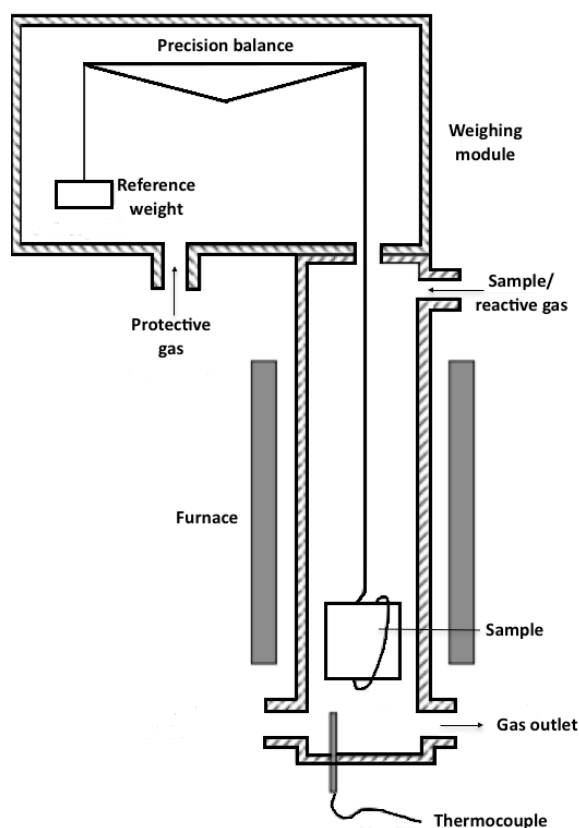
Figure 8: *Design for Thermo gravimetry Analysis*

3.3 Experimental I

Material Characterization

3.3.1 X-Ray Fluorescence

Sample preparation for XRF analysis

In order to avoid grain size effects and enhance reproducibility of the measurement, the dolomite powder is pelletized into pellets of 40 mm using boric acid as a binder. 200 mg of sample was mixed with 3 g of boric acid.

Four dolomite samples were chosen for XRF analysis in which a small amount of the sample (200 mg) were mixed by crushing them by hand with 3 g of Boric acid in a mortar. The boric acid was used as a binder to hold the pelletized dolomite intact into a disk shape. The disks were prepared in a casting die and they were 30 mm in diameter. and crushed in a mortar. The homogenized mixture was then pelletized into a disk of 40 mm diameter prior to loading into the XRF cell. The sample was then loaded into the XRF analyser (Rigaku Supermini200

Analyser).

3.3.2 Surface Area and Porosity Measurements

N_2-Physisorption analyses were carried out using the Micromeritics Tri Star 3020 Surface Area and Porosity Analyser and the VacPrep 061 Degasser (shown in figure 9a)

An empty clean dry sample tube holder was weighed and the weight recorded. A known mass (50-100 mg) of each of the calcined dolomite samples was then placed in the sample holder. The combined weight of the tube and sample was then taken. The sample was cooled for 1 hour by letting it to stand in an ambient environment then degassed overnight in a 4 μmmHg vacuum at 300 °C. The sample was ready for analysis when the degas unit indicated 100 mtorr pressure or less. A tube jacket and a glass stick were put onto sample tube prior to installing it on to the the surface area and porosity analyser. The weight of the sample after analysis were also taken to ensure that the correct sample weight were used in calculation of surface area and porosity parameters.

(a) *Sample degasser*   **(b)** *Surface Area and Porosity Analyser*
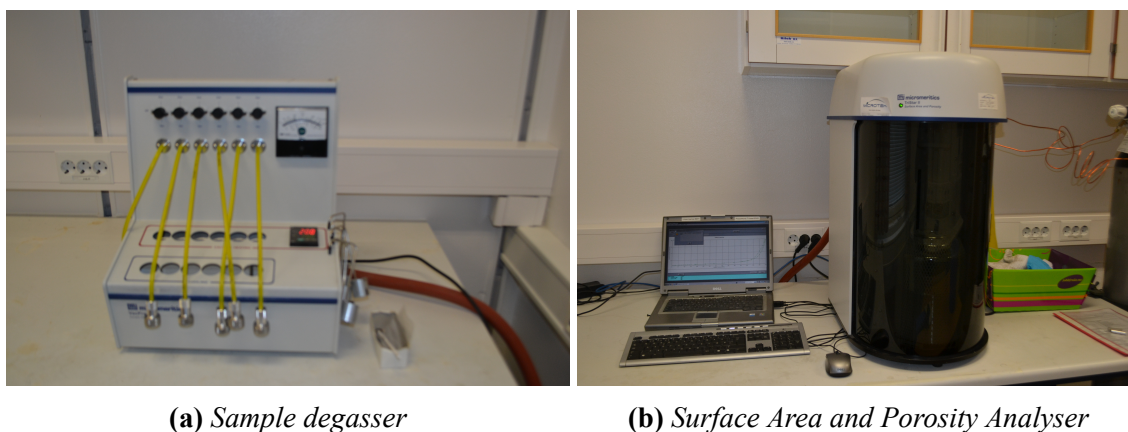
Figure 9: *Equipment for use in surface area and porosity measurements*

3.3.3 XRD Analysis

The main purpose of performing the XRD analyses on the dolomite sample was identify the different phases within each dolomite sample. This was performed using Bruker D8 Advance DaVinci X-ray Diffractometer: "DaVinci 1". The instrument used CuKα radiation with 2.5 °primary and secondary Soller slits with LynxEye^{TM} SuperSpeed Detector Variable divergence slit: "V6" which means that the divergence slit (the slit between the X-ray source and the sample) opens automatically such that the illuminated length on the sample always remained 6 mm (when using fixed divergence slit, the illuminated length on the sample changes from long to short). The X-Ray tube voltage was set to 40 kV and a current of 50 mA. A small amount of each of the samples was place on an XRD-sample tube holder and compressed using a glass slide. The samples were then loaded in the instrument and scanned in the 2θ range of 15-75°using a step size of 0.013°. The generated diffractograms were identified against a standard PDF-4+2016 RDB database using the Bruker EVA software.

3.3.4 Crystallite Size Determination

The size of the crystallites were calculated using a technique based on Scherrer equation. The LVol-IB crystallite size (based on Scherrer equation) was done using the Bruker TOPAS software (Bru, n.d.).

The variation in the crystallite sizes of CaO phase were used to study various dolomite samples.

$$L = \frac{K\lambda}{\beta Cos\theta}$$

(3.3.1)

where L is the size of the crystallites, K is a constant (0.94), β is the full breadth at half peak height of an XRD line, λ is the X-Ray wavelength, θ diffraction angle.Raw XRD data was converted using Bruker file exchange software. The least squares fit of this data was obtained using Standard TOPAS Refinement software Bru (n.d.). Instrument line broadening of double-Voigt approach are shown in appendix G.2.1. The line profile width in inversely proportional to crystalline size Cullity (1956), such that if the Scherrer constant K is introduced to relate ε to L_{Vol} using the equation then:

$$\varepsilon = \frac{\lambda}{\beta_{FWHM(s)} \cdot cos\theta} \qquad\qquad L_{vol} = \frac{K\lambda}{\beta_{FWHM(s)} \cdot cos\theta}$$

For cubic crystallites the value of K is chosen as 0.94 while 0.89 is chosen for spherical crystallites which depends on the line profile width is determined, the shape of the crystallites, and the size distribution. It is generally accepted that using the integral breadth (IB) rather than FWHM gives an evaluation that is approximately independent of the distribution in size and shape: K can be assumed to be 1 (IB is defined as the width of a rectangle with the same height and area as the line profile, obtained from dividing the line profile area by the line profile height) Bru (n.d.).

$$L_{vol} = \frac{\lambda}{\beta_{IB} \cdot cos\theta}$$

(3.3.2)

where L_{vol} volume weighted mean column lengths and β_{IB} and LVol-IB is the integral breadth based LVol calculation using Lorentzian and Gaussian type component convolutions (Cry Size L and Cry Size G).

3.3.5   Scanning elecron microscopy

SEM analysis was carried using the FEI Apreo scanning electron microscope in which a small mass of the sample was attached on to an adhesive tap which can be loaded into instrument's platform on the sample stage. Images of the sample were scanned at various magnification settings to obtain the best representative image and resolution. Figure 10 shows the actual image used for SEM characterization of sorbent particles. The instrument is equipped with the following Detectors; ETD (located within the chamber), back-scattered electron detector called T1, secondary electron detector called T2, a directional backscattered electron detector (DBS), and an EDX Oxford. An in chamber navigation camera (Chamber Camera CCD) is used to navigate between samples to be analysed. The SEM Apreo has an attainable resolution of upto 1 nm at 1 kV, an acceleration voltage ranging from 0.2–30 kV with a maximum beam current of 400 nA.
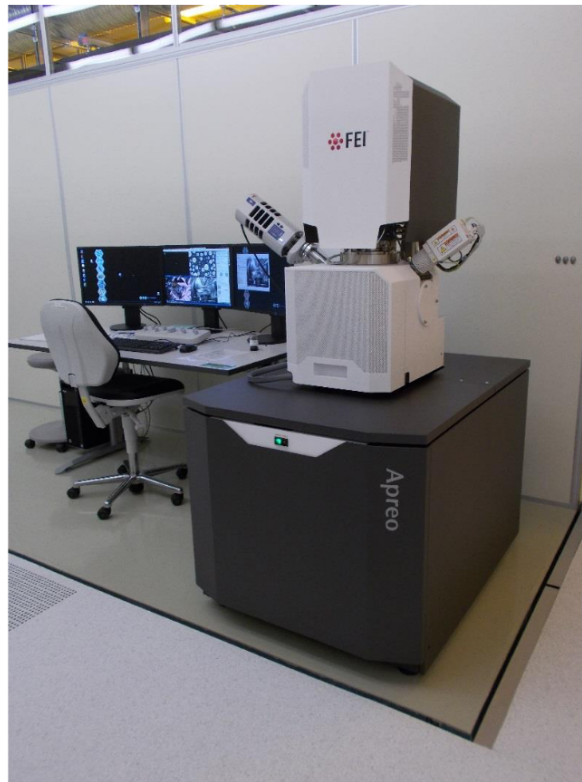
Figure 10: *FEI Apreo Scanning Electron Microscope*

3.3.6 Thermogravimetric Analysis

TGA experiments were the main focus of this study, as the stability of the sorbents during the multi cyclic CO_2 capture operation could be deduced from these experiments directly. Two TGA instruments; **TA instruments TGA Q500** and **Linseis Thermal Analysis STA PT1600** were used for the thermogravimetric analysis as shown in figure below. In both machines, the flow of the CO_2 and N_2 gases was controlled using mass flow controllers (MFC) installed within the machine.
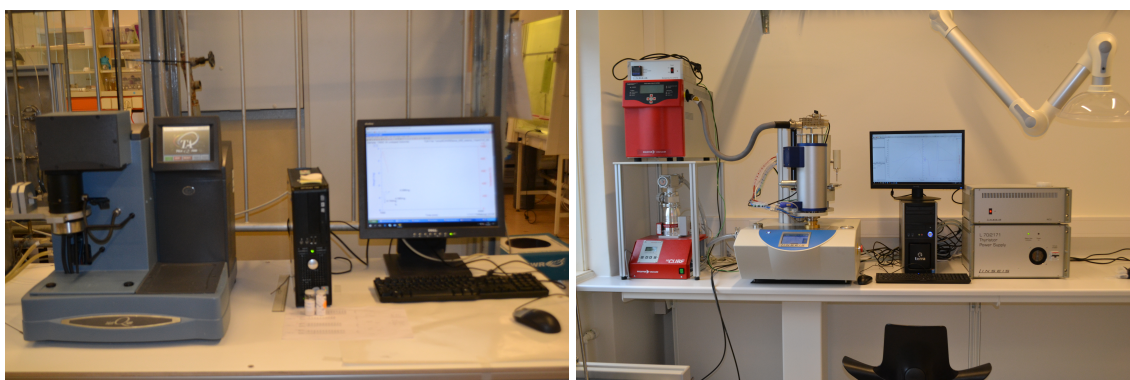
(a) *TGA Q500*   **(b)** *Linseis PT1600 TG Analyser*

Figure 11: *The thermo gravimetric analysers used for stability tests of the dolomite samples*

TGA temperature program

The experiment was then ran using a pre-defined temperature program. Figure **??** briefly shows the temperature program used for the TGA analysis of dolomite samples. A baseline measurement was

used to create a blank correction file for the measurements. To achieve this an empty clean crucible was weighed and loaded into the TGA furnace. The baseline measurement was subtracted from the actual material measurement so as to get the true thermal behaviour of the material without that of the either aluminium or platinum sample holders.
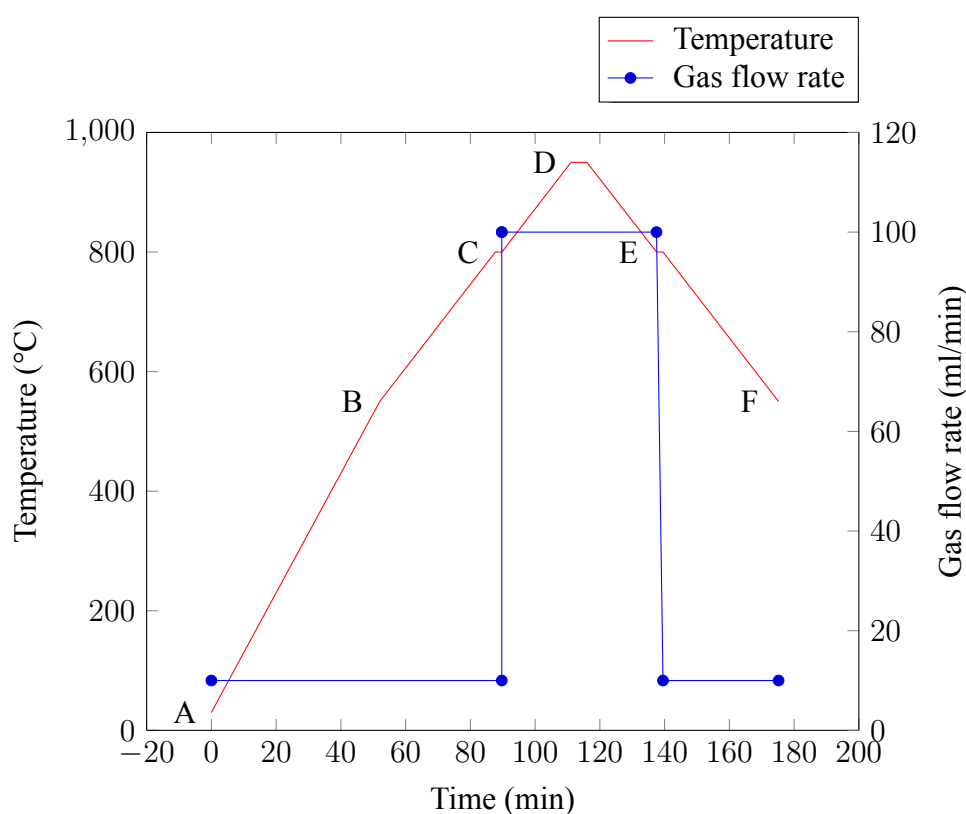
Figure 12: *TGA temperature program*

The main motivation for using this temperature program was due to the fact that from previous experiments, testing the stability of dolomite at fixed isothermal temperature of 570 °C for carbonation and 650 °C for decarbonation showed that the after several cycles, the decay of the capture capacity necessitates an increase in the sorption temperature from 570°C to 750°C in order to enhance the kinetics for the sorption. Similarly after several cycles while capturing at 750 °C, the decay and low kinetics are observed again, which again necessitates an increase in sorption temperature.

To correct for this, the test conditions were changed to a **temperature scanning** program where during carbonation, the temperature is scanned **from 550 to 800 °C** in a 10% CO_2 followed by decarbonation where temperature is scanned from **from 800 to 950 °C** in a 100% pure CO_2. The temperature program follows steps A-F described in a sequence as follows:

Step A-B   the temperature was raised from an ambient temperature (approximately 30°C) to 550°C at a heating rate is 10°C in a stream of 10% CO_2 balanced with 90% N_2. As temperature increases the sample is calcined and any volatile contaminants like water vapour or CO_2 that may have associated with the sample upon exposure to air are removed.

Step B-C   Further heating of the sample from 550 to 800°C at a heating rate of 7 °C/minute. This represented the carbonation phase where the sample is subjected to a stream of 10% CO_2. (90 ml/min N_2 in purge 1, 10 ml/min CO_2).

Step C   At 800 °C, the temperature is held isothermally for 2 minutes

Step C-D   Further heating of the sample from 800 to 950°C at a heating rate of 7 °C/minute. During this phase the gas is switched from 10% CO_2 to 100% CO_2. It is this stage that the desorption of CO_2 takes place hence called the regeneration stage. $CaCO_3$ decomposes back to CaO and CO_2 as shown by reaction 1.

Step D   At 950 °C, the temperature is held isothermally for 5 minutes in 100% CO_2 environment.

Step D-E   Cooling of the sample at rate of 10 °C/minute in a stream of pure CO_2

Step E   At 800 °C, the temperature is again held isothermally for 2 minutes

Step E-F   Cooling of the sample at rate of 10 °C/minute in a stream of 10% CO_2

Multi cycles   Steps B-F are repeated numerous times to so as to analyse the multi cyclic behaviour of the sorbent under the conditions described above. *Therefore it is important to note that each cycle comprised of two carbonation and two desorption stages.* For examples if 60 multi cycles were run, they comprise a total of 120 carbonation and desorption reactions.

The capture capacity was calculated from the TGA data by taking the difference in weight of sample during TGA measurement divided by the original weight owing to the fact that it is the sorption of CO_2 that is responsible for the weight change of the sample.

The ***maximum theoretical CO₂ capture capacity*** of the sorbent is calculated from the equation;

$$\text{Max. capture capacity} = \frac{\text{Mole of CaO reacted}}{\text{total moles of CaO present}}$$

According to the equation 1.2, CaO reacts with CO_2 in a 1:1 mole ratio. Also CaO and MgO in dolomite exists in equi molar quantities hence *moles of CaO = moles of MgO.*

$$\text{Max. capture capacity} = \frac{\text{Maximum CO}_2 \text{ weight captured}}{\text{Sorbent weight}}$$

$$X_N = \frac{n_{CO_2}}{n_{CaO,\ total}}$$

$$= \frac{n_{CO_2}}{n_{CaO,reacted} - n_{CaO,\ locked}}$$

where:

$n_{CaO,\ locked}$ refers to the amount of CaO reacted with Al_2O_3 and ZrO_2 to form Calcium Aluminate and Calcium Zirconate respectively and is thus unavailable for reaction with CO_2 and thus does not participate in the carbonation reaction.

$$\text{Max. capture capacity} = \frac{\text{Maximum CO}_2 \text{ weight captured}}{\text{Sorbent weight}}$$

$$\text{Max. capture capacity} = \frac{\left[\text{moles MgO} - \text{moles Al}_2\text{O}_3 - \text{moles ZrO}_2\right] \cdot 44}{\text{moles MgO} \cdot 40 + \text{moles MgO} \cdot 56 + \text{moles Al}_2\text{O}_3 \cdot 101.96}$$

where 44, 40, 56, 101.96 are the molecular weights for CO_2, CaO, MgO and Al_2O_3 respectively. This maximum theoretical capacity denoted as X_o is useful in the calculation of the actual conversion of the sorbent in a given number of cycles using the equation:

$$X_N = \frac{\Delta W}{W_{initial} \cdot X_o} \tag{3.3.3}$$

while the ***actual CO₂ capture capacity*** is calculated from the following equation using TGA data;

$$\text{Actual capture capacity} = \frac{\Delta W}{W_{initial}}$$

where:
n is the number of moles of a given compound,
Δ W is the change in weight of the sorbent during reaction
$W_{initial}$ is the initial weight of sorbent before commencement of the measurement.

4 Chapter

Results and Discussion

> "A month in the laboratory can often save an hour in the library."
> —*Frank Westheimer, 1988*

4.1 Characterization of CO_2 sorbents

The following chapter recounts the results from N_2 physisorption for surface area and porosity measurements, elemental composition by X-Ray fluorescence, phase identification and crystallite size determination as well as structure determination from X-Ray diffraction as well as thermo gravimetric analyses on various dolomite based sorbents.

The elemental composition of the samples as observed from XRF analysis reveals that the starting material after calcination is predominantly made up of CaO and MgO, with almost no SiO_2. The observed SiO_2 in the 1 %Al samples is thought be coming from the Nitrate precursors used during doping as these are not 100% pure. More so, the XRF reveals that the calculation of nitrate precursor quantities are quite accurate, for instance the intended Zirconia quantity of 1 %wt is observed as 0.92%wt from XRF analysis. Unfortunately, the malfunctioning of the XRF equipment did not permit determination of other sample for their elemental composition during the later stages of this work.

	Elemental Analysis Percentage by mass (% wt)						
Sample	CaO	MgO	Al_2O_3	ZrO_2	SiO_2	K_2O	Fe_2O_3
Dolomite	52.3	46.1	0.4	-	-	-	0.73
1% Al dolomite	51.9	43.3	3.2	-	0.85	0.62	0.15
1% Sp dolomite	62.4	33.7	2.22	-	0.85	0.65	0.18
1% Zr dolomite	45.9	51.7	0.15	0.92	0.77	0.42	0.09

Table 4.1.1: *XRF Elemental Analysis for dolomite samples for batch 2 samples. Sp stands for Spinel formed between Al and Mg in equal quantities*

The results from the N_2 physisoption experiments indicated that dolomite exhibits a Type IV isotherm which indicates presence of a mesoporous solid (IUPAC classification McCusker (2005)). The N_2 molecules undergo capillary condensation phenomena associated with mesoporosity of the dolomite. Further, the N_2 adsorption and desorption isotherm in figure 13 indicates a H3 hysteresis loop as observed from parallel adsorp-desorp branches and there exist as a non-rigid pore structures between particle grains. Non-rigidity characterised by lack of defined plateau region at $P/P_o = 1$ without any overlapping adsorp-desorp branches (Che and Védrine, 2012). The specific surface area of various dolomite samples are shown in the table below.

Batch	Calc. temp	Sample	SSA [m²/g]	Mesopor. volume [cm³/g]	Pore size (diameter) [Å]
Batch I	900 °C	Unmodified dolomite	28.15	0.126	152.29
		0.5% Al Dolomite	15.71	0.092	232.83
		1% Al Dolomite	14.43	0.090	232.50
		2% Al Dolomite	14.58	0.080	208.02
		1/2% Sp Dolomite	13.52	0.075	228.71
		1% Sp Dolomite	12.16	0.076	256.02
		2% Sp Dolomite	12.42	0.073	243.93
Batch II	1000 °C	Dolomite	13.50	0.084	255.59
		1/2% Al Dolomite	13.42	0.074	214.30
		1% Al Dolomite	12.62	0.073	235.07
		2% Al Dolomite	10.24	0.060	223.12
		1/2% Sp Dolomite	11.70	0.057	223.41
		1% Sp Dolomite	11.02	0.059	233.81
		2% Sp Dolomite	10.40	0.054	231.74
Batch III	1000 °C	Dolomite	11.14	0.061	232.42
		4%Al2%Zr Dolomite	4.77	0.031	261.50
		3 1/2%Al2%Zr Dolomite	5.35	0.037	276.23

Table 4.1.2: *N_2 adsorption results for dolomite samples calcined at 900°C and 1000°C. Sp stands for Spinel formed between Al and Mg in equal quantities*

The N_2 adsorption-desorption curve is shown below.
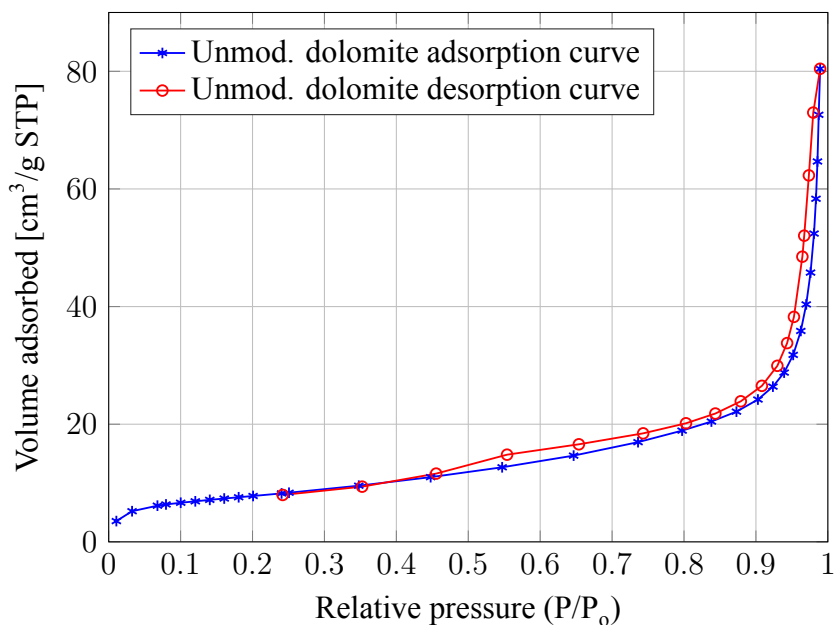
Figure 13: *Adsorption isotherm for undoped dolomite (calc. 950 °C -3 hrs)*

However, the adsorption desorption isotherms for the **doped** dolomite materials are shown in appendix and these show H1 hysteresis loop loops characterised by parallel adsorp-desorp branches. This is probably due to adsorption in unconnected mesopores with a relatively narrow pore size distribution. This implies that the dopant material actually occupies some of the original mesopores that

existed in the calcined dolomite.

It is also observed that upon subsequent doping and calcination, the specific surface area and meso-porous volume of dolomite will decrease significantly especially for the samples calcined at a lower temperature of 900°C. For instance the surface area of dolomite will decrease from 28 m^2/g to 12 m^2/g upon doping with 2% Alumina-Magnesia spinel.

From the comparison of the diffraction patterns obtained from uncalcined dolomite in figure 14 and that of calcined dolomite in figure 15 indicates that the peaks assigned to $CaMg(CO_3)_2$ (PDF-00-036-0426) completely disappeared upon 3 hour long calcination at 1000 °C while it gave rise to new diffraction patterns of CaO (PDF 01-070-4068) and MgO (PDF 00-043-1022). This indicates that at 1000 °C the calcination is sufficient to generate the required mixed CaO-MgO oxide.
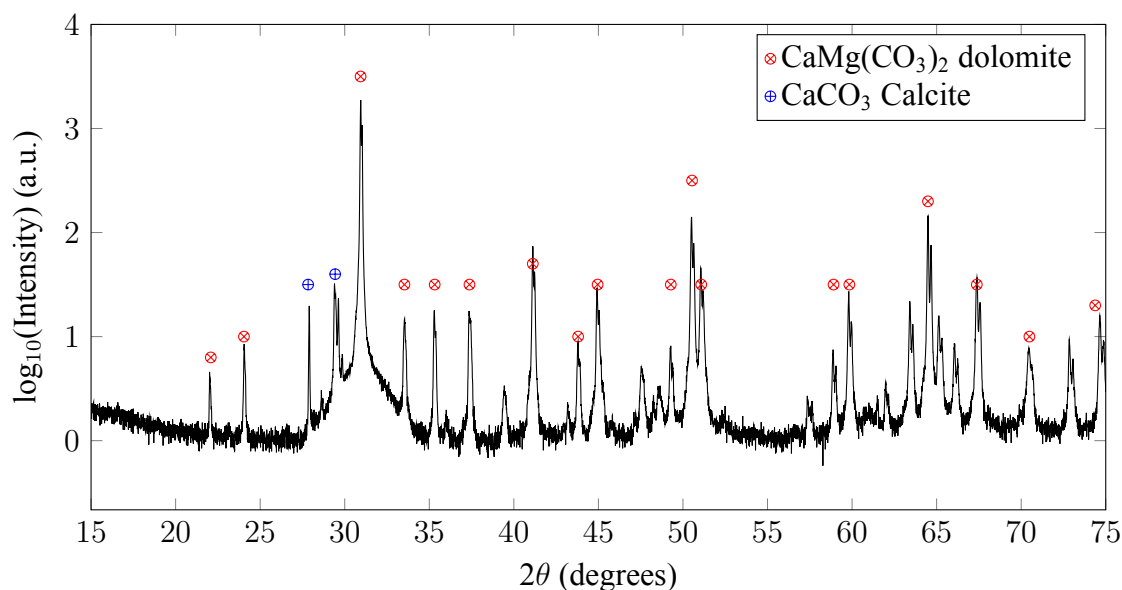
Figure 14: *XRD of uncalcined dolomite*
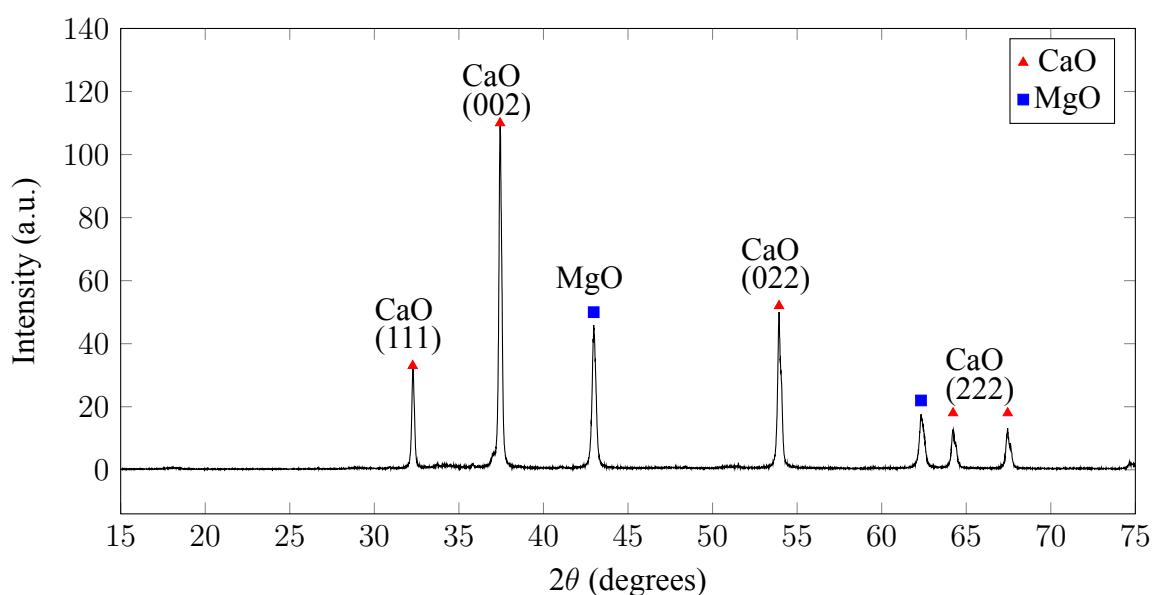
Figure 15: *XRD to identify phases in calcined dolomite*

4.1.1 Phase Identification
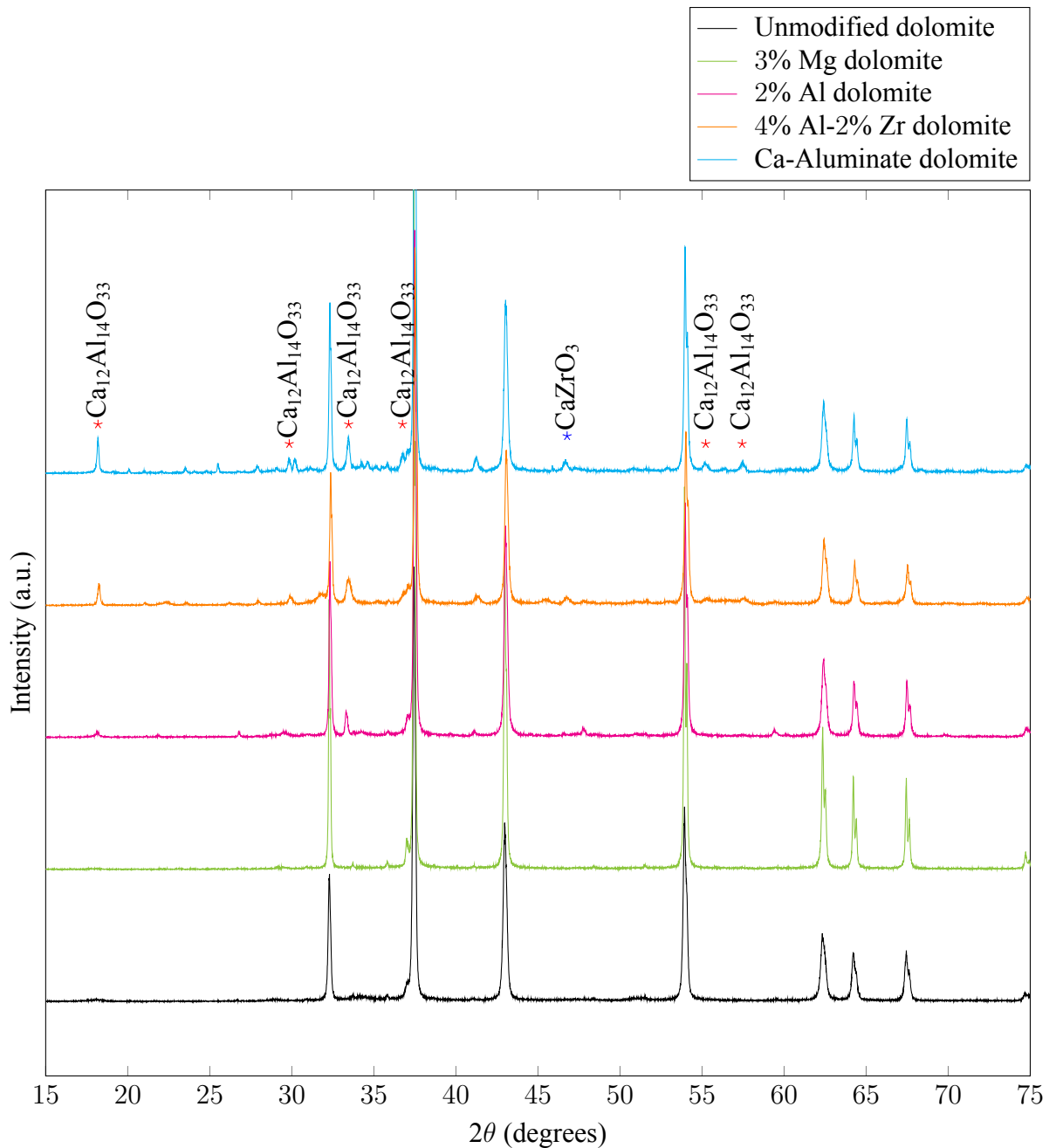
Figure 16: *X-Ray diffractograms of various dolomite-based sorbents*

The stacked XRD shows the various sorbents as scanned between a 2θ range of 15-75 °. As stated before, the unmodified calcined dolomite shows two predominant patterns belonging to CaO and Periclase (MgO) as identified by the PDF-2016+ RDB database. Furthermore, the diffraction pattern reveals that the subsequent impregnation with Al, Mg and Zr will introduce two very important phases; Calcium Aluminate $Ca_{12}Al_{14}O_{33}$, Calcium Aluminium Oxide Peroxide $Ca_6Al_7O_{16}(O)$ and Calcium Zirconate $CaZrO_3$. These phases are identified as Mayenite (PDF 04-015-0818), and Larkagiite (PDF 00-061-0228) as well as Larkagiite Syn (PDF 00-035-0615) respectively.

$Ca_{12}Al_{14}O_{33}$ phases are widely spread out across the 2θ in the the 4%Al-2%Zr and 3% Al Calcium

Aluminate dolomite samples. These can be obseved at 2θ positions of 18.2, 30.2, 34.6, 55.2 and 57.4 for the Mayenite phase and 46.7 for the Larkagiite phase. A detailed phase identification can be found in raw XRD data appendix. As outlined in literature, it is these newly formed phases that play an important role in stabilization of CaO crystalline structure against sintering.

4.1.2 CaO & MgO crystallite sizes

Tables 4.1.3 and 4.1.4 shows the results obtained from the calculation of the crystallite sizes of CaO and MgO in the calcined samples of unmodified dolomite, Calcium Aluminate dolomite and 4%Al2%Al-doped dolomite. In addition the tables show the *hkl phases* of CaO and MgO as well as the 2θ positions at which these phases exist. It can clearly be seen that the crystallite sizes of the CaO in each of the samples are greater that those of MgO in all the analysed samples. More so the crystallite size in the calcined dolomite is identical to that of the dolomite sample doped with 4%Al-2%Zr doped (67.9 nm and 68.4 nm) which implies that an almost negligible amount of CaO contributes to the formation of the Mayenite and Larkagiite phases. The increased crystallite size for the Calcium Aluminate dolomite is indicative of dopant intimately fusing with indigenous CaO hence contributing to the overall increase in size from 67.9 nm to 80.2 nm.

On the contrary, the crystallite size of MgO in all the samples analysed by TOPAS clearly show that it remain unchanged which is an implication that MgO is an inert phase and does not participate in the formation of new phases with the dopants and hence does not adversely undergo thermal sintering as the case with CaO.

hkl phase	Multi- plicity	d	2θ position (°)	Dol F^2	Dol LVol (nm)	CaAl F^2	CaAl LVol (nm)	4A1Z F^2	4A1Z LVol (nm)
111	8	2.78	32.17	23.33		24.031		19.11	
002	6	2.41	37.31	79.46		81.854		65.083	
022	12	1.702	53.80	98.83	67.89	101.81	80.25	80.95	68.40
311	24	1.451	64.08	39.15		40.335		32.071	
222	8	1.390	67.30	45.13		46.496		36.97	

Table 4.1.3: *CaO Crystallite Size for calcined unmodified and doped dolomite*

hkl phase	Multi- plicity	d	2θ position (°)	Dol F^2	Dol LVol (nm)	CaAl F^2	CaAl LVol (nm)	4A1Z F^2	4A1Z LVol (nm)
111	8	2.43	36.94	4.39		4.48		3.73	
002	6	2.10	42.92	54.61	41.92	55.68	42.85	46.37	47.82
022	12	1.49	62.31	98.83		64.78		53.96	
311	24	1.27	74.69	11.03		11.25		9.37	

Table 4.1.4: *MgO Crystallite Size for calcined unmodified and doped dolomite*

Otyo
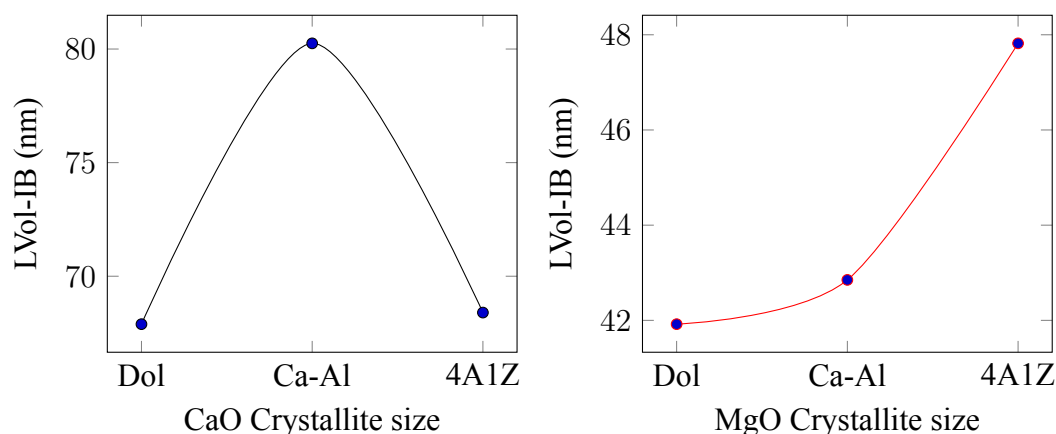
The PSD analysis on calcined dolomite before and after milling shows that it is possible to get as low as approximately 0.3 μm size upon sufficient milling. The milling is important towards ensuring the performance of dolomite-based sorbents in cyclic capture tests. During carbonation of dolomite,

Sample	Median size (μm)	Mean size (μm)	D(v,0.5) (μm)
	6.10	7.08	413.25
	6.04	6.98	408.84
Dolomite before milling	5.49	6.80	400.88
	6.08	7.02	411.39
	0.245	0.257	17.64
	0.245	0.256	17.42
Dolomite after milling & sieving	0.244	0.257	17.43
	0.245	0.258	17.26

Table 4.1.5: *(Macro) Particle size distribution of calcined dolomite before and after milling.*

the carbonation is initially rapid and will quickly changeover to a significantly slow reaction regime as shown in in figure 17 17b below. It is generally accepted that the fast carbonation is controlled by the kinetics of the reaction yet the slow regime is controlled by diffusion of CO_2 through the formed $CaCO_3$ product layer as observed by Dennis and Pacciani (2009). The figure further shows that the complete calcination will never reach the starting weight implying that the CaO will be below 1. This incomplete conversion is caused by the closure of the smallest pores due to the difference in the molar volume of $CaCO_3$ product and CaO of 36.9 and 16.9 cm^3/mol respectively.

The decomposition of one of the successful sorbents (4%Al-2%Zr doped dolomite) reveals that the first weight change of the material occurs between 100-150°C due to loss of water of crystallization and between 500-550°C due to probable decomposition of $Al(NO_3)_3$ and $ZrO(NO_3)_2$. The largest weight change occurs 750 and 866°C due to decomposition of $CaCO_3$ as dictated by the thermodynamics of the reaction.

(a) *4%Al-2%Zr dol. decomposition*

(b) *1 cycle carb/calc of undoped dolomite*
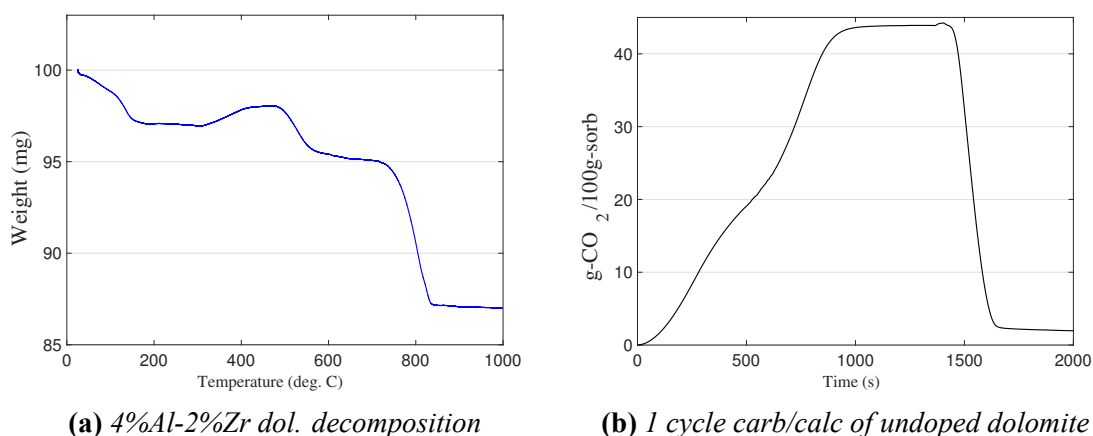
Figure 17: *The thermo gravimetric analysers used for stability tests of the dolomite samples*

4.1.3 First cycle in multi cyclic process

When calcined dolomite is subjected to a temperature corresponding to it's thermodynamic carbonation temperature, the reaction will be shifted towards formation of $CaCO_3$ and this is symbolised by an increase in weight of the sample. This weight increase is primarily due to the sorption of CO_2 on to the CaO hence forming $CaCO_3$. Figure 18 shows that during this first cycle, the weight of the sample will have four peaks which indicate carbonation phases and three troughs which indicate desorption phases and these are explained below:

- The first peak corresponds to the carbonation during a low concentration (10% CO_2) at relatively low temperature. As the temperature raises above approximately 728 °C, the weight of the sample decreases as dictated by the thermodynamics of the the reaction.
- The second peak depicts sorption in a 100% CO_2 (high) concentration at a high temperature and this corresponds to 847°C. As soon as temperature approaches 950 °C, desorption will rapidly take place, and the sample will be completely calcined.
- As the temperature drops in the high CO_2 environment, another carbonation phase occurs where is a maximum weight occurs at a temperature of 798 °C.
- Another low CO_2 carbonation occurs as temperature decreases reaching a maximum weight at around 550 °C.
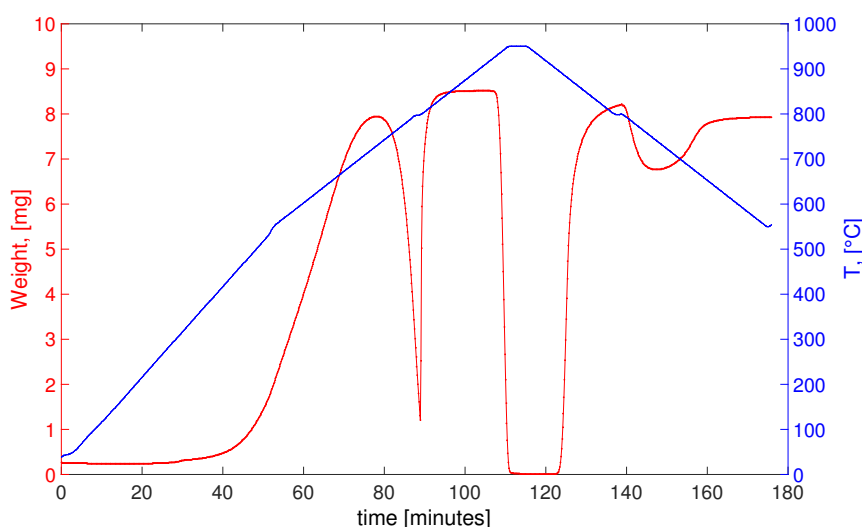
Figure 18: *The variation in weight of a calcined dolomite sample during the first cycle.*

For the stability testing, the multi cyclic CO_2 capture of four different dolomite samples were analysed on the TGA for the first 20 cycles and results are reported in figure **??** below.
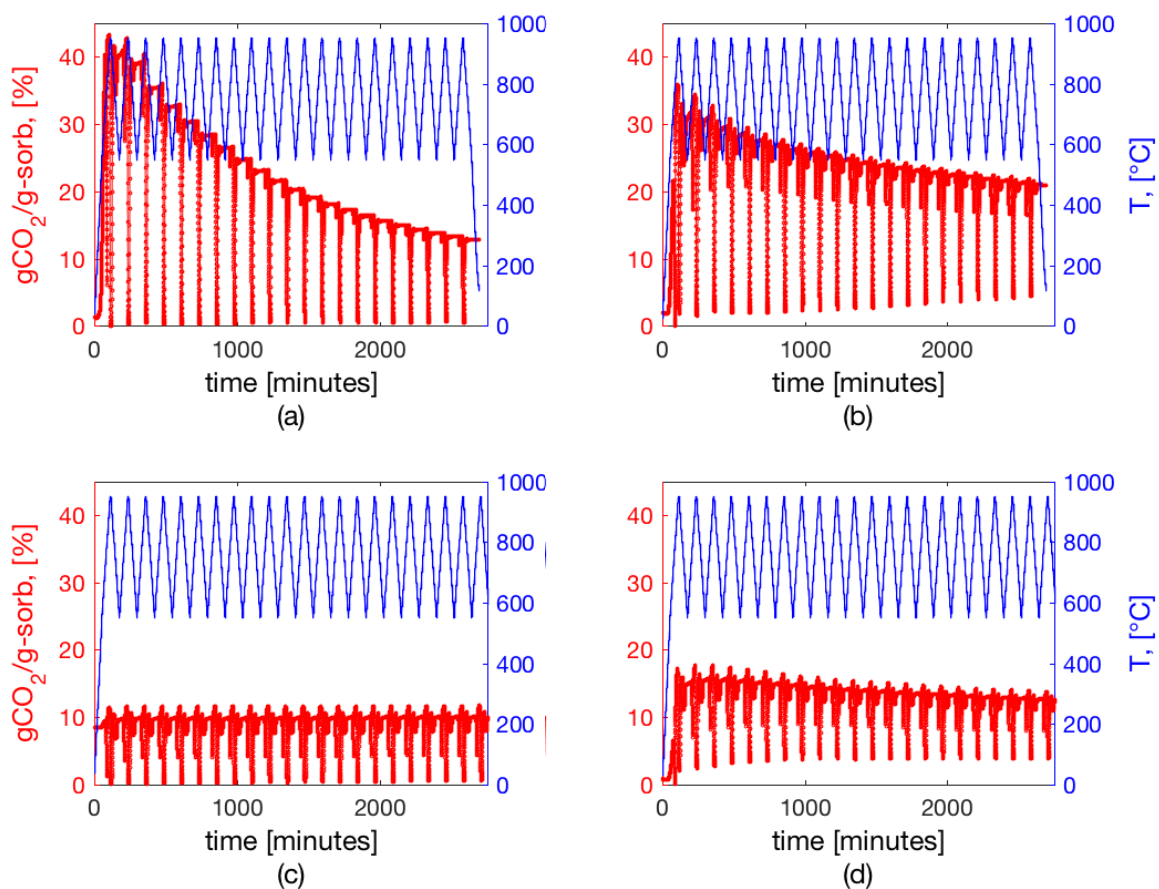
Figure 19: *Loss in the CO_2 capture capacity during the first 20 cycles. See below*

Figure 19 above shows the decay in the capture capacity during 20 cycles for (a): unmodified dolomite, (b): 2% Al doped dolomite, (c): 4%Al-2%Zr doped dolomite and (d): 3%Al-1%Zr doped dolomite. It was observed from these thermogravimetric measurement and analysis that the dolomite-based sorbents undergo a thermal sintering effect repeated multi cyclic sorption-desorption cycles. This sintering effect is depicted by *(i)* a gradual decrease in the maximum weight during carbonation and *(ii)* the shifting of the baseline during measurement.

The shifting of the baseline was be clearly observed in the graphs (b) and (c) above belonging to 2% Al doped dolomite and 3 %Al-1%Zr doped dolomite respectively. The degree of sintering is a material behaviour which indicates the degradation of the active active CaO crystalline as this become deactivated and unavailable for reaction upon multiple carbonation reaction. In order to accurately analyse the thermogravimetric data without interference cause by this baseline shift, all TGA data was re-analysed by recalculating the % capture capacity and % conversion using a MATLAB script shown in appendix **??**. The Matlab code was carefully developed in such a way that for each cycle, - it computes the minimum point, - subtracts all values within that cycle from this minimum point. An example of the recalculation result is shown in figure As seen in the figure, unmodified dolomite (calcined at 1000 °C) experienced rapid decay during the first 20 cycles from ca. 40 to around 6.7 gCO_2/100g-sorbent. The residue capture capacity of dolomite has been reported by Mastin et al. (2011) to be around 8 g-CO_2/100g-sorbent after 500 cycles. In this particular work, it was observed

that the residual capture capacity was 6.7 g-CO$_2$/100g-sorbent after just 134 cycles. This occurrence is attributed to the fact that the ingrained CaO crystallites within dolomite have a tendency to undergo sintering during high temperature carbonation reactions.

Upon introduction of an external phase of Alumina (Al$_2$O$_3$) and Zirconia (ZrO$_2$) through subsequent doping via the incipient wetness impregnation route and calcination, the decay in the CO$_2$ capture capacity is decreased at the expense of losing some initial capture capacity. Of this preliminary results, the sample of dolomite which shows the most promising potential for an efficient CO$_2$ capture while having the most stability is the 4 %Al-2 %Zr doped. This 4 %Al-2 %Zr doped dolomite sample showed a stable With this in mind, the sample was tested for an extended number of cycles, a total of $\approx$100 multi cycles.
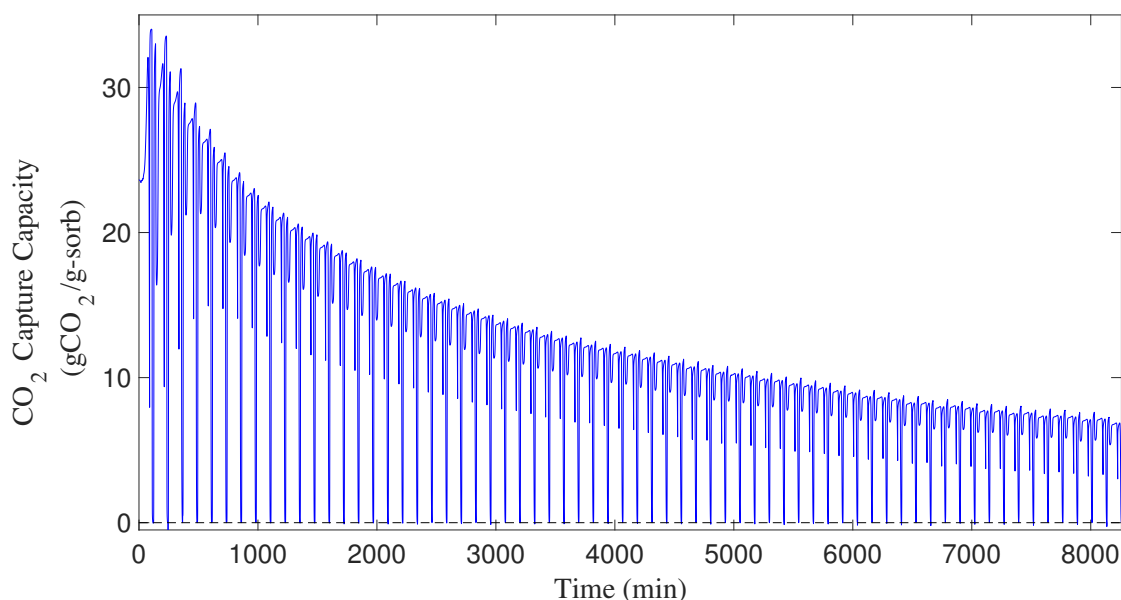
Figure 20: *Loss in the capture capacity of unmodified dolomite during 64 cycles*

In order to appreciate the role played doping the original dolomite sample with 4%Al-2%Zr the extended stability of was compared to that of undoped dolomite. In figures 22 and 21 the capture capacity of dolomite decrease to a meagre 6.7 gCO$_2$/100g-sorbent in just 64 cycles yet that of the 4%Al-2%Zr maintained a stable capacity of approximately 10.5 gCO$_2$/100g-sorbent in as many as 94 cycles. Unfortunately, at the time of testing the 4%Al-2%Zr doped dolomite, the TGA computer could only handle approximately 33 cycles at a time, hence there is a discontinuity in the results for the 94 as these were separately (Run# 1,Run# 2 and Run# 3 as shown in the figure) but with exactly the same sample.
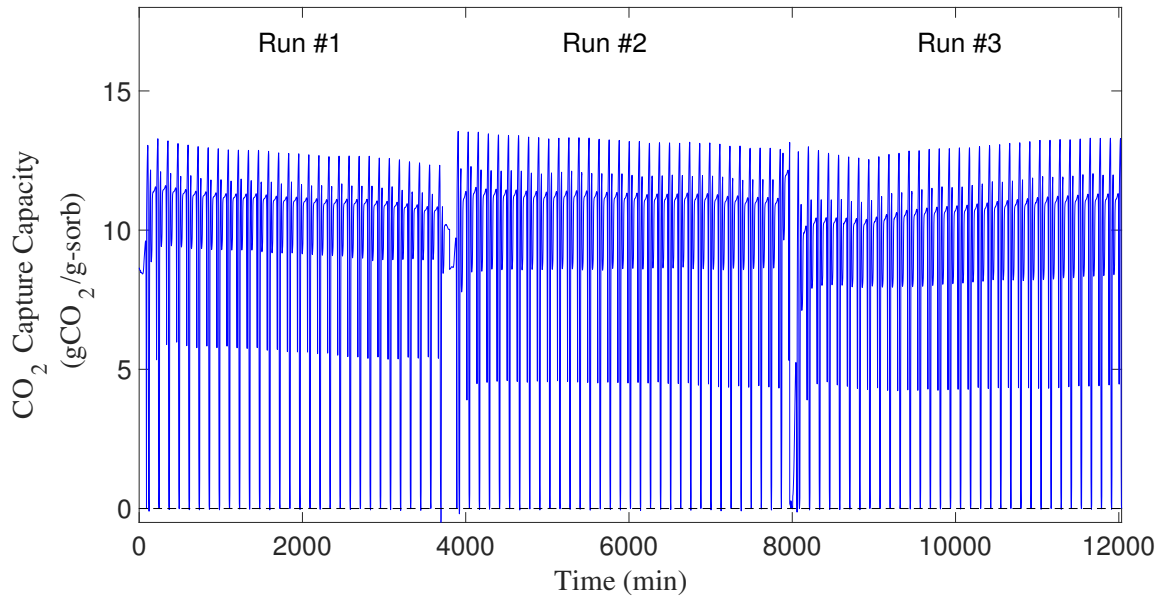
Figure 21: *Stability of 4%Al2%Zr doped dolomite (94 cycles)*
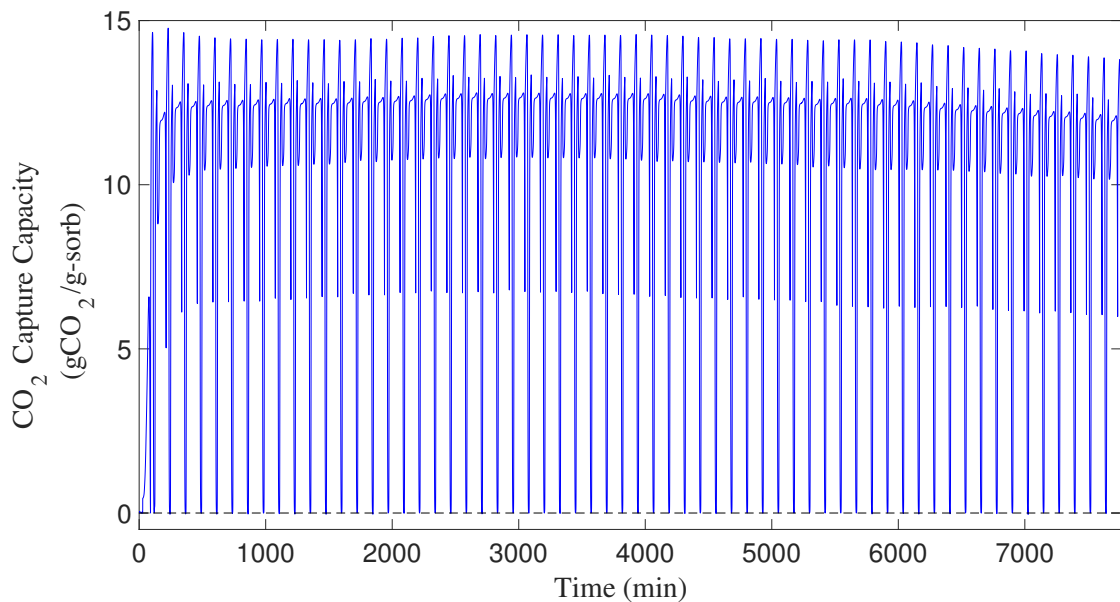
Figure 22: *Loss in the capture capacity of 3.5%Al-2%Zr dolomite during 63 cycles*

As seen in figure 4.1.6 below, all the tested sorbents showed a high initial capacity (above 30 g-CO_2/100g-sorb) but these capacities decayed tremendously over the next 20 cycles.

Batch I samples	Max. conversion	g-CO$_2$/100g-sorb in			total loss
		2nd	11th	21st	(20 cycles)
Undoped dolomite	0.458	40.89	21.02	12.38	28.5
0.5% Al dolomite	0.450	34.33	24.39	18.10	16.2
1% Al dolomite	0.442	36.62	25.88	21.60	15.0
2% Al dolomite	0.425	29.90	22.3	17.2	12.7
0.25% Al-0.25% Mg dol	0.450	36.75	24.29	17.3	19.5
0.5% Al-0.5% Mg dol	0.441	33.28	22.77	16.68	16.6
1% Al-1% Mg dolomite	0.423	31.38	21.89	16.72	14.7
2% Zr dolomite	0.449	30.65	21.92	16.57	14.1
Ca Aluminate dol.	0.4092	27.45	23.70	20.63	6.8
2%Al-2%Zr dol	0.4150	13.08	9.87	8.79	4.2

Table 4.1.6: *Capture capacity in 20 cycles test*

The figure 23 shows a quick comparison between the sorbents that the most interesting CO$_2$ capture capacities. It highlights the loss in the capture capacity of different dolomites over 20 and 30 cycles. It was observed that introducing two phases of dopant was beneficial toward maintaining the stability against sintering as observed in a lesser loss in the g-CO$_2$/100g-sorb. It was observed the loss in capacity of the 2 %Al doped dolomite over 20 cycles was 12.7 as compared to just a 4.2 loss in the 2 %Al-2 %Zr doped sample.
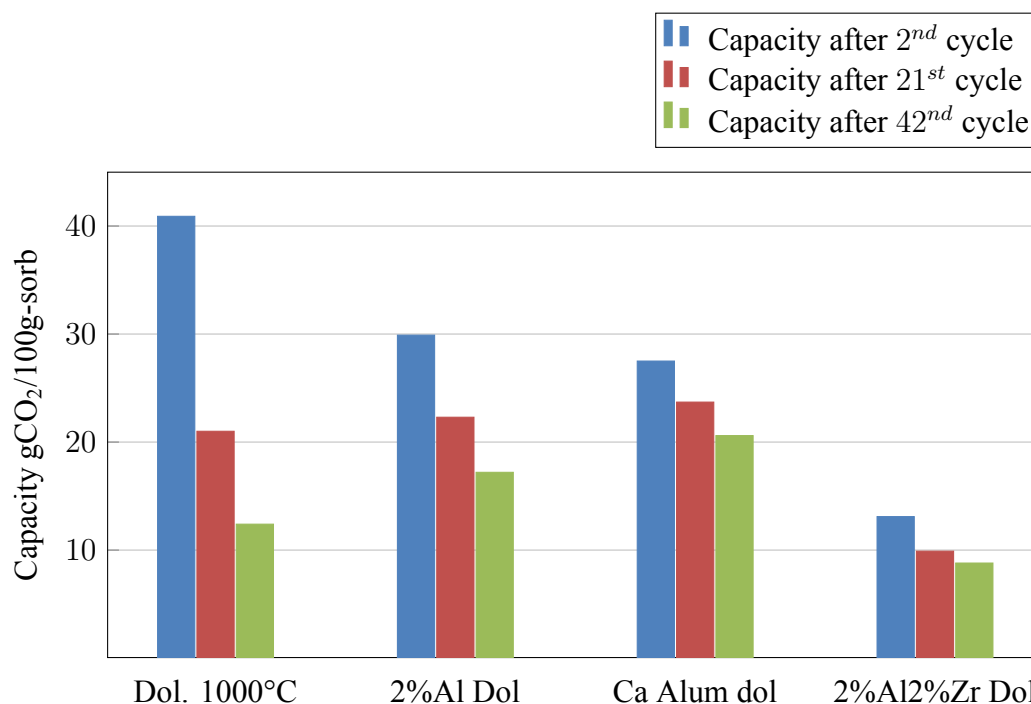
Figure 23: *Comparison of capture capacity of some sorbents*

As it was identified that mixed dopants showed better contribution towards stability of dolomite notably the Aluminium and Zirconium components, an attempt was made to mix them and part of the results are shown in table 4.1.7 below. The 3 %Al-1 %Zr doped dolomite showed a loss of 5.3 g-CO$_2$/100g-sorb over 33 cycles while single oxide doping with 3 %Mg achieved an almost similar loss. This can be explained by the very Tammann temperature of MgO which tends to stabilize CaO

crystallites against sintering. However no new phase is formed in this sorbent as shown in the XRD data.

Batch I	g-CO$_2$/100g-sorb in			total loss
samples	2nd	16th	33st	(33 cycles)
3%Al-1%Zr dol	13.25	9.52	7.948	5.3
3%Mg dol	12.38	8.92	7.18	5.2
6%Al-2%Zr dol	9.16	10.113	10.312	+1.15
4%Al-2%Zr dol	10.71	10.32	10.03	0.68
3$^1/_2$%Al-2%Zr dol	12.7	12.4	12.1	0.6

Table 4.1.7: *Capture capacity in 33 cycles test*
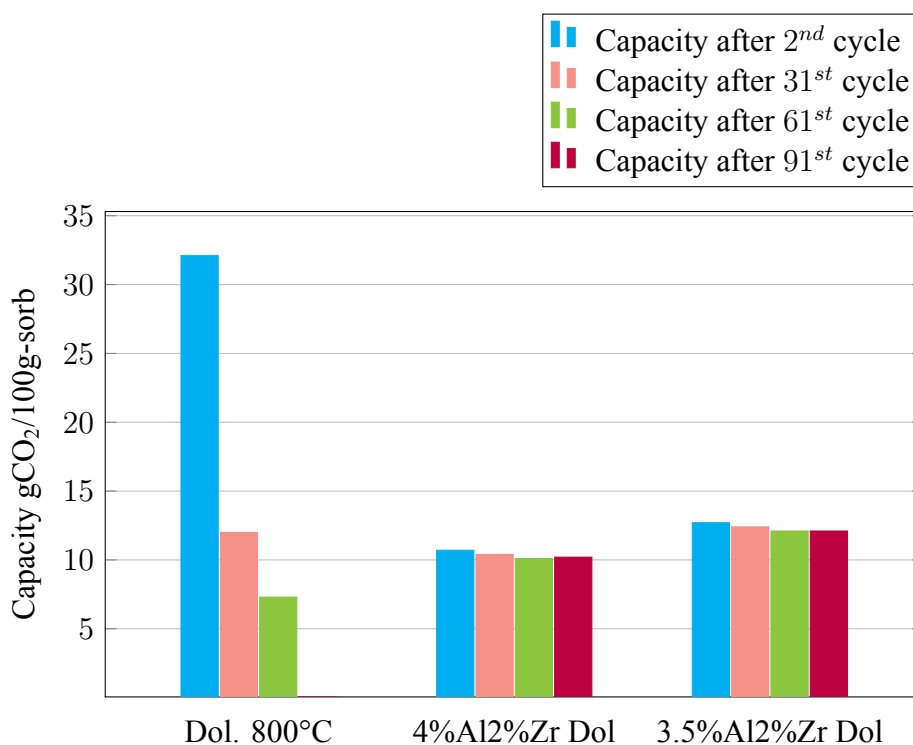
Figure 24: *Comparison of capture capacity with extended cycles*

4.2 Conversion of dolomite-based sorbents

The conversion for some of the developed sorbent samples are represented below as well as their oxide content calculated based on the starting amount of dolomite.

Sorbent	Max. theoretical conversion	Percent content of added oxide in doped sorbent (%)		
		Al_2O_3	ZrO_2	MgO
Unmod. Dolomite	0.4583			
0.5% Al dolomite	0.4499	0.94		
1% Al dolomite	0.4418	1.87		
2% Al dolomite	0.4253	3.71		
0.25% Al-0.25% Mg dol.	0.4496	0.47		1.05
0.5% Al-0.5% Mg dol.	0.4408	0.92		2.08
1% Al-1% Mg dol.	0.4232	1.81		4.08
1% Zr dolomite	0.4530		0.999	
2% Zr dolomite	0.4485		1.995	
3% Mg dolomite	0.4035			6.17
3% Al-1%Zr dolomite	0.4040	5.51	0.973	
6% Al-2%Zr dolomite	0.3514	10.73	1.89	
4% Al-1%Zr dolomite	0.3881	7.29	1.08	
2% Al-2%Zr dolomite	0.4150	3.70	2.19	
4% Al-2%Zr dolomite	0.3827	7.28	1.93	
3.5% Al-1%Zr dol.	0.3906	6.40	1.935	
3%Al ($CaAl_2O_4$) dol.	0.4092	5.51		

Table 4.2.1: *Max conversion and % oxide content of sorbents*
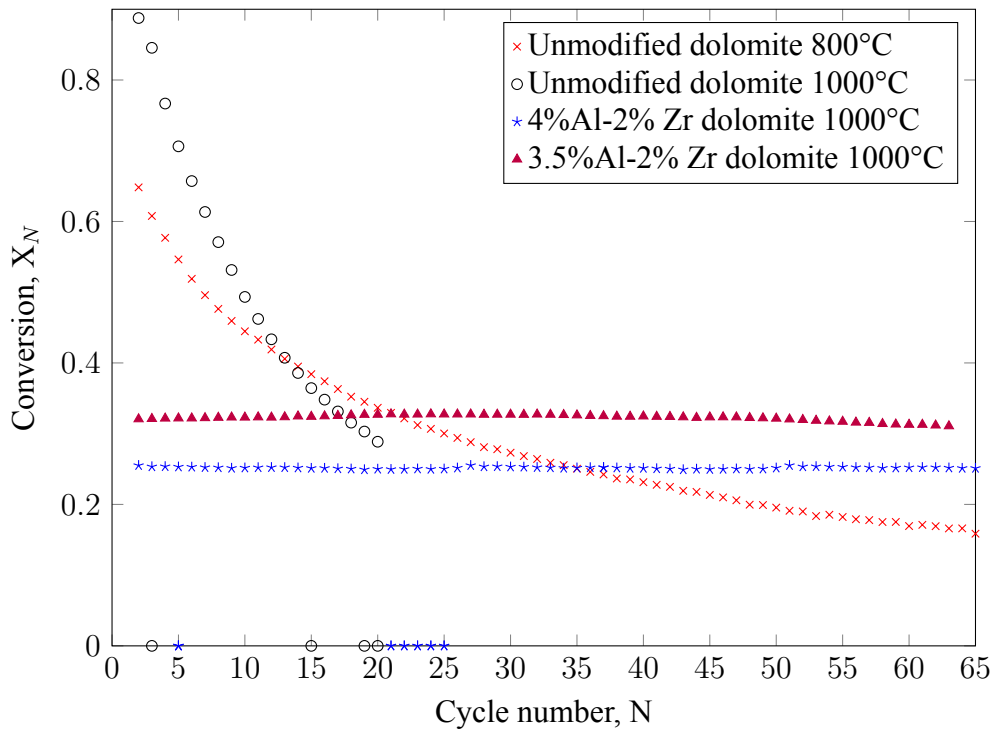
Figure 25: *Variation of conversion, X_N over multiple cycles, N*

4.3 Morphology of selected samples

Scanning electron microscopy of the tested indicates that the morphology of dolomite is significantly changed upon being subjected to multi cyclic desorption in a CO_2 environment. For instance unmodified calcined dolomite show a rough surface before the multi cyclic operation but this will become smoother or molten due to the sintered CaO nano particles as shown in figures 30 and 27. A similar observation is made in the dolomite sample doped with $CaAl_2O_4$ (with 3% Al).

(a) *Pre-testing*   **(b)** *After testing*
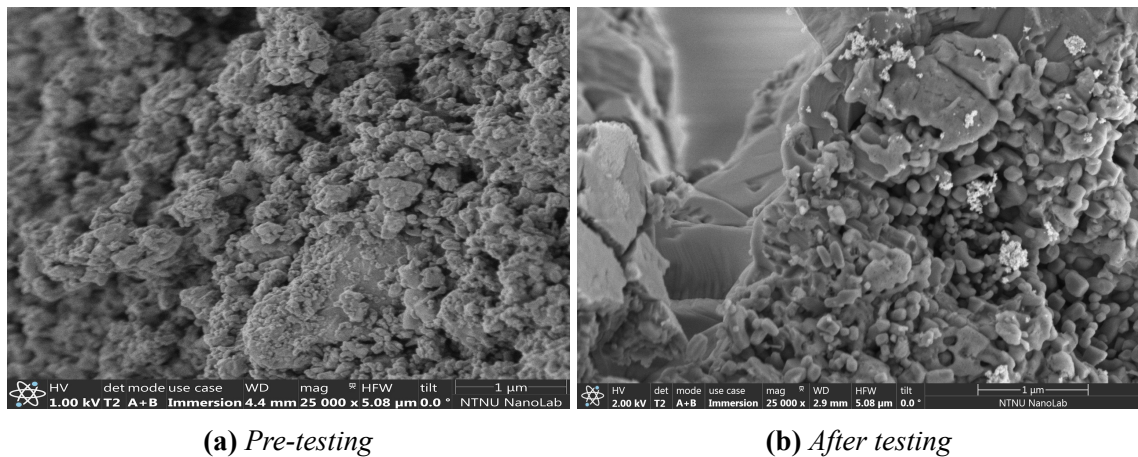
Figure 26: *Morphology of Calcined dolomite before and after 60 cycles*
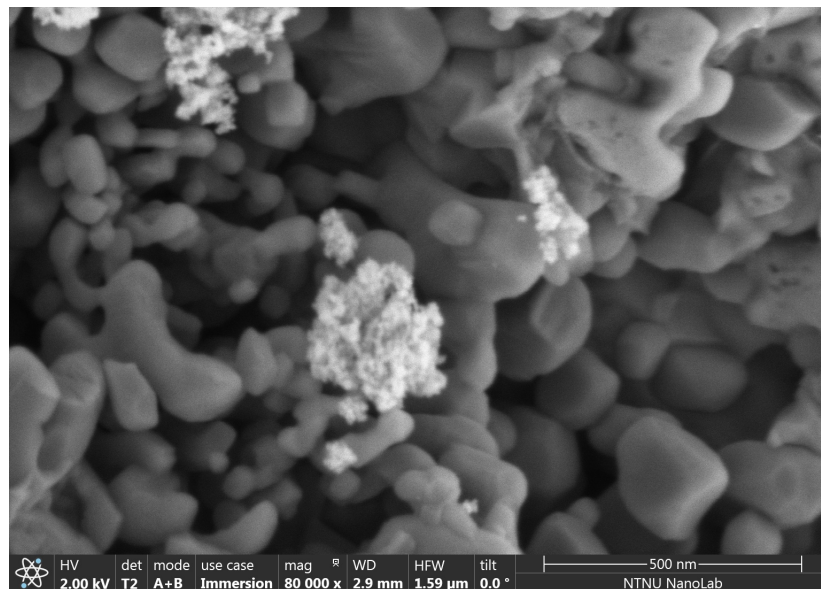
Figure 27: *screenshot*

For the 4%Al-2%Zr sample that was subjected to 94 cycles, the sample minimals less sintering but the size of the pores greatly increased as shown in figure 28.

(a) *Pre-testing*   **(b)** *After testing*
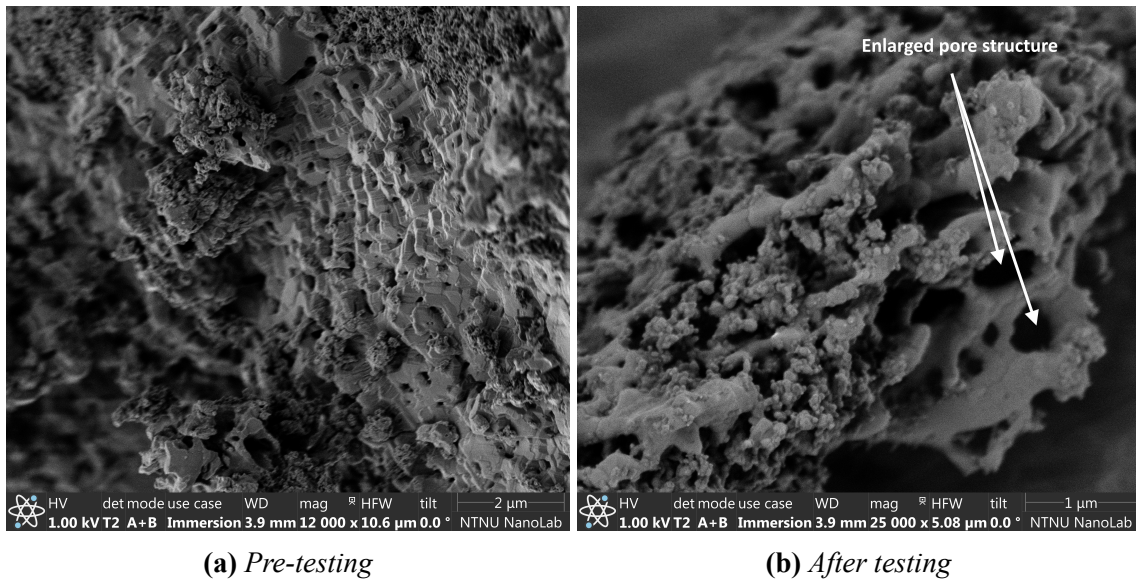
Figure 28: *Morphology of 4%Al2%Zr doped dolomite sample before and after 100 cycles*

The figure above indicates that there is an enlargement of pores when the 4%Al2%Zr doped dolomite sorbent is subject to repeated multi cycles. This observation is further corroborated from the pore size (BJH) analysis and can explain the reason behind the observed stable capture capacity of this particular sorbent.

(a) *Pre-testing*   **(b)** *After testing*
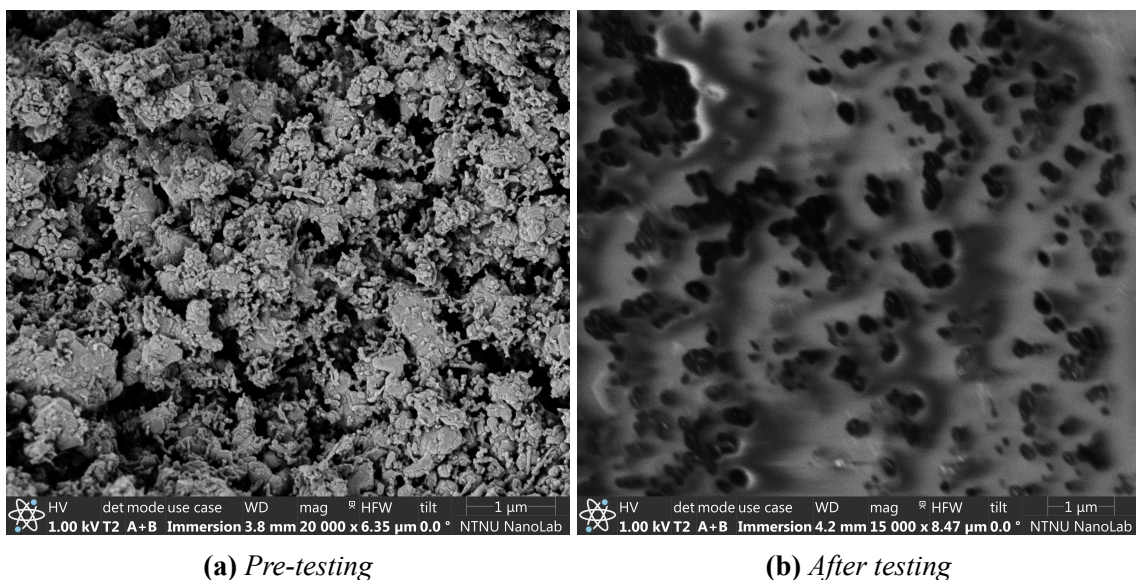
Figure 29: *Morphology of Calcium Aluminate (with 3 %Al) dolomite before and after 20 cycles*

However the 4%Al-2%Zr doped dolomite sample showed a considerable resistance against sintering as surface morphology of the area of interest did not change much after 20 cycles.

(a) *Pre-testing* (b) *After testing*
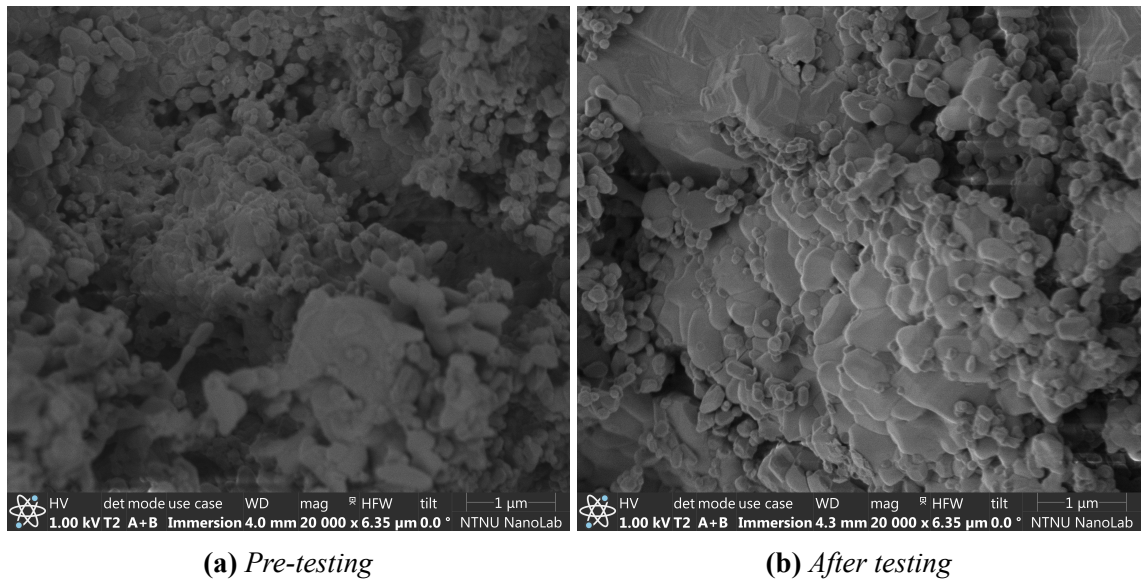
Figure 30: *Morphology of 4%Al2%Zr (fine) doped dolomite sample before and 20 cycles*

Chapter 5

Conclusion and Recommendations for Further Work

5.1 Further work on dolomite-based sorbents

Due to the limitations of the TGA as a tool for kinetic studies, it is suiting to analyse the developed dolomite-based sorbents in a laboratory-scale fixed bed reactor that can be used to test amount of sorbent than just a few milligrams permissible with the TGA. For recommendation purposes only a schematic diagram and brief description of the FBR is shown in figure 32. The operation of the fixed bed reactor is also described. Upon successful operation of this fixed bed reactor, the kinetics of the sorbents can be studied. The advantage of the fixed bed reactor over TGA is that more sorbents can be loaded in the reactor, up to 2 g as compared to only a few milligrams in the TGA.

More so, the diffusion limitations of gas flow to the sorbents is significantly decreased so that the kinetics of the reaction is the only controlling factor and can thus be ascertained. Figure 32 shows the piping and instrumentation diagram for the reactor setup used for testing the CO_2 sorbents. The fixed bed reactor is primarily used to determine the change in the weight of the sorbent sample as it is heated in a controlled gas environment. The flows of gases to the reactor are controlled by Mass Flow Controllers, MFC (Bronckhorst-type) which in turn are controlled by the computer.
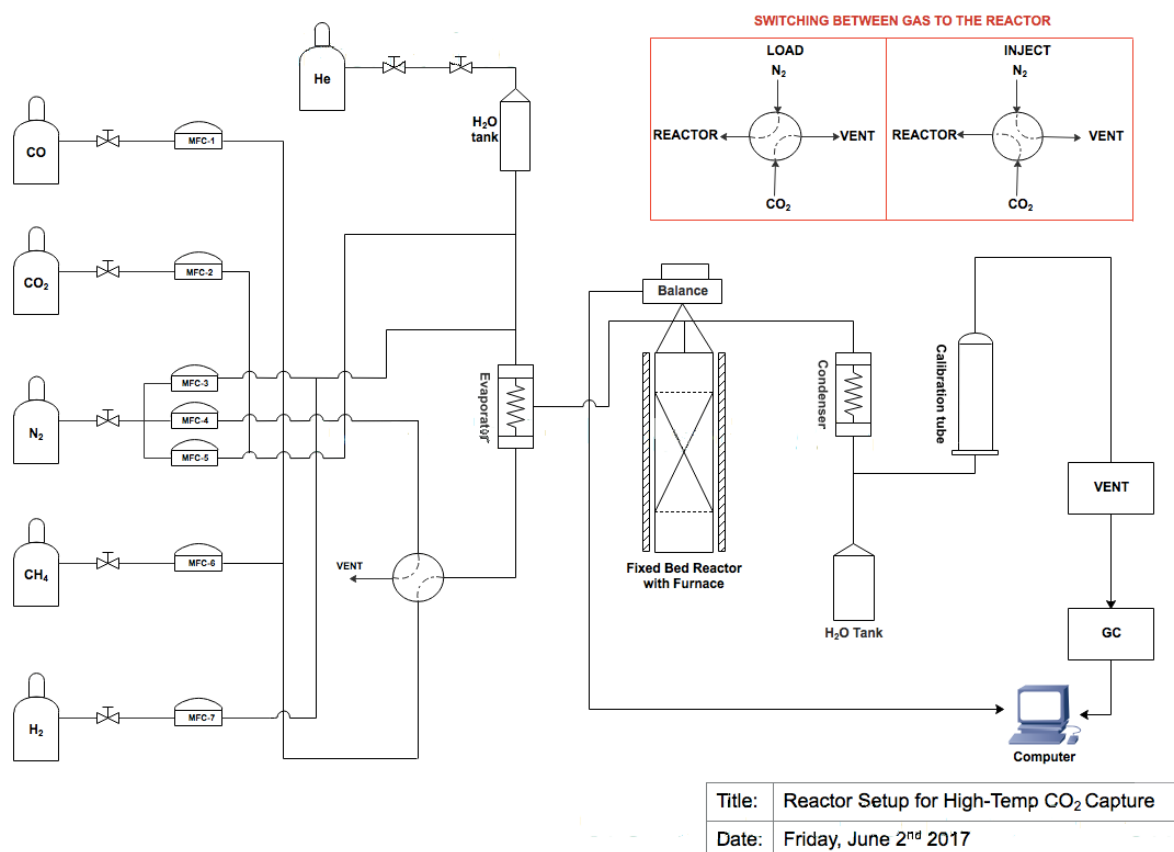
Figure 31: *Fixed bed reactor set up*

The reator set up conditions include:

- Reactor dimensions: 16 mm outer diameter, 22 cm height

- Maximum sample weight: 3 g

- Atmosphere: CO, Ar, CO_2, CH_4, N_2, H_2S, H_2O, steam.

- Maximum temperature: 1100 °C

The key parameters controlled by the computer software include:

- Furnace or sample temperature

- Gas flow rates and compositions

A Eurotherm Controller (not shown on the diagram) is used to control the temperature of the furnace. A VICI value is used to switch between the gases flowing into the reactor. When the VICI valve is in the LOAD position during desorption, Nitrogen gas will flow in the reactor. Contrariwise, when the VICI valve is in the INJECT position during the carbonation phase, carbon dioxide gas will flow into the reactor. All reactor and furnace parameters including set points and actual process values are programmed and recorded using a dedicated labview software

The fixed bed reactor was not used during the project work. However the plan for the future is to screen the dolomite samples through TGA characterization and later test them for stability using the FBR. Figure 32 shows the set up of the reactor to be used. A more detailed description of the working principle of the set-up will be given in subsequent reports.
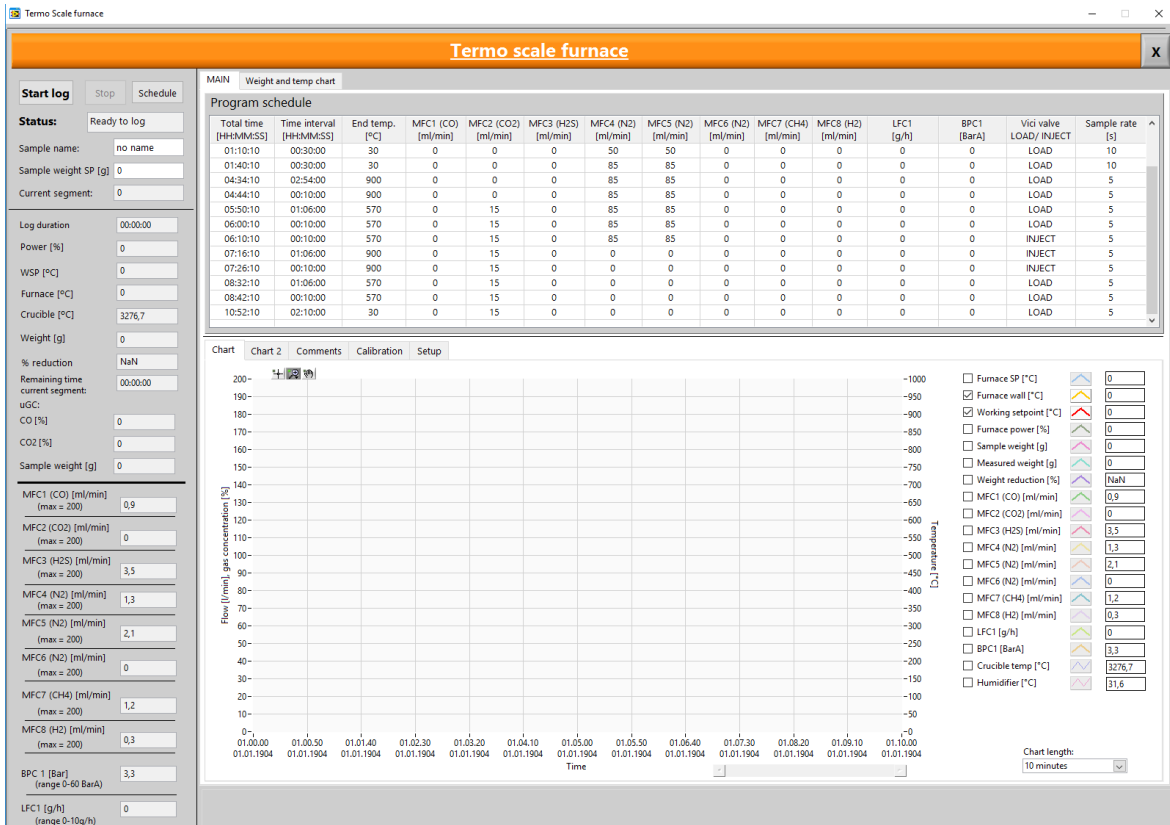
Figure 32: *LabView software screen used for fixed bed reactor operation and monitoring*

With sufficient kinetic data, modelling of the kinetics and model-fitting can be performed on the kinetic data using an expression like the one posulated by Grasa et al. (2007) shown below:

$$X_N = X_r + \frac{1}{\frac{1}{1-X_r} + kN}$$

(5.1.1)

where k is the deactivation constant (ranging between 0.28-1.96), X_r is the residual conversion and X_N is the CaO conversion in the $N^t h$ cycle.

Performance in presence of steam

In this work, only the dry conditions were used. No tests were performed in the wet condition due to limitation of the equipment. It would however be interesting to ascertain the performance of our developed sorbents in presence of steam as regards to stability and kinetic studies.

For instance, the effect of steam on the performance of dolomite based sorbents has been studied by various scientists (Wang et al. (2016), Zarghami et al. (2015), Abbasi et al. (2014)) and it has been reported that steam improves the kinetics of decomposition, modifies the radial distribution of pores, improves connectivity inside the dolomite particles. There is decreased diffusion resistance of the evolved CO_2 inside the particle. Wang et al. (2015) however found a detrimental effect of steam on dolomite performance. With these contradicting reports, it is crucial to perform an independent analysis to the effect of steam in our prevailing conditions.

5.2 Conclusion

In this Master's thesis, it was confirmed that naturally occurring unmodified Arctic dolomite upon sufficient calcination at 1000°C can be used to capture CO_2 due to it's high initially high through the carbonation reaction of CaO to $CaCO_3$. However this unmodified dolomite suffers from the dramatic loss of capacity to capture CO_2 from 43.2 to just 6.7 g-CO_2/100g-sorbent in just 120 carbonation-decarbonation cycles (60 cycles).

The stability of naturally occurring dolomite after sufficient calcination was thereby successfully improved by incorporation with an inert mixed oxide comprising of Al_2O_3 and ZrO_2 and identified that the optimal amount was xx 3.5%Al with 2%Zr based on multi cyclic tests conducted in a TGA. This finding is comparable to that of Arstad et al. (2014) who improved the stability of Seljelid dolomite using 1% Zr at a constant capture capacity of 1 mmol-CO_2/g-sorbent using different test conditions from the ones used in this work.

Further investigation revealed that this stabilization of calcined dolomite is brought about due to formation new mixed oxide phases of *Calcium Aluminate* and *Calcium Zirconate* which function in synergy to protect the CaO crystal structure against thermal sintering. Increasing the amount of oxide dopant beyond these value for instance to 6 %Al with 2 %Zr did not significantly improve the stability of dolomite.

Even though the primary objective of developing a stable dolomite-based sorbents was successfully achieved in this masters project, there is a tremendous room for improvement. The best case was achieved by doping 3.5%Al-2%Zr and it had a capture capacity of 12.4 g-CO_2/100g-sorbent and a constant conversion of 0.33 after 120 carb/decarb cycles (60 multi-cycles). The diminished specific surface area of this sorbent shows that areas of improvement can be made in the drying and calcination methods used. For example the thermal degradation of the 4 %Al-2 % showed the temperature should be held isothermally for atleast 1 hour at 150 and 550 °C during calcination temperature program to appropriately decompose the nitrate component.

Chapter 6

Glossary

Special and technical terms

Sorption	a physico chemical process by which one substance becomes attached to another where absorption and adsoprption occur simultaneously in a single process. Adsorption is the incorporation of a substance in one state into another of a different state, for instance CO_2 being taken up by a solid CaO whereas adsorption – the physical adherence or bonding of ions and molecules onto the surface of another phase.
CO_2 Capture capacity	is the amount of CO_2 in grams/moles that can be adsorbed by a given amount of sorbent that is; g-CO_2/g-sorbent
Conversion	the ratio of the amount (in moles) of active CaO component reacted to form $CaCO_3$ to the total amount (in moles) CaO present. Since not all CaO is able to react during the carbonation reaction due to formation inert Calcium Aluminate and Calcium Zirconate phases, the conversion will be reduced below unity. The presence of inert MgO in natural dolomite present in equi molar amounts as the active CaO also reduces the conversion of the sorbent. Thus the conversion X_N is calculated using the equation.

$$X_N = \frac{\Delta W}{W_{initial} \cdot X_o} \qquad (6.0.1)$$

	where: ΔW is the change in weight as measured by TGA, $W_{initial}$ is the initial weight of the sample used during the measurements X_o is the maximum (theoretical) conversion attainable.
Tammann temperature	the temperature above which the bulk atoms become mobile. This is the temperature above which the atoms and molecules of the solid acquire sufficient energy for the bulk mobility and reactivity to become appreciable. Tammann temperature is approximately equal to ½ the melting point temperature.
Baseline	is also known as the correction measurement is the measurement made by the TGA with an empty crucible (without the sample). This measure is usually subtracted from the actual measurement from the sample in order to remove measurement errors that might arise from contribution from the measurement system/crucible.

Bibliography

Abbasi, E., Hassanzadeh, A., Zarghami, S., Arastoopour, H. and Abbasian, J. (2014), 'Regenerable mgo-based sorbent for high temperature CO_2 removal from syngas: 3. CO_2 capture and sorbent enhanced water gas shift reaction', *Fuel* **137**, 260–268. cited By 5.
URL: *http://dx.doi.org/10.1016/j.fuel.2014.07.088*

Al-Jeboori, M. J., Nguyen, M., Dean, C. and Fennell, P. S. (2013), 'Improvement of limestone-based CO_2 sorbents for ca looping by hbr and other mineral acids', *Industrial & Engineering Chemistry Research* **52**(4), 1426–1433.
URL: *http://dx.doi.org/10.1021/ie302198g*

Arstad, B., Lind, A., Andreassen, K., Pierchala, J., Thorshaug, K. and Blom, R. (2014), In-situ xrd studies of dolomite based co2 sorbents, *in* 'In-situ XRD studies of dolomite based CO2 sorbents', Vol. 63, pp. 2082–2091. cited By 0.
URL: *http://dx.doi.org/10.1016/j.egypro.2014.11.224*

Barker, R. (1973), 'The reversibility of the reaction $CaCO_3 \leftrightarrow CaO+CO_2$ ', *Journal of Applied Chemistry and Biotechnology* **23**(September), 733–742.
URL: *http://doi.wiley.com/10.1002/jctb.5020231005*

Bhatia, S. K. and Perlmutter, D. D. (1983), 'Effect of the product layer on the kinetics of the CO_2-lime reaction', *AIChE Journal* **29**(1), 79–86.
URL: *http://doi.wiley.com/10.1002/aic.690290111*

Broda, M., Kierzkowska, A. M. and Muller, C. R. (2014), 'Development of Highly Effective CaO-based, MgO-stabilized CO_2 Sorbents via a Scalable One-Pot Recrystallization Technique', *Advanced Functional Materials* **24**(36), 5753–5761.

Bru (n.d.), *TOPAS 5 Technical Reference*.

Che, M. and Védrine, J. (2012), *Characterization of solid materials and heterogeneous catalysts. From structure to surface reactivity*, Wiley-VCH.

Coutures, J. P. and Rand, M. H. (1989*a*), 'Melting temperatures of refractory oxides - Part II: Lanthanoid sesquioxides', *Pure and Applied Chemistry* **61**(8), 1461–1482.

Coutures, J. and Rand, M. (1989*b*), 'International Union of Pure Commission on High Temperature and Solid State Chemistry * Melting Temperatures of Refractory Oxides : Part I1 Lanthanoid Sesquioxides', *Pure and Applied Chemistry* **61**(8), 1461–1482.

Cullity, B. D. (1956), 'Elements of x-ray diffraction', pp. 3–531.

De Jong, K. (2009), *Synthesis of Solid Catalysts*, Wiley VCH Verlag GmbH & Co. KGaA.

Dennis, J. and Pacciani, R. (2009), 'The rate and extent of uptake of CO_2 by a synthetic, cao-containing sorbent', *Chemical Engineering Science* **64**(9), 2147 – 2157.
URL: *http://www.sciencedirect.com/science/article/pii/S000925090900061X*

Fennel, P. and Anthony, B. (2015), *Calcium and Chemical Looping Technology for Power Generation and Carbon Dioxide (CO2) Capture*, Vol. 1, Woodhead Publishing publications.
URL: *http://www.sciencedirect.com/science/article/pii/B9780857092434000136*

Fennell, P. S., Pacciani, R., Dennis, J. S., Davidson, J. F. and Hayhurst, A. N. (2007), 'The effects of repeated cycles of calcination and carbonation on a variety of different limestones, as measured in a hot fluidized bed of sand', *Energy & Fuels* **21**(4), 2072–2081.
URL: *http://dx.doi.org/10.1021/ef060506o*

Filitz, R., Kierzkowska, A. M., Broda, M. and Müller, C. R. (2012), 'Highly efficient CO_2 sorbents: Development of synthetic, calcium-rich dolomites', *Environmental Science & Technology* **46**(1), 559–565. PMID: 22129091.
URL: *http://dx.doi.org/10.1021/es2034697*

Gil, M. V., Fermoso, J., Rubiera, F. and Chen, D. (2015), 'H_2 production by sorption enhanced steam reforming of biomass-derived bio-oil in a fluidized bed reactor: An assessment of the effect of operation variables using response surface methodology', *Catalysis Today* **242**(PartA), 19–34.
URL: *http://dx.doi.org/10.1016/j.cattod.2014.04.018*

Grasa, G., González, B., Alonso, M. and Abanades, J. C. (2007), 'Comparison of CaO-based synthetic CO_2 sorbents under realistic calcination conditions', *Energy and Fuels* **21**(6), 3560–3562.

Johnson, J. (2010), 14 - sintering of refractory metals, *in* Z. Z. Fang, ed., 'Sintering of Advanced Materials', Woodhead Publishing Series in Metals and Surface Engineering, Woodhead Publishing, pp. 356 – 388.
URL: *http://www.sciencedirect.com/science/article/pii/B9781845695620500145*

Kierzkowska, A. M., Pacciani, R. and Müller, C. R. (2013), 'Cao-based CO_2 sorbents: From fundamentals to the development of new, highly effective materials', *ChemSusChem* **6**(7), 1130–1148.
URL: *http://dx.doi.org/10.1002/cssc.201300178*

Kierzkowska, A. M., Poulikakos, L. V., Broda, M. and Müller, C. R. (2013), 'Synthesis of calcium-based, Al_2O_3-stabilized sorbents for CO_2 capture using a co-precipitation technique', *International Journal of Greenhouse Gas Control* **15**, 48 – 54.
URL: *http://www.sciencedirect.com/science/article/pii/S1750583613000777*

Li, Y., Sun, R., Liu, H., Zhao, J., Han, K. and Lu, C. (2011), 'Process analysis of cyclic CO_2 capture using limestone and dolomite at high temperature [j]', *CIESC Journal* **6**, 033.

Manovic, V. and Anthony, E. J. (2009), 'CaO-Based Pellets Supported by Calcium Aluminate Cements for High-Temperature CO_2 Capture', *Environmental Science & Technology* **43**(18), 7117–7122.
URL: *http://dx.doi.org/10.1021/es901258w*

Mastin, J., Aranda, A. and Meyer, J. (2011), 'New synthesis method for CaO-based synthetic sorbents with enhanced properties for high-temperature CO_2-capture', *Energy Procedia* **4**, 1184–1191.
URL: *http://dx.doi.org/10.1016/j.egypro.2011.01.172*

McCusker, L. B. (2005), 'IUPAC nomenclature for ordered microporous and mesoporous materials and its application to non-zeolite microporous mineral phases', *Reviews in Mineralogy and Geochemistry* **57**(1), 1–16.
URL: *http://rimg.geoscienceworld.org/content/57/1/1*

Perejón, A., Miranda-Pizarro, J., Perez-Maqueda, L. A. and Valverde, J. M. (2016), 'On the relevant role of solids residence time on their CO_2 capture performance in the Calcium Looping technology', *Energy* **113**, 160–171.

Retsch Technology (n.d.), 'Laser Light Scattering particle analyzer horiba la-960', http://www.retsch-technology.com/products/laser-light-scattering/la-960/function-features/. Online; accessed 2017-06-23.

Valverde, J. M., Perejón, A., Medina, S. and Perez-Maqueda, L. A. (2015), 'Thermal decomposition of dolomite under CO_2: insights from TGA and in situ XRD analysis.', *Physical chemistry chemical physics : PCCP* **17**(44), 30162–76.
URL: *http://pubs.rsc.org/en/Content/ArticleHTML/2015/CP/C5CP05596B*

Valverde, J. M., Sanchez-Jimenez, P. E. and Perez-Maqueda, L. A. (2015), 'Ca-looping for postcombustion CO2 capture: A comparative analysis on the performances of dolomite and limestone', *Applied Energy* **138**, 202–215.
URL: *http://dx.doi.org/10.1016/j.apenergy.2014.10.087*

Wang, K., Hu, X., Zhao, P. and Yin, Z. (2016), 'Natural dolomite modified with carbon coating for cyclic high-temperature CO2 capture', *Applied Energy* **165**, 14–21.
URL: *http://dx.doi.org/10.1016/j.apenergy.2015.12.071*

Wang, K., Yin, Z., Zhao, P., Han, D., Hu, X. and Zhang, G. (2015), 'Effect of Chemical and Physical Treatments on the Properties of a Dolomite Used in Ca Looping', *Energy Fuels* **29**(7), 4428.

Zarghami, S., Ghadirian, E., Arastoopour, H. and Abbasian, J. (2015), 'Effect of steam on partial decomposition of dolomite', *Industrial and Engineering Chemistry Research* **54**(20), 5398–5406. cited By 3.
URL: *http://dx.doi.org/10.1021/acs.iecr.5b00049*

Appendix A

Risk Assessment

Evaluation and assessment of risk associated with the laboratory work performed during this Master's project are outlined in this appendix. The Risk assessment was performed with help with the HSE mananger at IKP, NTNU. Material Safety Data Sheets (MSDS) for the chemicals, instrument manuals as well as NTNU/SINTEF HSE handbook were used guidelines when generating this risk assessment form.

A.0-2

Detailed Risk Report

			Status	Date
ID	11174		Status	Date
Risk Area	Risikovurdering: Helse, miljø og sikkerhet (HMS)		Created	20.07.2016
Created by	Moses Mawanga		Assessment started	20.07.2016
Responsible	Moses Mawanga		Actions decided	
			Closed	

CAT, master/project, 2017 Moses Mawanga

Valid from-to date:

1/23/2017 - 6/19/2017

Location:

3 - Gløshaugen / 315 - Kjemi 5 / 1040 - 4. etasje / 448

Goal / purpose

Risk assessment of the work performed by Moses Mawanga on the new Balance reactor during a master project.
Lab work involves synthesis and characterization of CaO based materials.

Background

Experimentation with a balance reactor with pre-treated dolomite. Activities include; ball-milling, sieving, calcination with a high temperature furnace, TGA, XRD, Raman, BET setups.

Description and limitations

Pressurized non-combustible gases; Carbon dioxide and Nitrogen during testing with the reactor.

Prerequisites, assumptions and simplifications

Few serious dangers
Protection during the execution of the experiment is a prerequisite: fume-hood, goggles, lab coat, gloves, fire blankets, fire extinguisher, gas detection system

Attachments

[Ingen registreringer]

References

TGA apparatus(https://avvik.ntnu.no/Risk/EditRiskAssessment/1532)

A.0-2

Detailed Risk Report

Summary, result and final evaluation

The summary presents an overview of hazards and incidents, in addition to risk result for each consequence area.

Final evaluation

Risk is of general nature.
No remaining risk is associated with this experimentation exercise.

Units this risk assessment spans

 - Institutt for kjemisk prosessteknologi

Participants

Gunn Torill Wikdahl

Karin Wiggen Dragsten

De Chen
Li He

Readers

Kumar Ranjan Rout

Shirley Elisabeth Liland

Others involved/stakeholders

De Chen
Kumar Ranjan Rout
Rune Lødeng
Li He

The following accept criteria have been decided for the risk area Risikovurdering: Helse, miljø og sikkerhet (HMS):

Helse	Materielle verdier	Omdømme	Ytre miljø
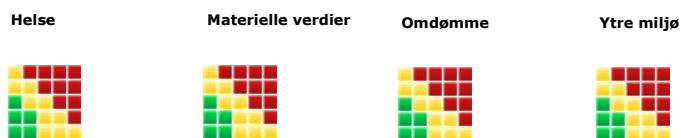
Overview of existing relevant measures which have been taken into account for this risk assessment

The table below presents existing measures, which have been take into account when assessing the likelihood and consequence of relevant incidents.

Hazard	Incident	Mesures taken into account
Chemical handling	Spillage on skin, inhalation or eyes	Personal Protective Equipment.
	Spillage on skin, inhalation or eyes	Safety Data Sheets
	Spillage on skin, inhalation or eyes	Fume hood

Existing relevant measures with descriptions:

A.0-4

Detailed Risk Report

Personal Protective Equipment.

Safety google   Nitrile gloves
Lab coat   Face shield
nose masks

Safety Data Sheets

CO2 MSDS   N2 MSDS
Dolomite MSDS   Calcium Nitrate MSDS
Aluminium nitrate nonahydrate MSDS   Aluminium nitrate nonahydrate MSDS
Zirconyl nitrate 35 wt% solution MSDS

Gas leakage detection

Before every experimental run, gas leakage is detected.

Fume hood

[Ingen registreringer]

Risk analysis with evaluation of likelyhood and consequence

This part of the report presents detailed documentation of hazards, incidents and causes which have been evaluated. A summary of hazards and associated incidents is listed at the beginning.

The following hazards and incidents has been evaluated in this risk assessment:

- **Chemical handling**
  - Spillage on skin, inhalation or eyes

Overview of risk mitigating actions which have been decided, with description:

Chemical handling/Spillage on skin, inhalation or eyes (incident)

Non-toxic chemicals. But care should be taken not to spill,
Protective equipment should be used always.

Overall assessed likelihood of the incident: Unlikely (1)

Comment to likelihood assessment:

[Ingen registreringer]

Assessment of risk for the consequence area: Helse

Assessed likelihood (common for incident):   Unlikely (1)

Assessed consequence: Medium (2)

Comment to consequence assessment:

[Ingen registreringer]

Overview of risk mitigating action which have been decided:

Below is an overview of risk mitigating actions, which is intended to contribute towards minimizing the likelihood and/or consequence of incidents:

Overview of risk mitigating actions which have been decided, with description:

Norges teknisk-naturvitenskapelige universitet (NTNU)	Print date:	Printed by:	Page:
Unntatt offentlighet jf. Offentlighetsloven § 14	07.03.2017	Moses Mawanga	3/5

B

Incipient Wetness Impregnation

B.1 Calculation of amount Nitrate Precursor used

Zinconyl Nitrate	$ZrO(NO_3)_2$
Zirconium tetrachloride	$ZrCl_4$
Magnesium Nitrate	$Al(NO_3)_3 \cdot 9\,H_2O$
Aluminium Nitrate	$Mg(NO_3)_2 \cdot 6\,H_2O$

Table B.1.1: *Nitrate Precursors*

To demonstrate how the amounts of nitrate precursors were calculated based on the starting amount of calcined dolomite.
starting with 10 g of calcined dolomite, with the target of doping it with 2 wt% Al, the following procedure was employed.
With 2 wt % Al, the remaining wt of dolomite corresponds to 98 wt %
98 wt % correspond to 10 g of sorbent material

2 wt % correspond to $\frac{10 \cdot 2}{98} = 0.2041$ g of Al

Moles of Al $= \frac{0.2041}{27} = 7.56 \cdot 10^3$ g of Al

From the reaction:
$$Al(NO_3)_3 \longrightarrow Al$$
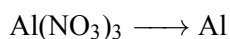
One mole of $Al(NO_3)_3 \cdot 9\,H_2O$ liberates one mole of Al.

Moles of $Al(NO_3)_3 \cdot 9\,H_2O = 7.56 \cdot 10^3$

Mass of $Al(NO_3)_3 \cdot 9\,H_2O = \frac{7.56 \cdot 10^3}{375.13} = 2.8357$ g.

Adjust for purity $= 2.8357$ g

This implies that 2.8357 g of the Aluminium nitrate nonahydrate precursor in needed to be fused with calcined dolomite via the incipient wetness method in order to have approximately 2 wt % Al doped dolomite.

The maximum CO_2 capture capacity of the doped dolomite sorbent was calculated using the following equation. The equation hold based on the assumption that dolomite has equimolar amount of CaO and MgO.

$$\text{Max. capture capacity} = \frac{\left[\text{moles MgO} - \text{moles Al}_2\text{O}_3 - \text{moles ZrO}_2\right] \cdot 44}{\text{moles MgO} \cdot 40 + \text{moles MgO} \cdot 56 + \text{moles Al}_2\text{O}_3 \cdot 101.96}$$

where 44, 40, 56, 101.96 are the molecular weights for CO_2, CaO, MgO and Al_2O_3 respectively. This maximum theoretical capacity denoted as X_o is useful in the calculation of the actual conversion of the sorbent in a given number of cycles.

Appendix C

Calibration

C.1 Calibration of the TGA Q500 instrument

C.1.1 MFC calibration

The sample and balance gas mass flow controllers were calibrated using the soap bubble method and the results shown below.

Calibration of TGA Q500 Sample gas purge MFC							
Volume [ml]	1	1	1	1	9	90	90
Nominal flowrate [ml/min]	**7**	**10**	**15**	**20**	**30**	**160**	**180**
Time [s]	46.29	19.78	8.97	5.62	28.28	44.53	40.03
	45.87	20	8.66	5.44	28.54	44.38	39.88
	48.75	20.21	8.6	5.5	28.12	44.34	39.91
	41.41	19.78	8.78	5.75	28.5		39.62
				5.94			
Avg. Time [s]	45.58	19.9425	8.7525	5.65	28.36	44.4167	39.86
Observed flowrate [ml/min]	**1.31637**	**3.00865**	**6.85518**	**10.6195**	**19.0409**	**121.576**	**135.474**

MFC Calibration curve for CO_2 purge

$y = 0.783x - 4.6478$
$R^2 = 0.9999$

Obs. flowrate [ml/min] vs Nom. flowrate [ml/min]
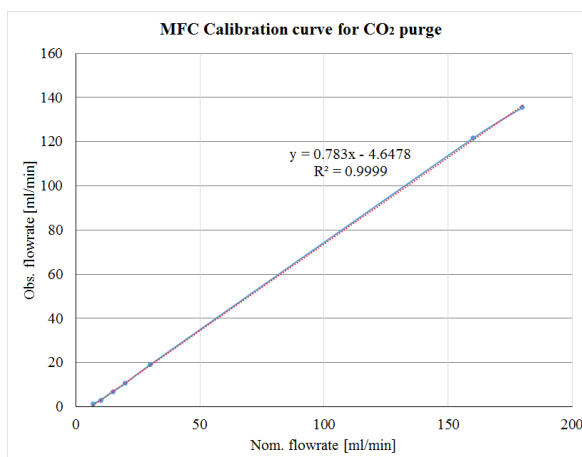
Calibration of TGA Q500 Balance gas purge MFC			
Volume [ml]	1	9	90
Nominal flow rate [ml/min]	**10**	**50**	**90**
Time [s]	4.34	8.31	44.19
	4.59	8.31	44.18
	4.66	8.28	44.5
	4.47	8.29	44.62
	4.57	8.31	44.72
			44.88
Avg. Time [s]	4.526	8.3	44.515
Observed flowrate [ml/min]	13.2567	65.0602	121.307

MFC Calibration curve for N2 purge

$y = 1.3506x - 0.9902$
$R^2 = 0.9994$

Obs. flowrate [ml/min] vs Nom. flowrate [ml/min]
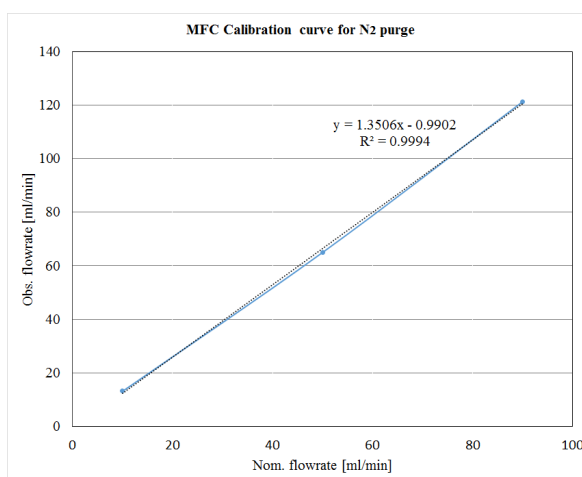
C.1.2 Weight Calibration

The weight calibration of the TGA Q500 instrument was performed using a standard method based on the decomposition of Calcium Oxalate Monohydrate. In this technique, Calcium Oxalate Mono-hydrate (20 g) which is used as a tutorial sample was decomposed in a stream of Nitrogen gas at a

heating rate of 5°C/min from ambient to 900°C.

1. $CaC_2O_4 \cdot H_2O \longrightarrow CaC_2O_4 + H_2O$ (C.1.1)

2. $CaC_2O_4 \longrightarrow CaCO_3 + CO$ (C.1.2)

3. $CaCO_3 \longrightarrow CaO + CO_2$ (C.1.3)

         (C.1.4)
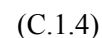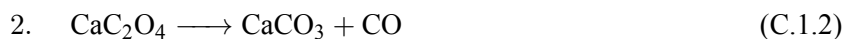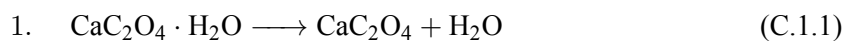
The material decomposes in three consecutive reactions given above. The weight loss during the heating up of the material from ambient to 900°C is shown in the graph below.
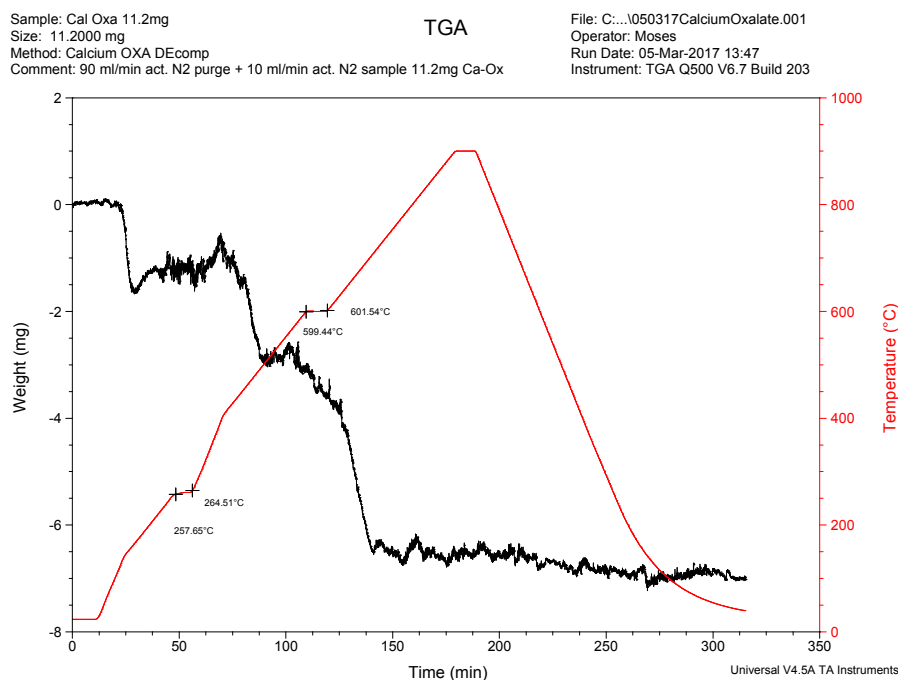
Figure C.1.1: *CaC$_2$O$_4$ decomposition curve for TGA weight calibration*

The TGA curve above shows the three weight loss steps of $CaC_2O_4 \cdot H_2O$ to be in agreement with the the three-step reaction scheme given above.

The loss of water of crystallization yielded a weight loss   =   1.5 g
First decomposition yielded a weight loss of   =   1.0 g
Second decomposition yielded a weight loss of   =   5.5 g

This was found to be in good agreement with the theoretical stoichiometric values based on the factoid that 1 mole of $CaC_2O_4 \cdot H_2O$ gives rise to 1 mole each of H_2O and CO.

Appendix D

XRF Raw Data

D.1   XRF

The supporting information obtained from the XRF analysis are given below in the following appendix.

SQX Calculation Result

Sample : Undoped dolomite
Application : F-U_Solid_S_209
Binder : H3BO3

Sample type : Oxide Powder
Ratio : 27.7872
Sample film corr. : P.P.Film
File : 201703111948

Date analyzed : 2017- 3-11 19:48
Balance :
Matching library :
Impurity corr. :

No.	Component	Result	Unit	Det. limit	El. line	Intensity	w/o normal
1	CaO	70.6	mass%	0.09612	Ca-KA	9.2227	32.6434
2	MgO	26.0	mass%	0.89586	Mg-KA	0.0754	12.0092
3	K2O	1.71	mass%	0.11125	K -KA	0.1607	0.7899
4	SiO2	1.25	mass%	0.11409	Si-KA	0.0261	0.5776
5	Al2O3	0.473	mass%	0.12271	Al-KA	0.0095	0.2188

Rigaku

SQX Calculation Result

Sample : 0.5%Aldolomite
Application : F-U_Solid_S_203
Binder : H3BO3

Sample type : Oxide Powder
Ratio : 24.9319
Sample film corr. : P.P.Film
File : 201703112018

Date analyzed : 2017- 3-11 20:18
Balance :
Matching library :
Impurity corr. :

No.	Component	Result	Unit	Det. limit	El. line	Intensity	w/o normal
1	CaO	65.1	mass%	0.09092	Ca-KA	9.0863	29.1608
2	MgO	28.8	mass%	0.81662	Mg-KA	0.0900	12.9122
3	Al2O3	2.64	mass%	0.16293	Al-KA	0.0569	1.1829
4	SiO2	2.00	mass%	0.13969	Si-KA	0.0447	0.8958
5	K2O	1.38	mass%	0.10146	K -KA	0.1390	0.6195

Rigaku

2017- 3-13 09:53

SQX Calculation Result

Sample : 1%Aldolomite
Application : F-U_Solid_S_204
Binder : H3BO3

Sample type : Oxide Powder
Ratio : 28.3932
Sample film corr. : P.P.Film
File : 201703112048

Date analyzed : 2017- 3-11 20:48
Balance :
Matching library :
Impurity corr. :

No.	Component	Result	Unit	Det. limit	El. line	Intensity	w/o normal
1	CaO	63.2	mass%	0.09279	Ca-KA	8.0255	28.9646
2	MgO	29.1	mass%	1.02334	Mg-KA	0.0822	13.3604
3	Al2O3	4.07	mass%	0.19728	Al-KA	0.0794	1.8669
4	SiO2	1.90	mass%	0.14275	Si-KA	0.0385	0.8725
5	K2O	1.72	mass%	0.11377	K -KA	0.1566	0.7882

Rigaku

2017- 3-13 09:54

SQX Calculation Result

Sample : 2%Aldolomite
Application : F-U_Solid_S_205
Binder : H3BO3

Sample type : Oxide Powder
Ratio : 27.6075
Sample film corr. : P.P.Film
File : 201703112119

Date analyzed : 2017- 3-11 21:19
Balance :
Matching library :
Impurity corr. :

No.	Component	Result	Unit	Det. limit	El. line	Intensity	w/o normal
1	CaO	68.0	mass%	0.09553	Ca-KA	11.2041	39.3979
2	MgO	24.2	mass%	0.87685	Mg-KA	0.0884	13.9967
3	SiO2	4.42	mass%	0.15622	Si-KA	0.1164	2.5625
4	Al2O3	2.18	mass%	0.19662	Al-KA	0.0554	1.2652
5	K2O	1.23	mass%	0.11135	K -KA	0.1462	0.7153

Rigaku

2017- 3-13 09:55

SQX Calculation Result

Sample : 0.5%spdolomite
Application : F-U_Solid_S_206
Binder : H3BO3

Sample type : Oxide Powder
Ratio : 24.7731
Sample film corr. : P.P.Film
File : 201703112149

Date analyzed : 2017- 3-11 21:49
Balance :
Matching library :
Impurity corr. :

No.	Component	Result	Unit	Det. limit	El. line	Intensity	w/o normal
1	CaO	66.3	mass%	0.08259	Ca-KA	8.4729	27.0606
2	MgO	28.1	mass%	0.82350	Mg-KA	0.0804	11.4686
3	SiO2	2.18	mass%	0.10890	Si-KA	0.0448	0.8915
4	Al2O3	1.77	mass%	0.17429	Al-KA	0.0349	0.7214
5	K2O	1.67	mass%	0.09999	K -KA	0.1536	0.6800

Rigaku

```
                              SQX Calculation Result

Sample : 1%spdolomite                              Date analyzed : 2017- 3-11 22:20
Application : F-U_Solid_S_207    Sample type : Oxide Powder    Balance :
Binder : H3BO3                   Ratio : 28.1001               Matching library :
                                Sample film corr. : P.P.Film   Impurity corr. :
                                File : 201703112220

No.    Component    Result    Unit      Det. limit    El. line    Intensity    w/o normal
 1     CaO          61.7      mass%     0.09221       Ca-KA       7.8872       28.1918
 2     MgO          31.2      mass%     0.98310       Mg-KA       0.0886       14.2517
 3     Al2O3        4.19      mass%     0.16780       Al-KA       0.0821        1.9140
 4     K2O          1.67      mass%     0.11053       K -KA       0.1525        0.7605
 5     SiO2         1.20      mass%     0.14162       Si-KA       0.0243        0.5471
```

Rigaku

2017- 3-13 09:58

```
                              SQX Calculation Result

Sample : 2%spdolomite                              Date analyzed : 2017- 3-11 22:50
Application : F-U_Solid_S_208    Sample type : Oxide Powder    Balance :
Binder : H3BO3                   Ratio : 26.4656               Matching library :
                                Sample film corr. : P.P.Film   Impurity corr. :
                                File : 201703112250

No.    Component    Result    Unit      Det. limit    El. line    Intensity    w/o normal
 1     CaO          60.8      mass%     0.09189       Ca-KA       7.2129       24.4402
 2     MgO          29.1      mass%     0.77811       Mg-KA       0.0769       11.6840
 3     Al2O3        7.61      mass%     0.16914       Al-KA       0.1392        3.0606
 4     K2O          1.78      mass%     0.10838       K -KA       0.1520        0.7172
 5     SiO2         0.789     mass%     0.13713       Si-KA       0.0149        0.3173
```
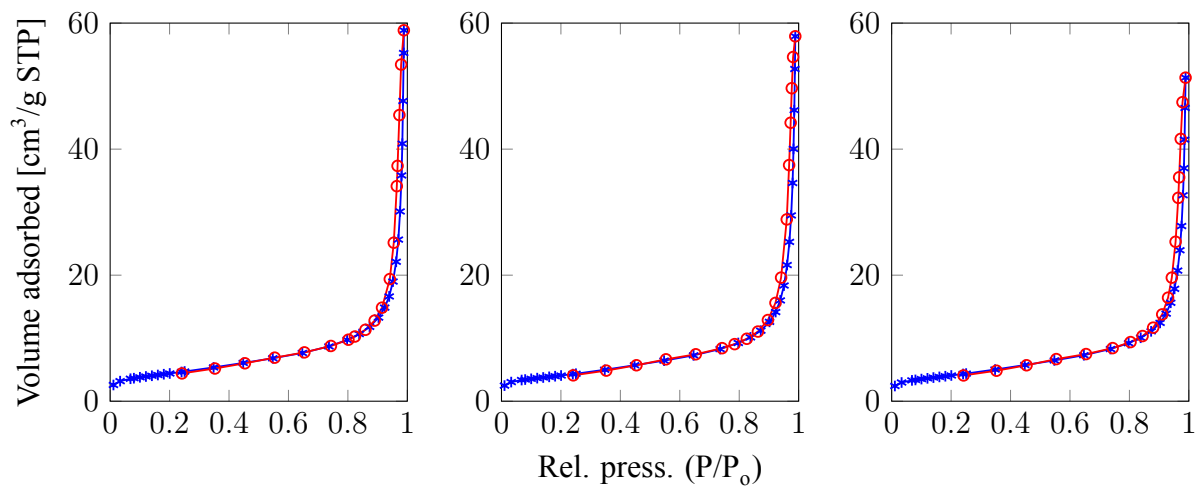
Rigaku

Appendix E

N₂ physisorption of doped samples

Figure E.0.1: *X-Ray Diffractograms of for samples calcined at 900°C. (L-R): 0.5% Al dol, 1% Al dol, 2% Al dol.*
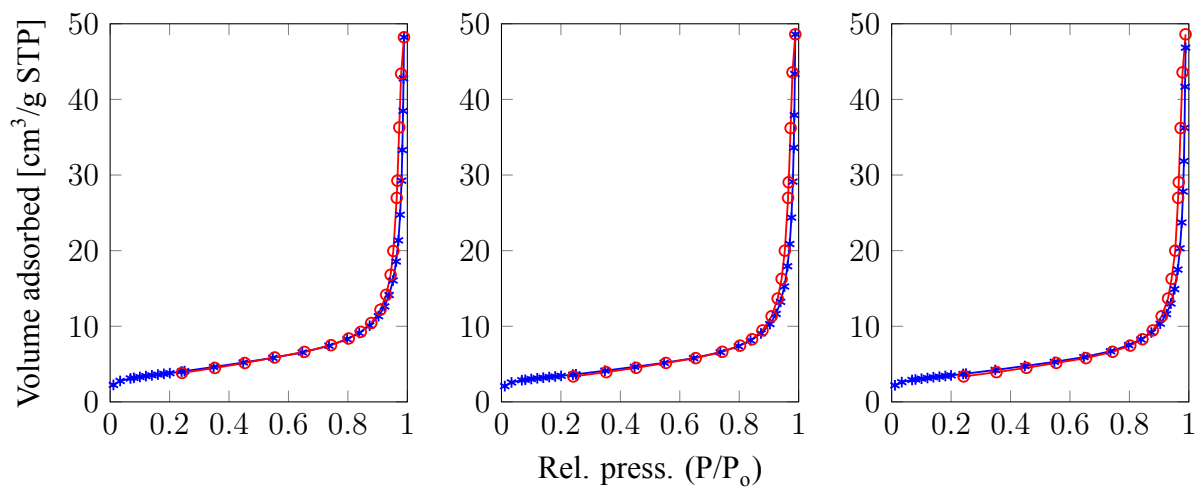

Figure E.0.2: *X-Ray Diffractograms of for samples calcined at 900°C. (L-R) bottom: 0.25% Al-0.25% Mg dol, 0.5% Al-0.5% Mg dol, 1% Al-1% Mg dol.*
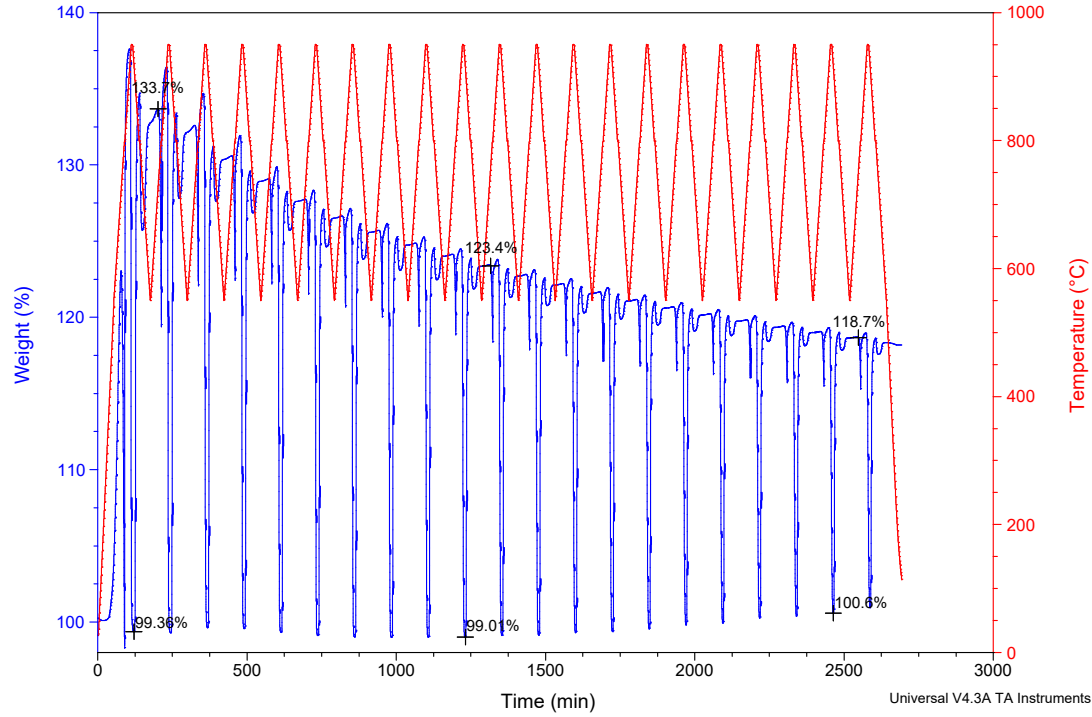
Appendix F

Raw data plots from the TGA Q500

Left panel:

Sample: 0904_pt5perAldol1000_3h_20cycle
Size: 19.7000 mg
Method: 20cycle operation baseline
Comment: 1000C 3hr 0.5%Al Calc.Doped Dolomite. Weight 19.7mg
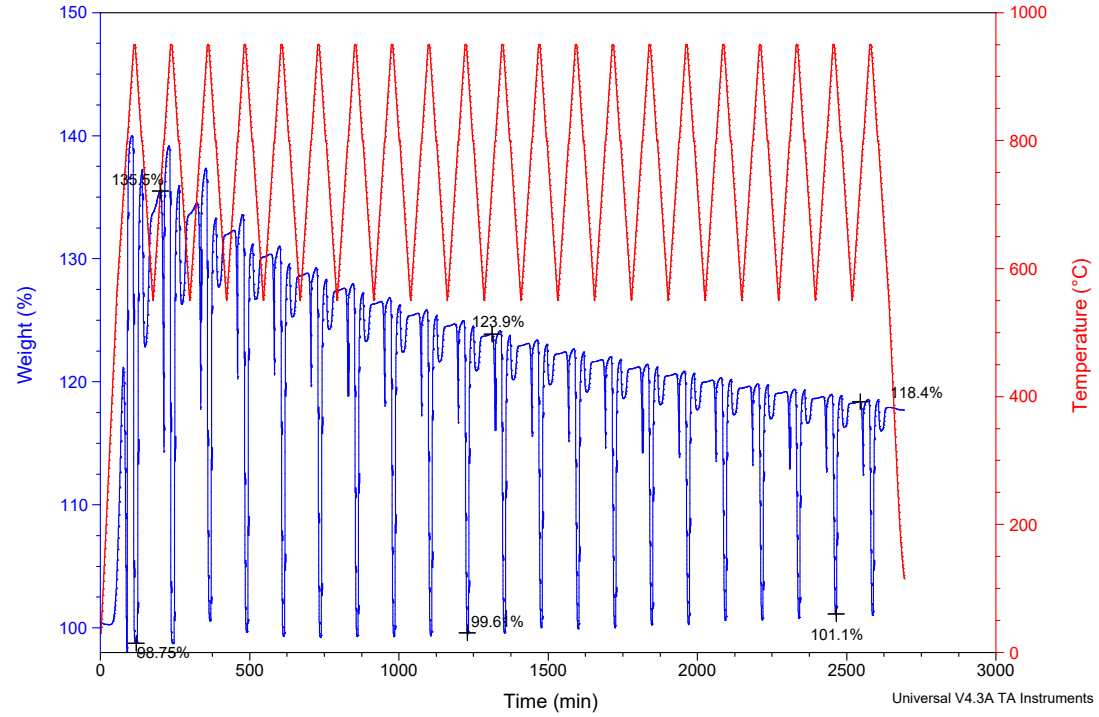
TGA

File: TempSCAN550sorp_950_desorp_10perCO2_2..
Operator: Moses
Run Date: 09-Apr-2017 12:44
Instrument: TGA Q500 V6.7 Build 203

133.7%
123.4%
118.7%
100.6%
99.36%
99.01%

Weight (%)
Temperature (°C)
Time (min)

Universal V4.3A TA Instruments

Right panel:

Sample: 0704_pt5perSpdol1000_3h_20cycle
Size: 19.9000 mg
Method: 20cycle operation baseline
Comment: 1000C 3hr 0.5%Sp Calc.Doped Dolomite. Weight 19.9mg
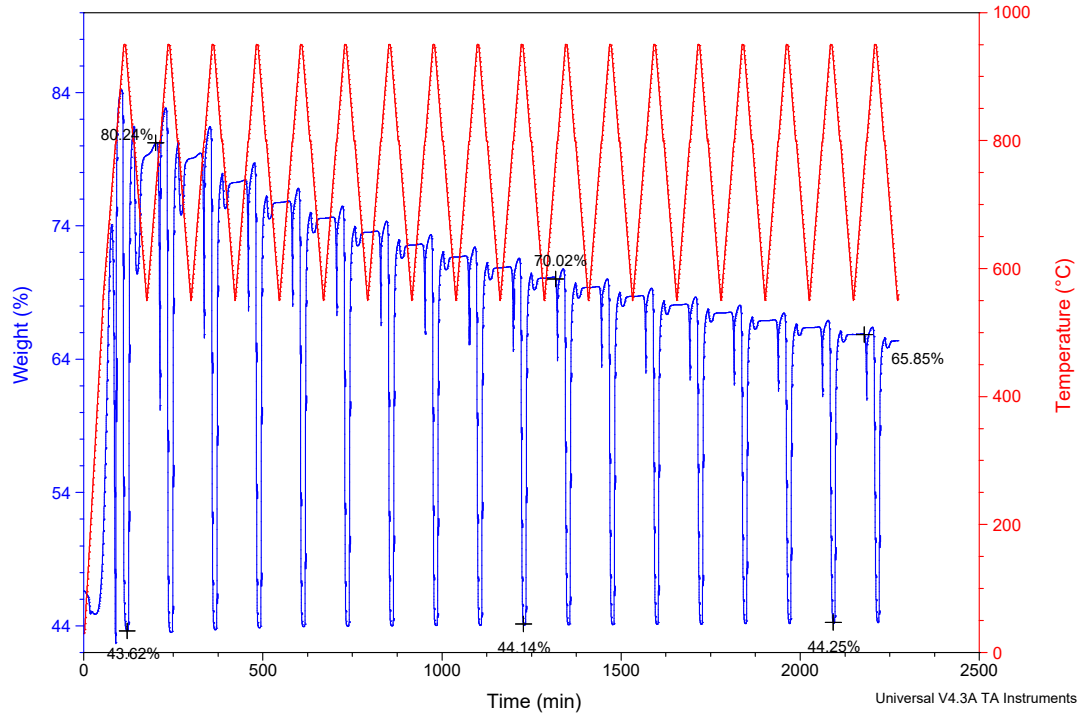
TGA

File: TempSCAN550sorp_950_desorp_10perCO2_2..
Operator: Moses
Run Date: 07-Apr-2017 11:18
Instrument: TGA Q500 V6.7 Build 203

135.5%
123.9%
118.4%
101.1%
99.6%%
98.75%

Weight (%)
Temperature (°C)
Time (min)

Universal V4.3A TA Instruments

Left panel:
Sample: 3103_dol1000_3h_20cycles
Size: 15.0000 mg
Method: 20cycle operation baseline
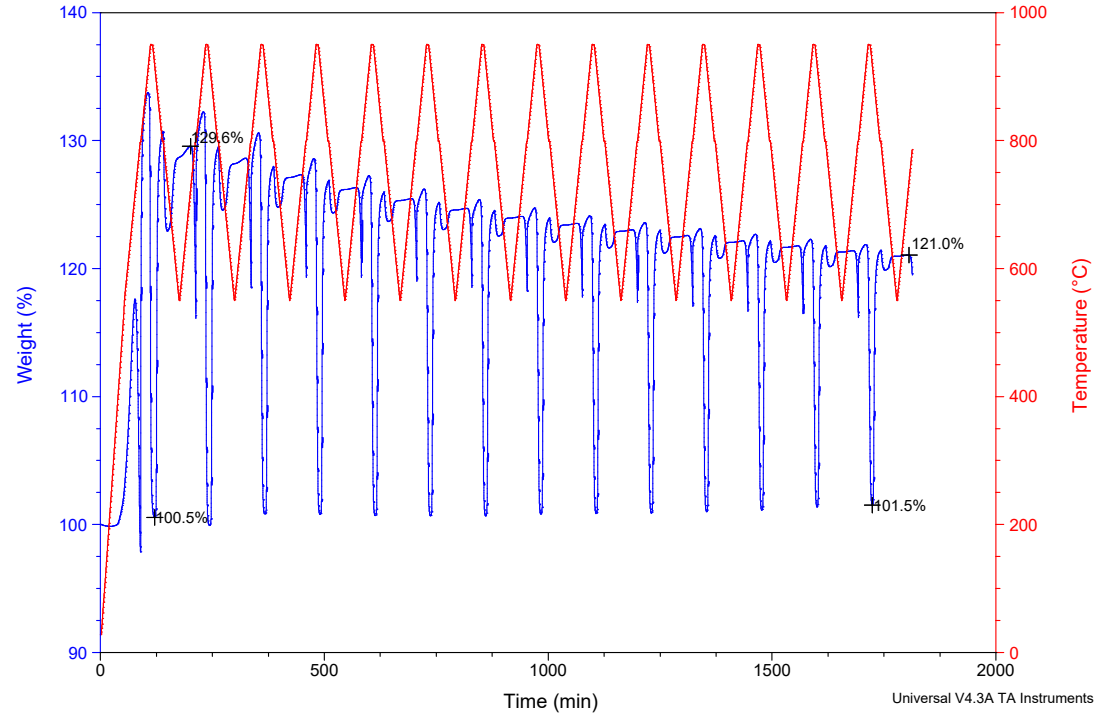Comment: 1000C 3hr 1% Al Calc.Doped Dolomite. Weight c.a 10 mg

TGA

File: Temp SCAN 550sorp_950_desorp_10perCO2...
Operator: Moses
Run Date: 31-Mar-2017 11:59
Instrument: TGA Q500 V6.7 Build 203

Right panel:
Sample: 1504_2%Aldol1000_3h_20cycle
Size: 18.6810 mg
Method: 20cycle operation baseline
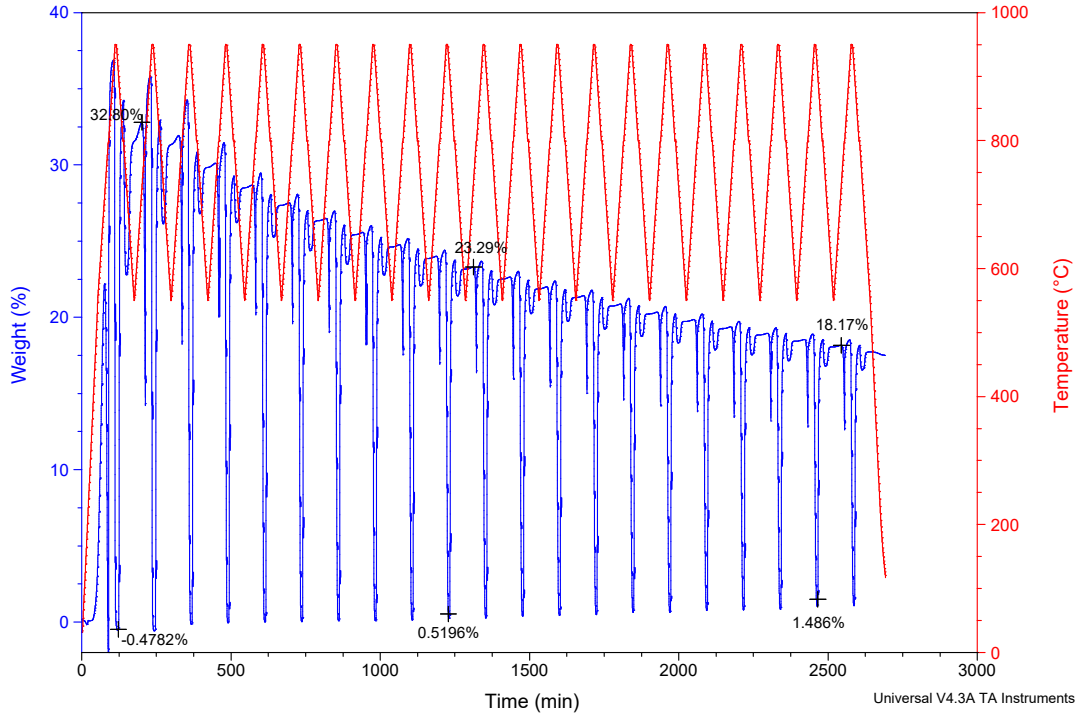Comment: 1000C 3hr 2%Al Calc.Doped Dolomite. Weight 18.6mg

TGA

File: TempSCAN550sorp_950_desorp_10perCO2_2.
Operator: Moses
Run Date: 15-Apr-2017 15:41
Instrument: TGA Q500 V6.7 Build 203

Universal V4.3A TA Instruments

Left panel:

TGA

Sample: 0204_1perSpdol1000_3h_20cycles
Size: 18.1000 mg
Method: 20cycle operation baseline
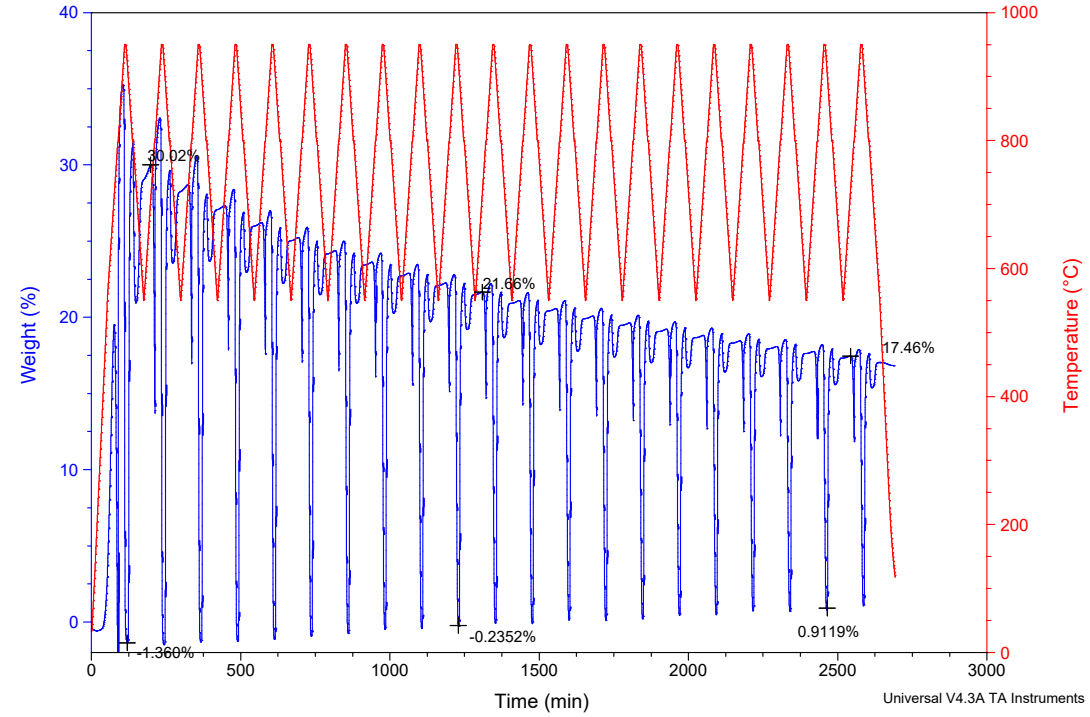Comment: 1000C 3hr 1% Sp Calc.Doped Dolomite. Weight 18.1mg

File: Temp SCAN 550sorp_950_desorp_10perCO2...
Operator: Moses
Run Date: 02-Apr-2017 20:00
Instrument: TGA Q500 V6.7 Build 203

32.80%

23.29%

18.17%

-0.4782%

0.5196%

1.486%

Universal V4.3A TA Instruments

Right panel:

TGA

Sample: 0504_2perSpdol1000_3h_20cycle
Size: 19.8000 mg
Method: 20cycle operation baseline
Comment: 1000C 3hr 2%Sp Calc.Doped Dolomite. Weight 19.8mg

File: TempSCAN550sorp_950_desorp_10perCO2_2.
Operator: Moses
Run Date: 05-Apr-2017 11:16
Instrument: TGA Q500 V6.7 Build 203

30.02%

21.66%

17.46%

-1.360%

-0.2352%

0.9119%

Universal V4.3A TA Instruments

Left panel:

Sample: 1704_2%Aldol1000_3h_20cycle
Size: 19.7000 mg
Method: 20cycle operation baseline
Comment: 1000C 3hr 2%Al Calc.Doped Dolomite. Weight 19.7 mg

TGA

File: TempSCAN550sorp_950_desorp_10perCO2_2...
Operator: Moses
Run Date: 17-Apr-2017 17:03
Instrument: TGA Q500 V6.7 Build 203

Weight (%) / Temperature (°C) vs Time (min)

Annotations: 130.7%, 123.7%, 120.4%, 100.8%, 101.4%, 103.2%

Universal V4.3A TA Instruments

Right panel:

Sample: 2404_2%ZrDol1000_3h_20cycle
Size: 19.8000 mg
Method: 20cycle operation baseline
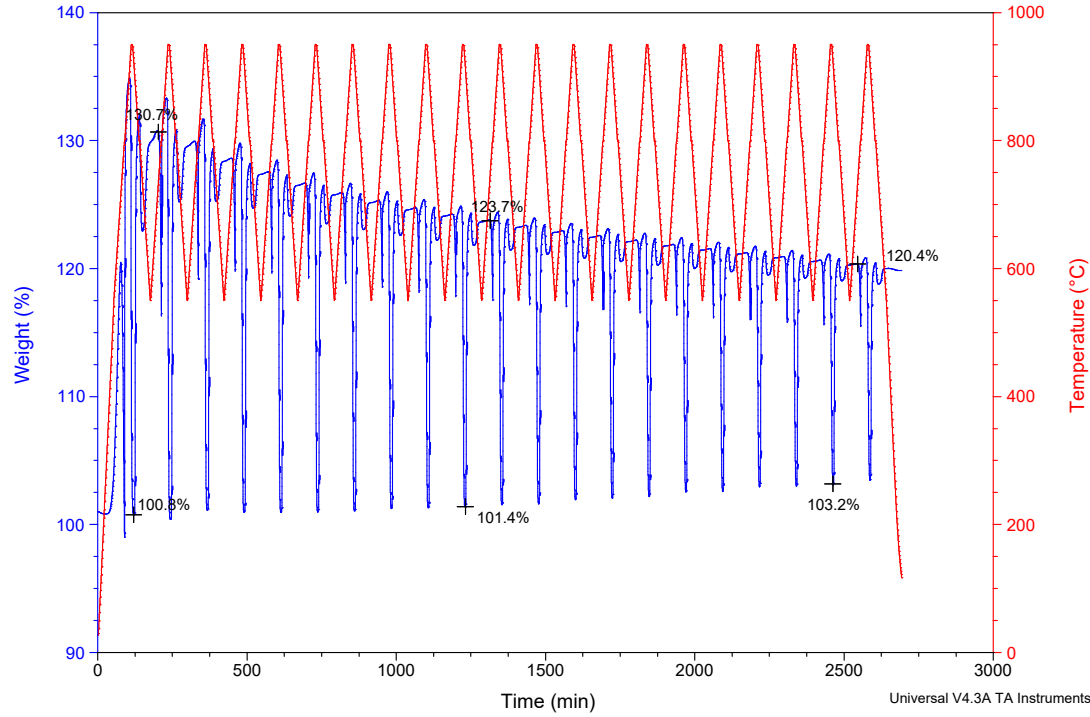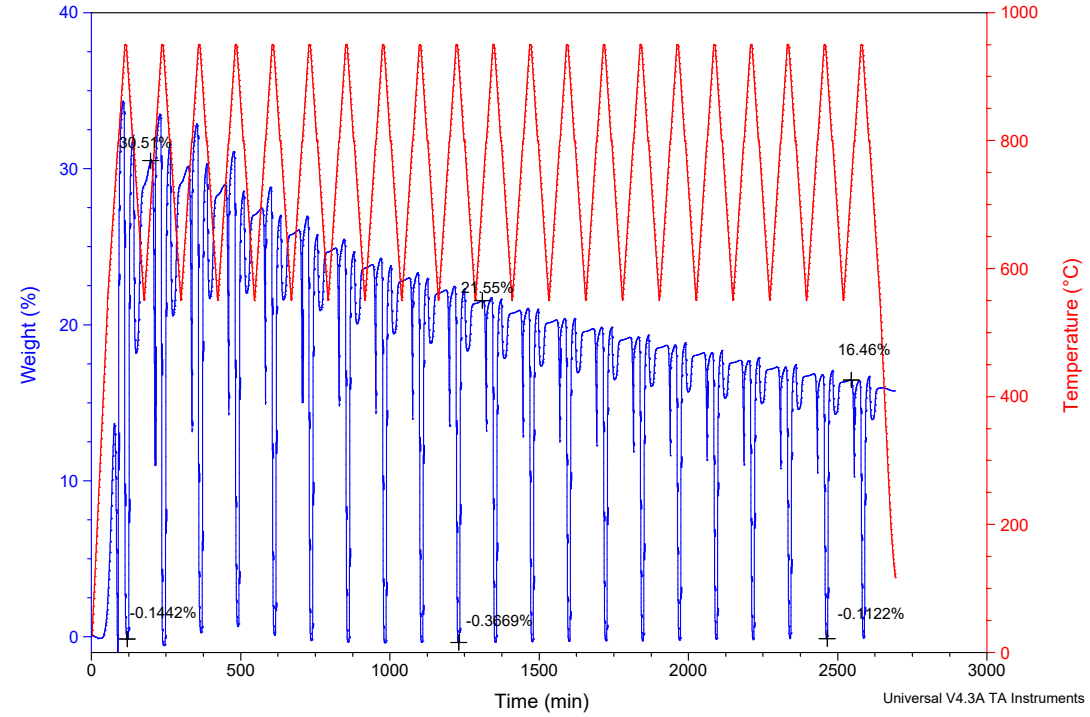Comment: 1000C 3hr 2%Zr Calc.Doped Dolomite. Weight 19.8 mg

TGA

File: TempSCAN550sorp_950_desorp_10perCO2_2...
Operator: Moses
Run Date: 24-Apr-2017 10:57
Instrument: TGA Q500 V6.7 Build 203

Weight (%) / Temperature (°C) vs Time (min)

Annotations: 30.51%, 21.55%, 16.46%, -0.1442%, -0.3669%, -0.1122%

Universal V4.3A TA Instruments

Left panel:

Sample: 1005_3MgDol1000_3h_50cycle
Size: 19.8000 mg
Method: 50cycle operation baseline
Comment: 1000C 3hr 3%Mg Dolomite. Weight 19.8 mg

TGA

File: TempSCAN550sorp_950_desorp_10perCO2_2..
Operator: Moses
Run Date: 10-May-2017 09:57
Instrument: TGA Q500 V6.7 Build 203

Right panel:

Sample: 2104_CaAluminDol1000_3h_20cycle
Size: 19.8000 mg
Method: 20cycle operation baseline
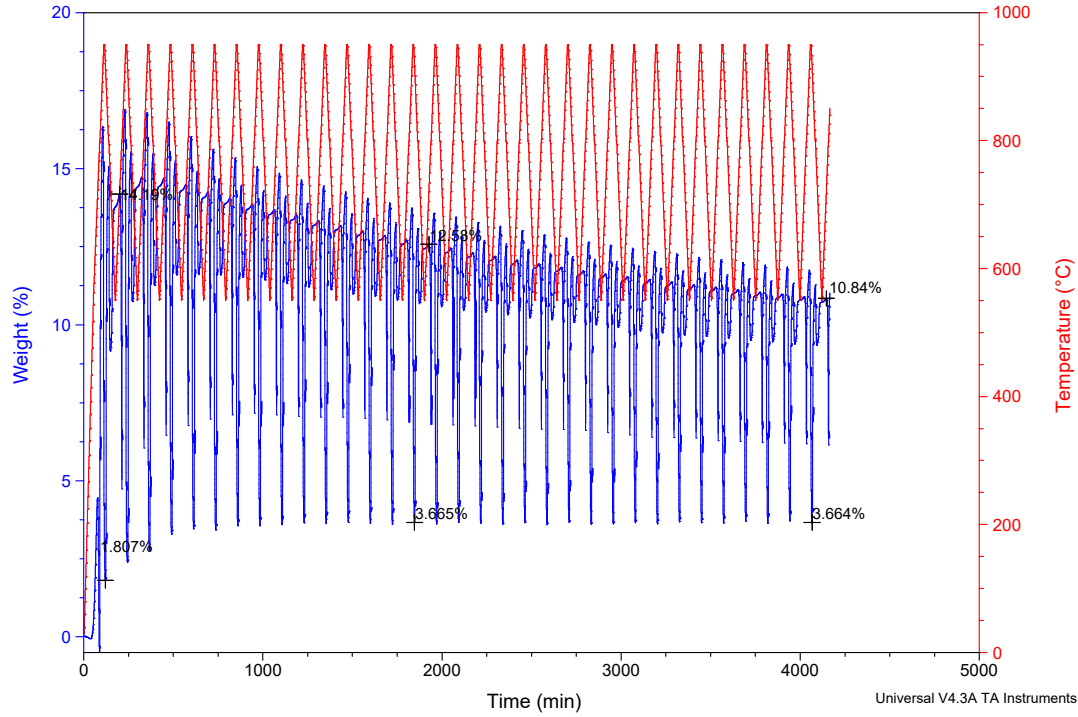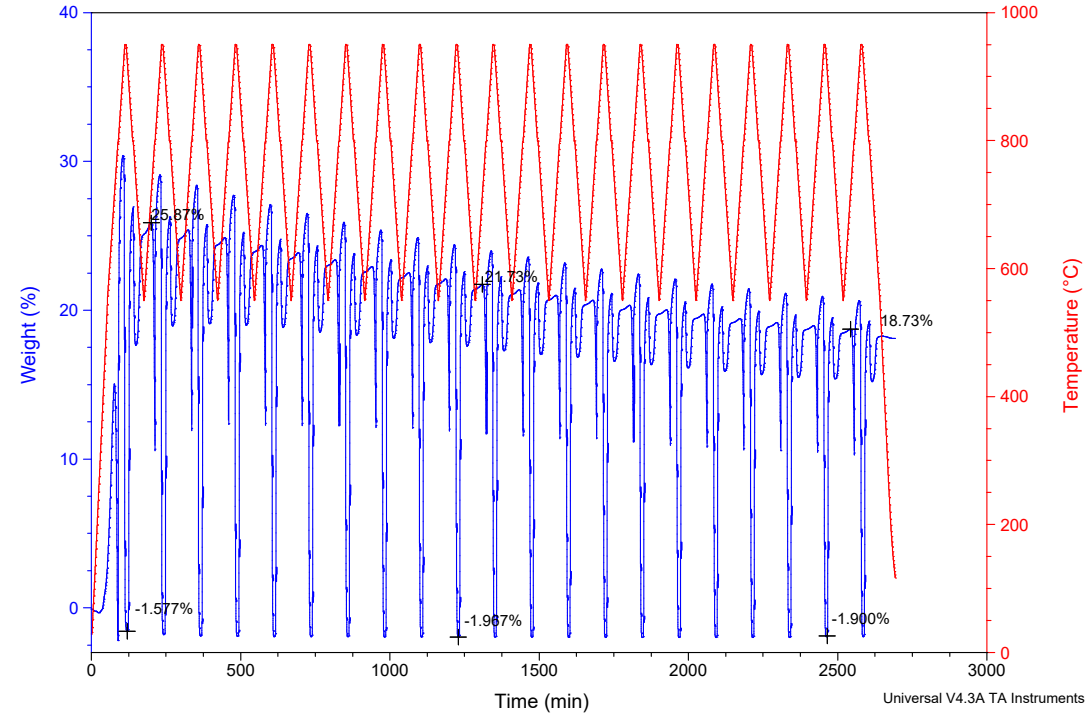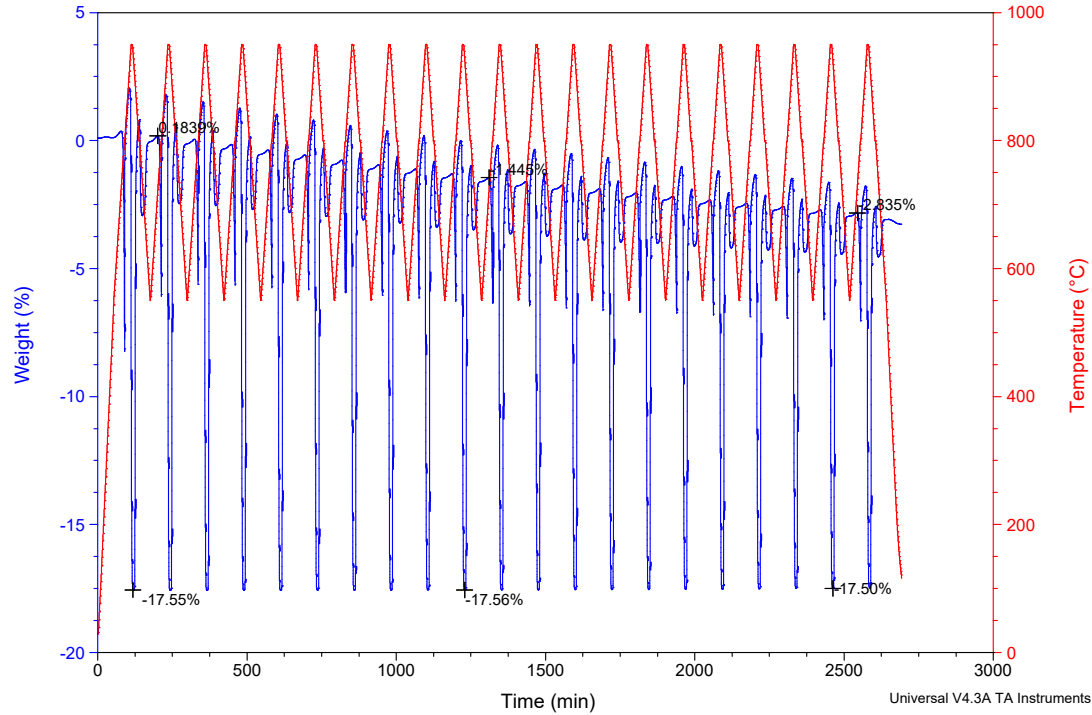Comment: 1000C 3hr 2%Al Calc.Doped Dolomite. Weight 19.8 mg

TGA

File: TempSCAN550sorp_950_desorp_10perCO2_2..
Operator: Moses
Run Date: 21-Apr-2017 17:27
Instrument: TGA Q500 V6.7 Build 203

Universal V4.3A TA Instruments

TGA

Sample: 2604_Ca-AlDol1000_3h_20cycle
Size: 19.2000 mg
Method: 20cycle operation baseline
Comment: 1000C 3hr Ca-AlDolomite. Weight 19.2 mg (contd)

File: TempSCAN550sorp_950_desorp_10perCO2_2..
Operator: Moses
Run Date: 26-Apr-2017 14:27
Instrument: TGA Q500 V6.7 Build 203

Sample: 1000C 3h 3%Al1%Zr Dolomite
Size: 20.0000 mg
Method: 30cycle operation baseline
Comment: 1000C 3h 3%Al1%Zr Dolomite 20.0mg after 50 cycles

File: TempSCAN550sorp_950_desorp_10perCO2_2..
Operator: Moses
Run Date: 19-May-2017 11:29
Instrument: TGA Q500 V6.7 Build 203

Universal V4.3A TA Instruments

TGA

Universal V4.3A TA Instruments

TGA

Universal V4.3A TA Instruments

Sample: 1000C 3h 4%Al2%Zr Dolomite
Size: 19.8000 mg
Method: 30cycle operation baseline
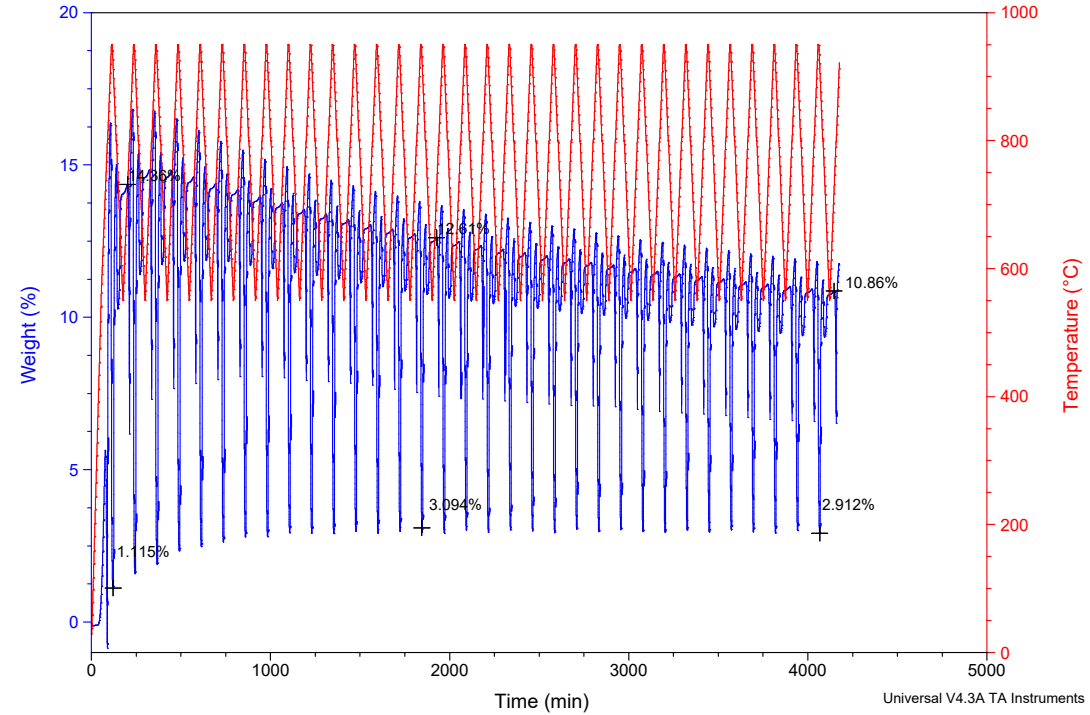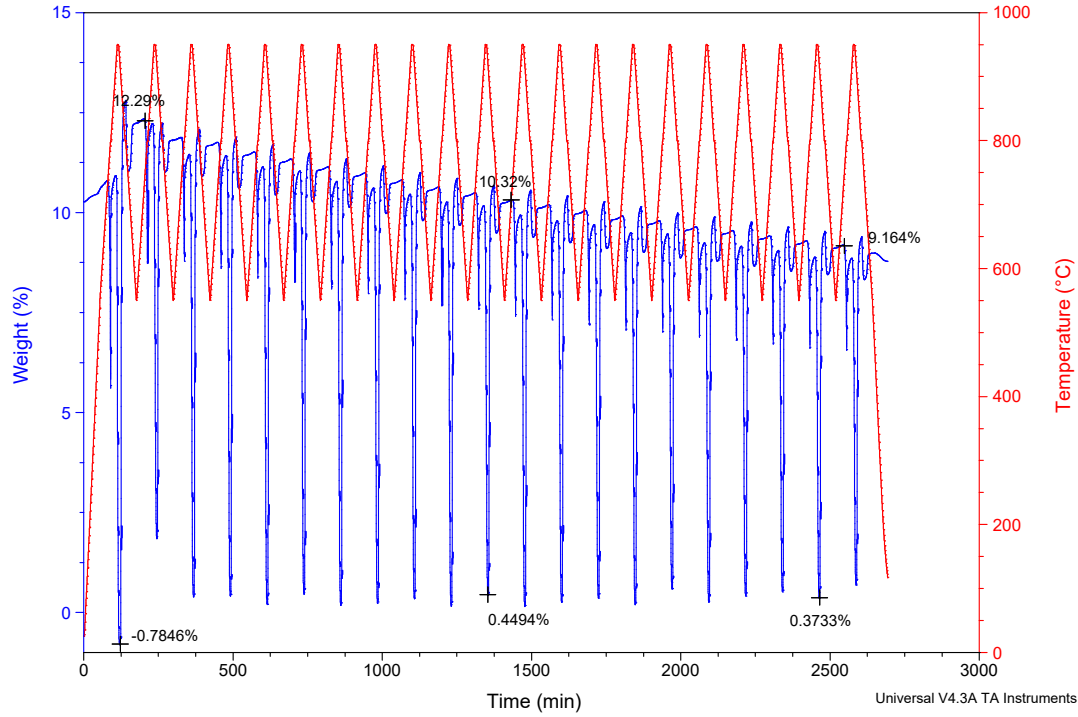Comment: 1000C 3h 4%Al2%Zr Dolomite 19.8mg after 50 cycles

TGA

File: TempSCAN550sorp_950_desorp_10perCO2_2...
Operator: Moses
Run Date: 16-May-2017 17:34
Instrument: TGA Q500 V6.7 Build 203
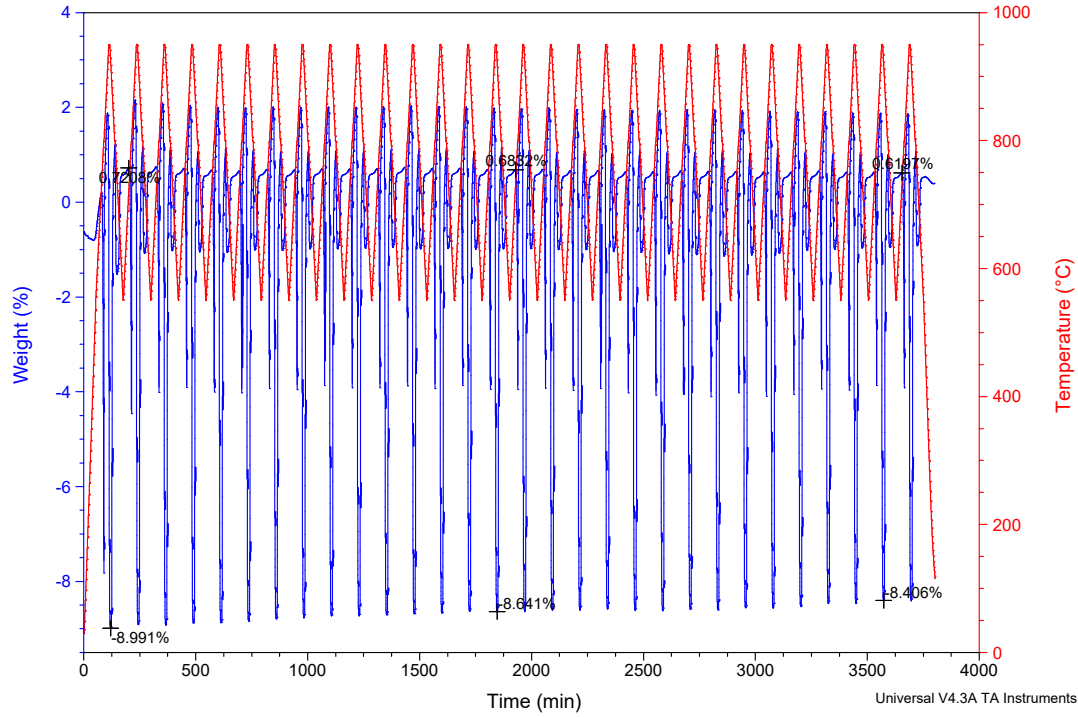
Sample: 1000C 3h 4%Al2%Zr Dolomite
Size: 16.5000 mg
Method: 30cycle operation baseline
Comment: 1000C 3h 4%Al2%Zr Dolomite 19.8mg after 50 cycles

TGA

File: take#3 - TempSCAN550sorp_950_desorp_1...
Operator: Moses
Run Date: 16-May-2017 17:34
Instrument: TGA Q500 V6.7 Build 203

Universal V4.3A TA Instruments

TGA

Sample: 1000C 3h 6%Al2%Zr Dolomite
Size: 19.9000 mg
Method: 30cycle operation baseline
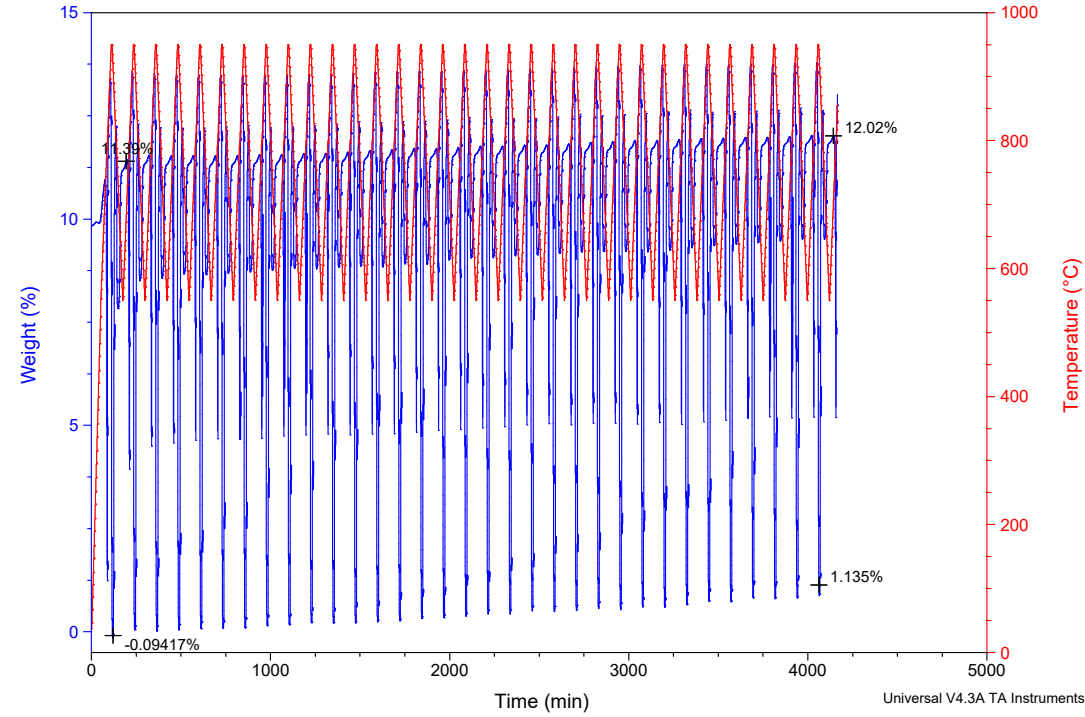Comment: 1000C 3h 6%Al2%Zr Dolomite 19.9mg after 100 cycles

File: TempSCAN550sorp_950_desorp_10perCO2_2..
Operator: Moses
Run Date: 25-May-2017 14:56
Instrument: TGA Q500 V6.7 Build 203
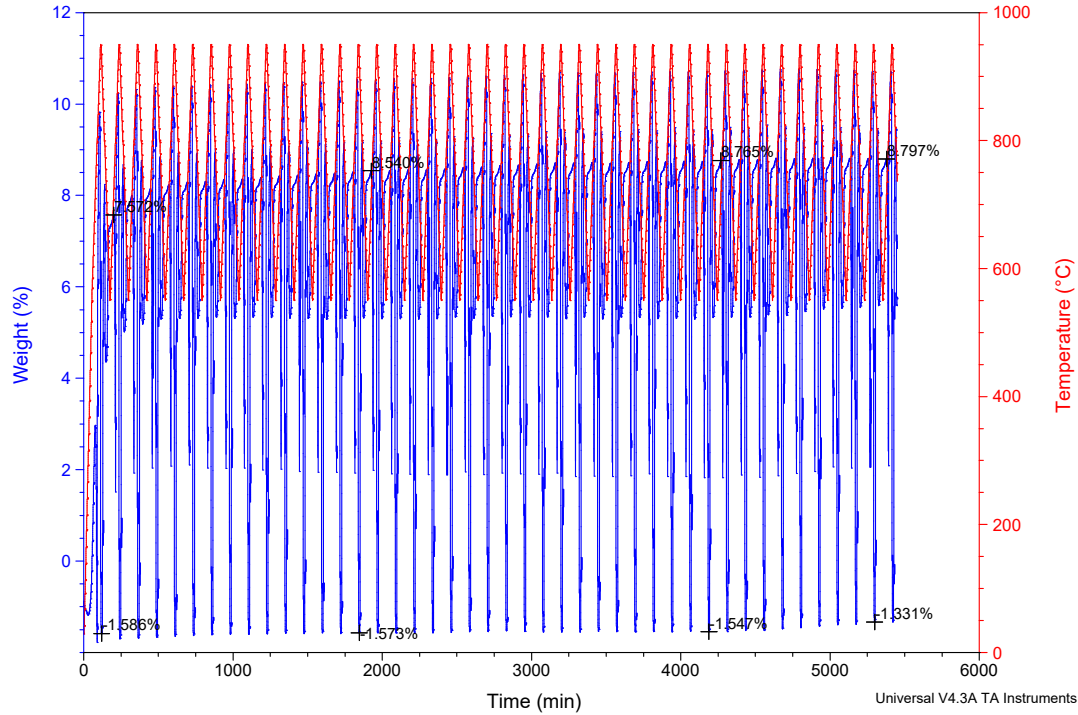
Sample: 1000C 3h 3.5Al2Zr dolomite
Size: 22.9000 mg
Method: 30cycle operation baseline
Comment: 1000C 3h 3.5Al2Zr dolomite 22.9mg

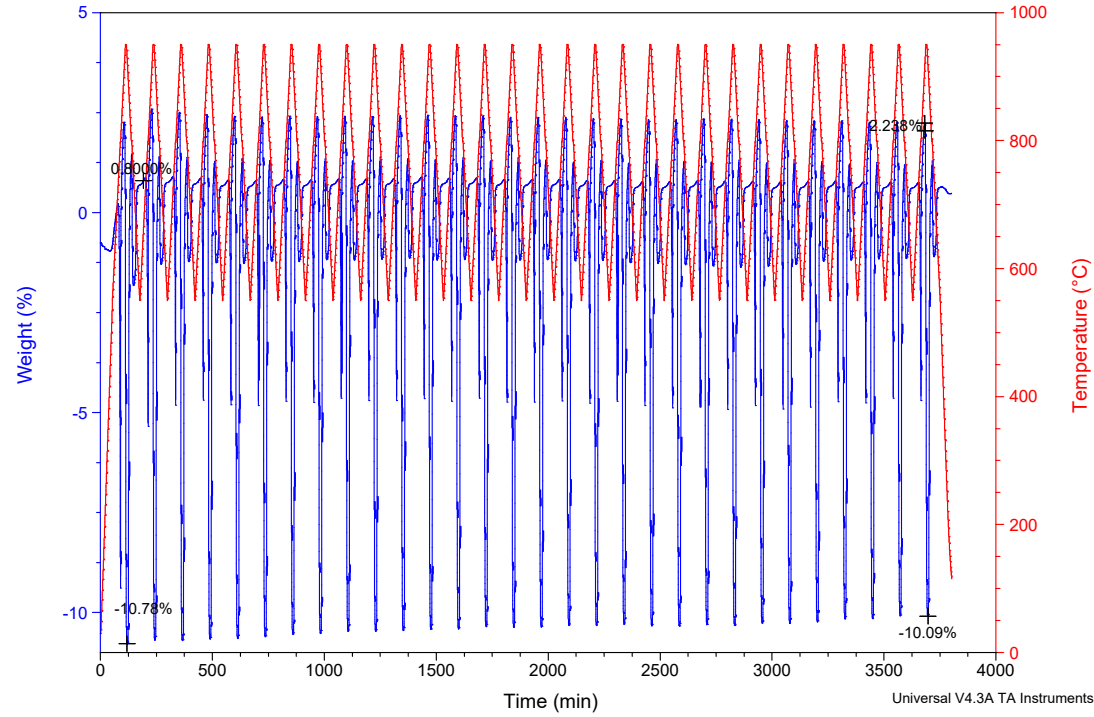File: TempSCAN550sorp_950_desorp_10perCO2_6..
Operator: Moses
Run Date: 19-Jun-2017 23:27
Instrument: TGA Q500 V6.7 Build 203

Universal V4.3A TA Instruments
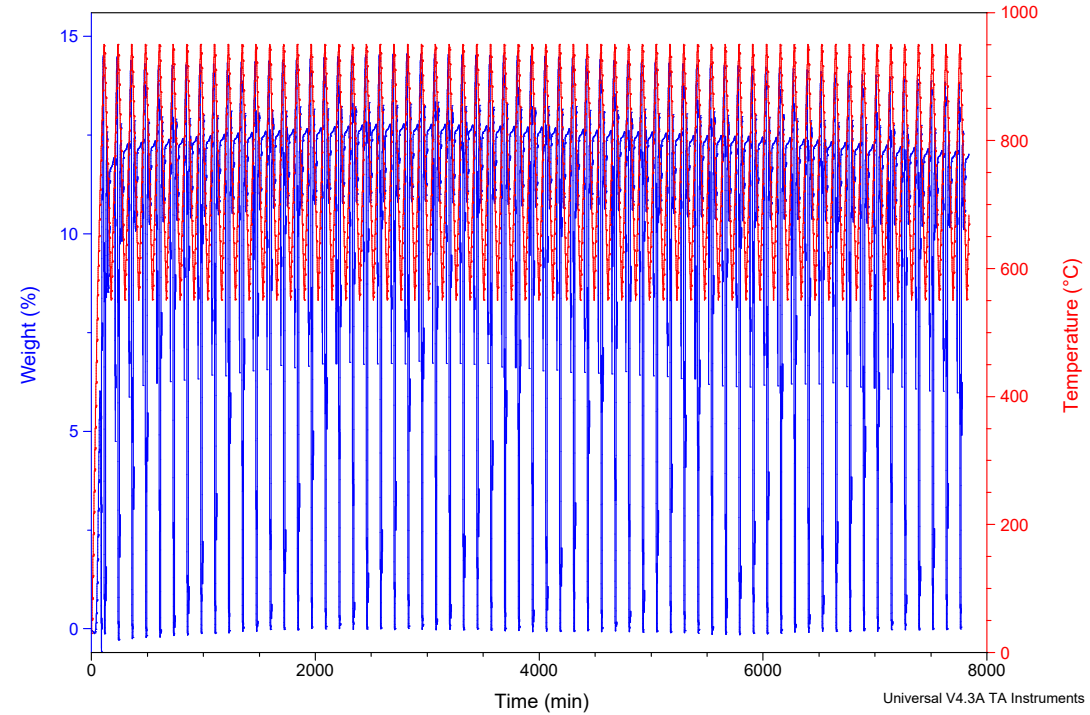
XRD Phase Identification

G.1 XRD raw diffractograms

The individual X-Ray diffraction patterns are shown here. Using PDF-4 RDB data base various peaks were identified for each sample. These identified phases are shown as legend items.

Furthermore, the miller indices (*hkl* phases) for the active CaO component were computed from the diffractogram and Bragg angle together with the information of the CaO lattice parameter, the Scherrer equation was used together with geometry relation of a cubic system.

Figure G.1.1: *X-Ray Diffractograms of for dolomite calcined at 1000 °C for 3hrs. The diffraction peaks show two predominant phases; CaO and periclase (MgO).*

Figure G.1.2: *X-Ray Diffractograms of for Calcium Aluminate (containing 3 %Al) dolomite calcined at 1000 °C for 3 hrs. The diffraction peaks show two predominant phases; CaO and periclase (MgO).*
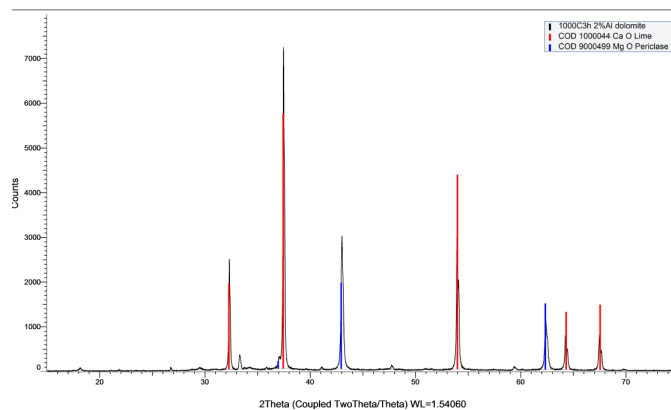
Figure G.1.3: *X-Ray Diffractograms of for 2 %Al dolomite calcined at 1000 °C for 3 hrs. The diffraction peaks show two predominant phases; CaO and periclase (MgO). The unidentified phase were found to belong to new formed phase of Mayenite as it is positioned on the same 2θposition as Mayenite found in Calcium Aluminate (equivalent to 3 %Al) dolomite sample.*
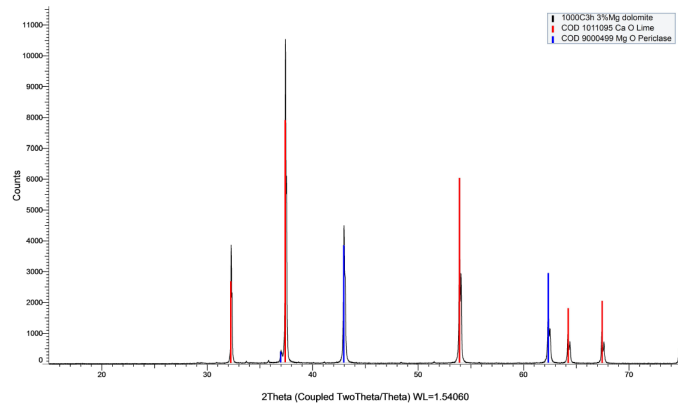
Figure G.1.4: *X-Ray Diffractograms of for 3 %Al dolomite dolomite calcined at 1000 °C for 3 hrs. The diffraction peaks show two predominant phases; CaO and periclase (MgO). No new phases are observed in the sample due to the low concentration of added Mg present in the sample.*
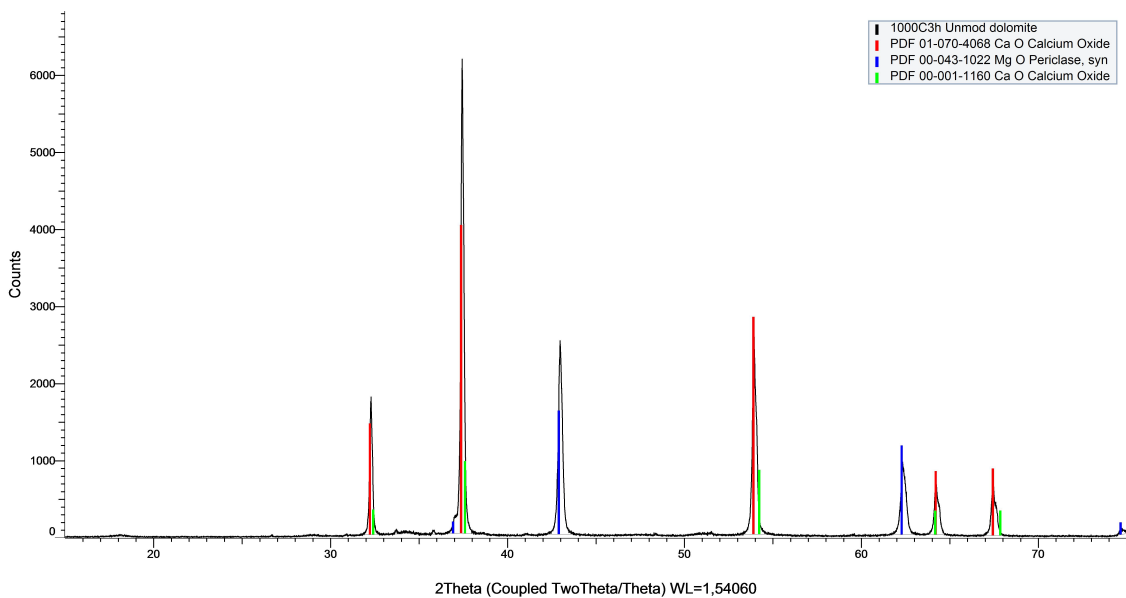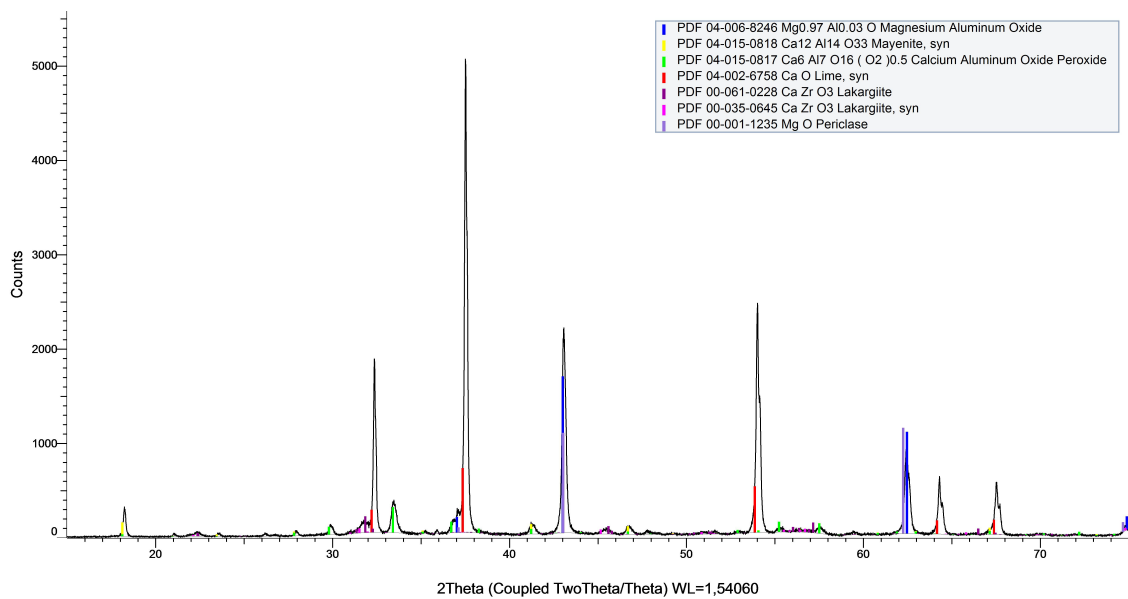

Figure G.1.5: *X-Ray Diffractograms of for 4 %Al 2% Zr dolomite calcined at 1000°C for 3 hrs. The diffraction peaks 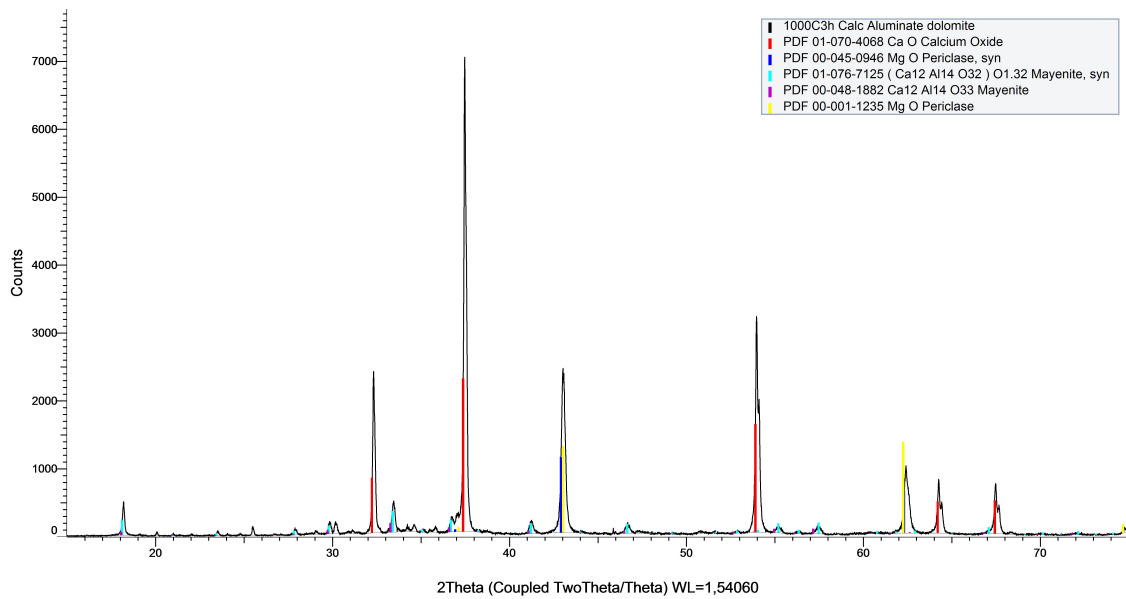show two predominant phases; CaO and periclase (MgO) with presence of new formed mixed oxide phases of Mayenite and Larkagiite.*

G.2 TOPAS Refinement parameters for Crystallite size calculation

Table G.2.1: *Standard TOPAS^{TM} Refinement Parameters (version 3)*

D8 DaVinci-1	
Parameter	Value
Peak Shape function	FP
Emission Profile	Cu Kα 5
Background	Order 3+
Instrument	
$\rightarrow$ Primary Radius	280
$\rightarrow$ Secondary Radius	280
$\rightarrow$ Point Detector	-
$\rightarrow$ Receiving Slit	-
$\rightarrow$ FDS Shape	-
$\rightarrow$ Linear PSD	Y
$\rightarrow$ LPSD angle range	3
$\rightarrow$ FDS angle	As chosen
$\rightarrow$ Full Axial Model	Y
$\rightarrow$ Source Length	12
$\rightarrow$ Sample Length	15
$\rightarrow$ RS Length	12
$\rightarrow$ Prim Soller	2.5
$\rightarrow$ N beta 2.5	
$\rightarrow$ Simple Axis Model	30
Corrections	-
$\rightarrow$ Zero Error	Off
$\rightarrow$ Sample Displ	Refine
$\rightarrow$ LP factor	"0", Fixed

HM:R-3
a=4.806Å
b=4.806Å
c=16.006Å
α=90.000°
β=90.000°
γ=120.000°
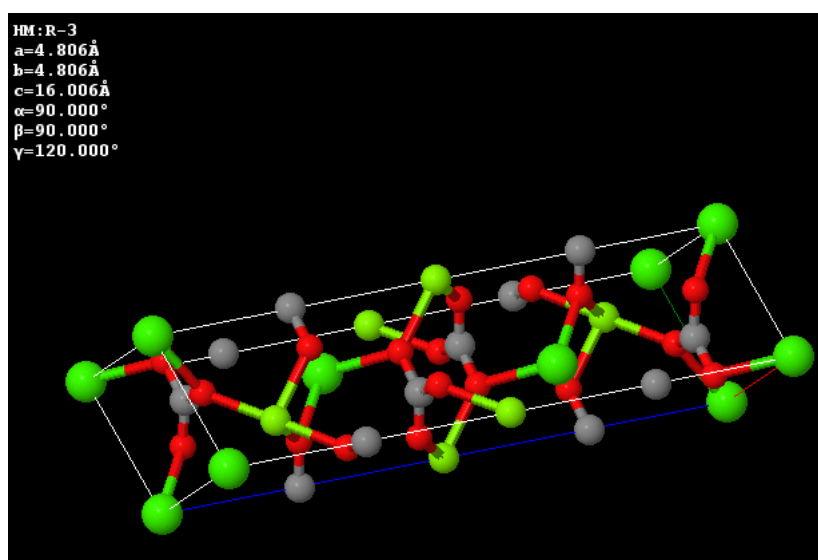
Figure G.2.1: *Unit cell structure for CaMg(CO$_3$)$_2$*

The unit cell structure of $CaMg(CO_3)_2$ as determined by the diffraction of uncalcined dolomite reveals a rhombohedral system which breaks down into a face-centered cubic systems of CaO and MgO upon sufficient calcination. The formation of new phases of Mayenite and Larkagiite are thought to occur through a subtle reaction between CaO and Al_2O_3 and ZrO_2 especially during the very first calcination step.

These new phases exhibit unit cell structures similar to those of CaO and MgO; i.e. cubic system for Mayenite $Ca_{12}O_{14}O_{33}$ and an orthorhombic sytem for Larkagiite $CaZrO_3$

(a) *CaO*   **(b)** *MgO*
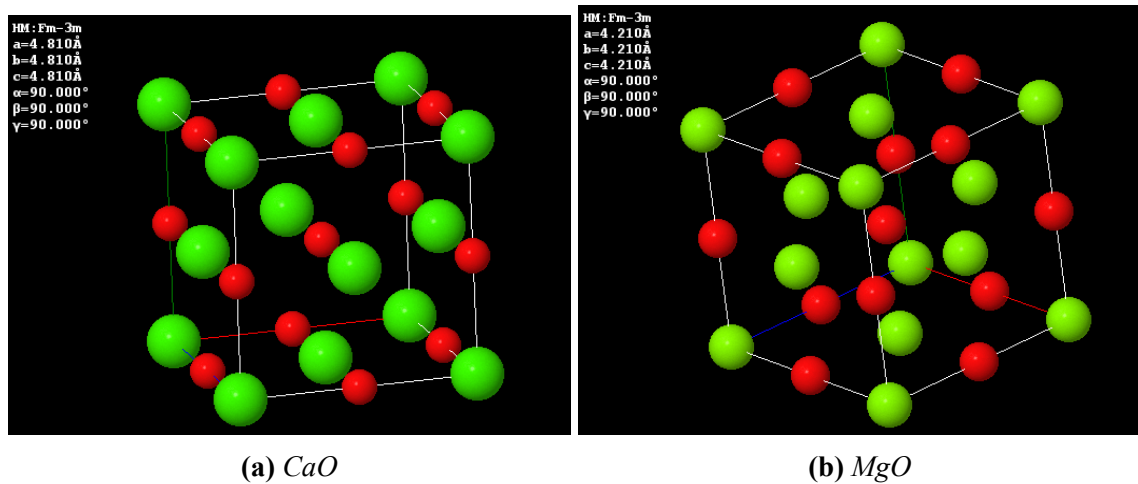
Figure G.2.2: *Unit cell structures for CaO and MgO as visualized from calcined dolomite*

(a) *Pre-testing*   **(b)** *After testing*

Figure G.2.3: *Unit cell structure for CaZrO3 and Ca12Al14O33 as visualised from doped dolomite samples*

The software generated particle size distribution report for unmilled calcined dolomite is shown below.

2017.04.21 14:12:11

HORIBA Laser Scattering Particle Size Distribution Analyzer LA-960

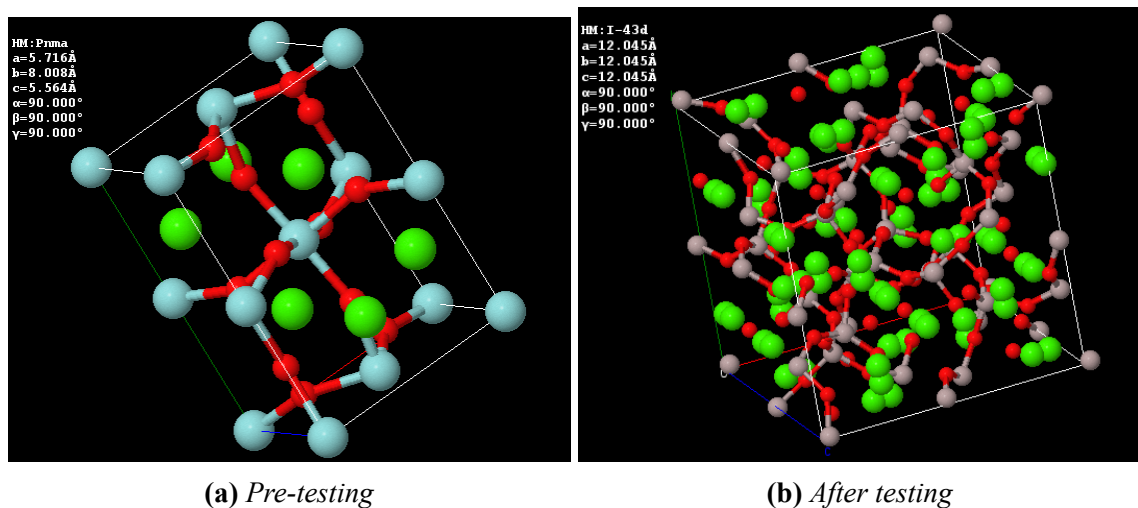|			
Batch	: Dolomite	Sample number : 001	Median size : 427.78174 (μm)
ID#	: 201704211411682	Operator : Moses	Mean size : 465.14481 (μm)
Data name	: 201704211411682	Source :	St. Dev. : 273.3889 (μm)
Transmittance (R)	: 74.2 (%)		Geo. mean size : 363.3972 (μm)
Transmittance (B)	: 69.6 (%)		Geo. St. Dev. : 2.4022 (μm)
Circulation speed	: 10		Mode size : 481.7667 (μm)
Agitation speed	: 10		Span : Off
Ultrasound	: 01:00 (7)		Diameter on cumulative % : (2)10.00 (%)- 153.4829 (μm)
Iteration mode	: Manual		
Distribution base	: Volume		
Refractive index (R)	: Dolomite		
	[Dolomite(1.680 - 0.000i),water(1.333)]		
Refractive index (B)	: Dolomite		
	[Dolomite(1.680 - 0.000i),water(1.333)]		
Material	: Dolomite		
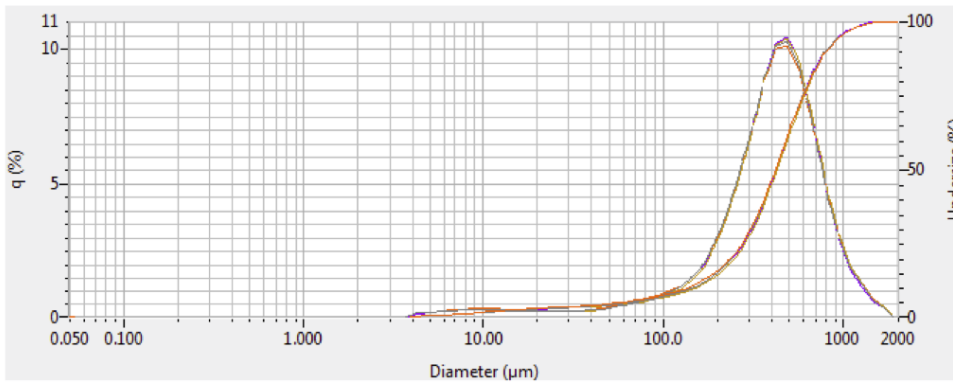
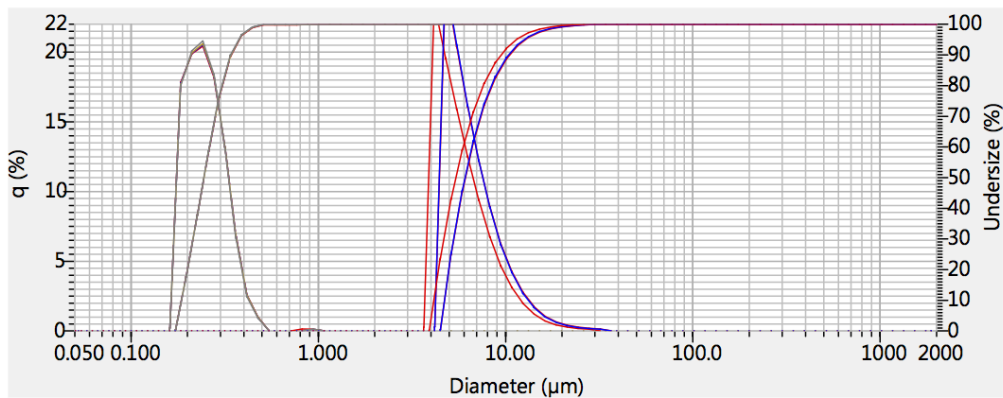| No.	Diameter (μm)	q (%)	Undersize (%)	No.	Diameter (μm)	q (%)	Undersize (%)	No.	Diameter (μm)	q (%)	Undersize (%)	No.	Diameter (μm)	q (%)	Undersize (%)
1	0.051	0.000	0.000	26	1.510	0.000	0.000	51	44.938	0.251	3.582	76	1337.481	1.228	98.939
2	0.058	0.000	0.000	27	1.729	0.000	0.000	52	51.471	0.306	3.887	77	1531.914	0.682	99.621
3	0.067	0.000	0.000	28	1.981	0.000	0.000	53	58.953	0.374	4.261	78	1754.613	0.379	100.000
4	0.076	0.000	0.000	29	2.269	0.000	0.000	54	67.523	0.456	4.717	79	2000.000	0.000	100.000
5	0.087	0.000	0.000	30	2.599	0.000	0.000	55	77.339	0.547	5.264				
6	0.100	0.000	0.000	31	2.976	0.000	0.000	56	88.583	0.647	5.911				
7	0.115	0.000	0.000	32	3.409	0.000	0.000	57	101.460	0.753	6.663				
8	0.131	0.000	0.000	33	3.905	0.000	0.000	58	116.210	0.859	7.522				
9	0.150	0.000	0.000	34	4.472	0.114	0.114	59	133.103	1.043	8.566				
10	0.172	0.000	0.000	35	5.122	0.141	0.256	60	152.453	1.345	9.911				
11	0.197	0.000	0.000	36	5.867	0.171	0.427	61	174.616	1.795	11.706				
12	0.226	0.000	0.000	37	6.720	0.201	0.627	62	200.000	2.450	14.156				
13	0.259	0.000	0.000	38	7.697	0.226	0.853	63	229.075	3.340	17.496				
14	0.296	0.000	0.000	39	8.816	0.243	1.096	64	262.376	4.453	21.949				
15	0.339	0.000	0.000	40	10.097	0.252	1.349	65	300.518	5.757	27.706				
16	0.389	0.000	0.000	41	11.565	0.253	1.602	66	344.206	7.285	34.991				
17	0.445	0.000	0.000	42	13.246	0.242	1.844	67	394.244	8.921	43.912				
18	0.510	0.000	0.000	43	15.172	0.223	2.067	68	451.556	10.122	54.033				
19	0.584	0.000	0.000	44	17.377	0.200	2.267	69	517.200	10.341	64.375				
20	0.669	0.000	0.000	45	19.904	0.180	2.447	70	592.387	9.649	74.023				
21	0.766	0.000	0.000	46	22.797	0.166	2.613	71	678.504	8.185	82.209				
22	0.877	0.000	0.000	47	26.111	0.161	2.775	72	777.141	6.258	88.467				
23	1.005	0.000	0.000	48	29.907	0.166	2.941	73	890.116	4.426	92.892				
24	1.151	0.000	0.000	49	34.255	0.181	3.122	74	1019.515	2.932	95.824				
25	1.318	0.000	0.000	50	39.234	0.208	3.331	75	1167.725	1.887	97.711				

1 / 1

Figure G.2.4: *PSD of unmilled dolomite*

The software generated particle size distribution report for milled calcined dolomite is shown below. The sample after milling was sieved throw a 45 μm to ensure uniform texture of the final powder.

2017.05.10 11:00:49

HORIBA Laser Scattering Particle Size Distribution Analyzer LA-960

Batch	: Dolomite	Material	: CaMgO2	Median size	: 0.24466 (µm)	Diameter on cumulative
ID#	: 201705101049826	Sample number	:	Mean size	: 0.25678 (µm)	
Data name	: 800C_fine_dolomite	Operator	: Moses	St. Dev.	: 0.0651 (µm)	
Transmittance (R)	: 87.7 (%)	Source	:	Geo. mean size	: 0.2497 (µm)	
Transmittance (B)	: 77.1 (%)			Geo. St. Dev.	: 1.2584 (µm)	
Circulation speed	: 10			Mode size	: 0.2403 (µm)	
Agitation speed	: 10			Span	: Off	
Ultrasound	: 01:00 (7)					
Iteration mode	: Manual					
Distribution base	: Number					
Refractive index (R)	: Dolomite					
	[Dolomite(1.680 – 0.000i),water(1.333)]					
Refractive index (B)	: Dolomite					
	[Dolomite(1.680 – 0.000i),water(1.333)]					

No.	Diameter (µm)	q (%)	Undersize (%)	No.	Diameter (µm)	q (%)	Undersize (%)	No.	Diameter (µm)	q (%)	Undersize (%)	No.	Diameter (µm)	q (%)	Undersize (%)
1	0.051	0.000	0.000	26	1.510	0.000	100.000	51	44.938	0.000	100.000	76	1337.481	0.000	100.000
2	0.058	0.000	0.000	27	1.729	0.000	100.000	52	51.471	0.000	100.000	77	1531.914	0.000	100.000
3	0.067	0.000	0.000	28	1.981	0.000	100.000	53	58.953	0.000	100.000	78	1754.613	0.000	100.000
4	0.076	0.000	0.000	29	2.269	0.000	100.000	54	67.523	0.000	100.000	79	2000.000	0.000	100.000
5	0.087	0.000	0.000	30	2.599	0.000	100.000	55	77.339	0.000	100.000				
6	0.100	0.000	0.000	31	2.976	0.000	100.000	56	88.583	0.000	100.000				
7	0.115	0.000	0.000	32	3.409	0.000	100.000	57	101.460	0.000	100.000				
8	0.131	0.000	0.000	33	3.905	0.000	100.000	58	116.210	0.000	100.000				
9	0.150	0.000	0.000	34	4.472	0.000	100.000	59	133.103	0.000	100.000				
10	0.172	0.000	0.000	35	5.122	0.000	100.000	60	152.453	0.000	100.000				
11	0.197	17.601	17.601	36	5.867	0.000	100.000	61	174.616	0.000	100.000				
12	0.226	20.094	37.695	37	6.720	0.000	100.000	62	200.000	0.000	100.000				
13	0.259	20.795	58.490	38	7.697	0.000	100.000	63	229.075	0.000	100.000				
14	0.296	18.400	76.890	39	8.816	0.000	100.000	64	262.376	0.000	100.000				
15	0.339	13.054	89.944	40	10.097	0.000	100.000	65	300.518	0.000	100.000				
16	0.389	6.634	96.578	41	11.565	0.000	100.000	66	344.206	0.000	100.000				
17	0.445	2.424	99.001	42	13.246	0.000	100.000	67	394.244	0.000	100.000				
18	0.510	0.891	99.892	43	15.172	0.000	100.000	68	451.556	0.000	100.000				
19	0.584	0.000	99.892	44	17.377	0.000	100.000	69	517.200	0.000	100.000				
20	0.669	0.000	99.892	45	19.904	0.000	100.000	70	592.387	0.000	100.000				
21	0.766	0.000	99.892	46	22.797	0.000	100.000	71	678.504	0.000	100.000				
22	0.877	0.000	99.892	47	26.111	0.000	100.000	72	777.141	0.000	100.000				
23	1.005	0.108	100.000	48	29.907	0.000	100.000	73	890.116	0.000	100.000				
24	1.151	0.000	100.000	49	34.255	0.000	100.000	74	1019.515	0.000	100.000				
25	1.318	0.000	100.000	50	39.234	0.000	100.000	75	1167.725	0.000	100.000				

1/1

Figure G.2.5: *PSD milled and sieved dolomite*

Appendix H

Calculation of conversion, X_N

The capture capacity was calculated from the TGA data by taking the difference in weight of sample during TGA measurement divided by the original weight owing to the fact that it is the sorption of CO_2 that is responsible for the weight change of the sample.

The ***maximum theoretical CO_2 capture capacity*** of the sorbent is calculated from the equation;

$$\text{Max. capture capacity} = \frac{\text{Mole of CaO reacted}}{\text{total moles of CaO present}}$$

According to the equation 1.2, CaO reacts with CO_2 in a 1:1 mole ratio. Also CaO and MgO in dolomite exists in equi molar quantities hence *moles of CaO = moles of MgO*.

$$\text{Max. capture capacity} = \frac{\text{Maximum } CO_2 \text{ weight captured}}{\text{Sorbent weight}}$$

$$X_N = \frac{n_{CO_2}}{n_{CaO, \, total}}$$

$$= \frac{n_{CO_2}}{n_{CaO, reacted} - n_{CaO, \, locked}}$$

where $n_{CaO, \, locked}$ refers to the amount of CaO reacted with Al_2O_3 and ZrO_2 to form Calcium Aluminate and Calcium Zirconate respectively and is thus unavailable for reaction with CO_2 and thus does not participate in the carbonation reaction.

$$\text{Max. capture capacity} = \frac{\left[\text{moles MgO} - \text{moles } Al_2O_3 - \text{moles } ZrO_2\right] \cdot 44}{\text{moles MgO} \cdot 40 + \text{moles MgO} \cdot 56 + \text{moles } Al_2O_3 \cdot 101.96}$$

where 44, 40, 56, 101.96 are the molecular weights for CO_2, CaO, MgO and Al_2O_3 respectively.

Table H.0.1: *Example of calculation of amount of precursor used and final max capture capacity*

MgO g/mol	40
CaO g/mol	56
Al2O3 g/mol	101.96
ZrO2 g/mol	123.2

	Al using Al(NO3)3.9H2O; ZrO(NO3)2	Al using Al(NO3)3.9H2O; ZrO(NO3)2	Al using Al(NO3)3.9H2O; ZrO(NO3)2
Desired %age for Al / Desired %age	4.000	3.500	3.000
Desired %age for Zr / Desired %age	2.000	2.000	2.000
Mass of dolomite calcined g	10.000	10.000	10.000
Mass of Al /g	0.426	0.370	0.316
Mass of Zr /g	0.213	0.212	0.211
Mole of MgO in dolomite	0.104	0.104	0.104
MW : Al g/mol	27.000	27.000	27.000
Moles of Al2O3	0.008	0.007	0.006
Mass of Al2O3 /g	0.803	0.699	0.596
MW : Zr g/mol	91.224	91.224	91.224
Moles of ZrO2	0.002	0.002	0.002
Mass of ZrO2 /g	0.238	0.237	0.235
Mg/Al mol/mol	13.219	15.188	17.813
MW Al(NO3)3.9H2O g/mol	375.130	375.130	375.130
Moles of Al(NO3)3.9H2O	0.016	0.014	0.012
Mass of Al(NO3)3.9H2O	5.912	5.146	4.387
MW ZrO(NO3)2 g/mol	231.230	231.230	231.230
Moles of ZrO(NO3)2	0.002	0.002	0.002
Mass of ZrO(NO3)2 /g	0.539	0.536	0.534
Weight for Al precursor g	5.912	5.146	4.387
Weight for Zr precursor g	0.539	0.536	0.534
Check:			
Dopant % (wt.Al to wt.dol)	3.854	3.387	2.915
Al2O3 in sorbent (dol.+Al2O3+ZrO2) %	7.277	6.395	5.505
Dopant % (wt. Zr to wtdol)	1.927	1.935	1.944
ZrO2in sorbent (dol.+ZrO2+Al2O3) %	2.154	2.163	2.172
Max. CO2 capture capacity % CO2 mass / sorbent mass	38.265	39.063	39.868

Matlab Code for calculation of conversion, $\mathbf{X}_N$

I.1 Capture Capacity Calculation

??

I.2 Capture Capacity Calculation

An example of a script used in the calculation of the CO_2 capture capacity of, for example, 4 %Al-2 %Zr doped dolomite from the TGA data with 94 cycles. The main purpose of code is simplify the handling of large amounts of data and helps in alleviating errors made by hand calculation. It helps to calculate the capacity beginning with the same zero starting capacity for all repeated cycles since the baseline will sometime shift as exemplified by:
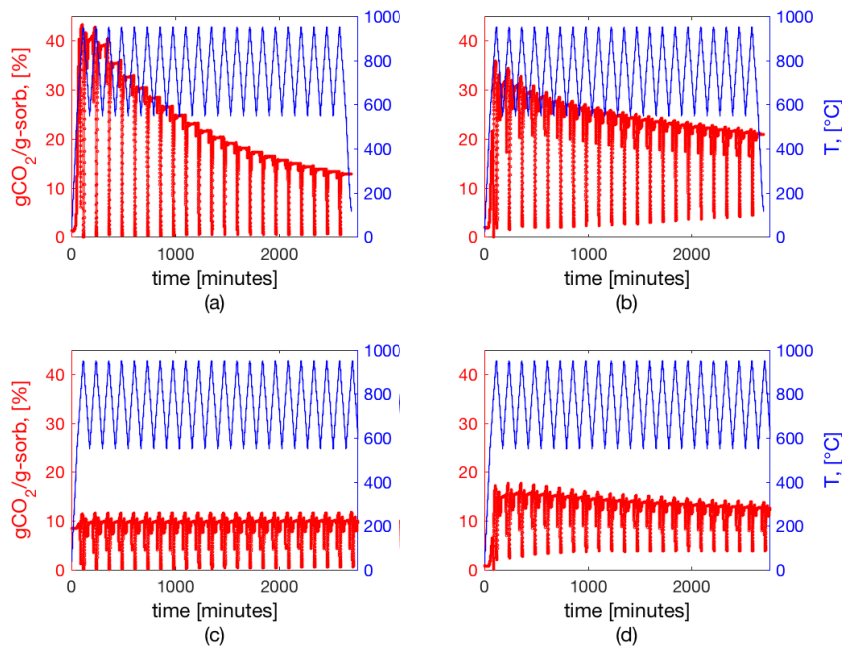

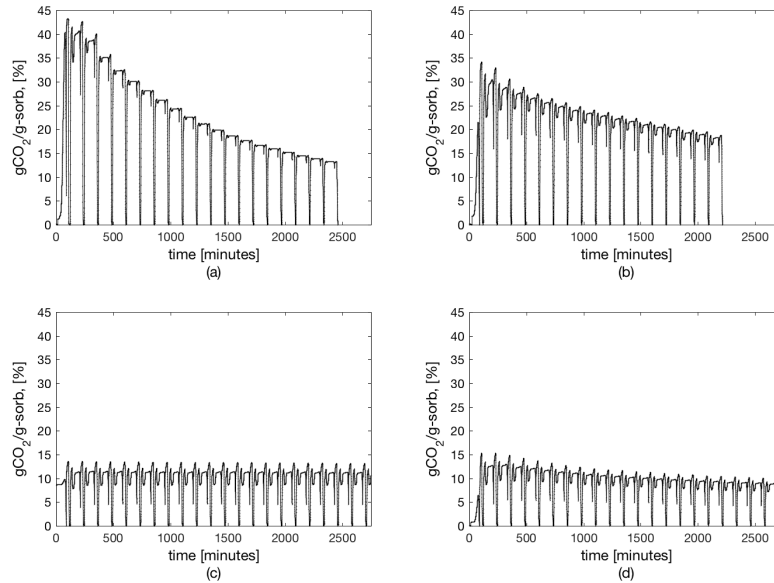**Figure I.2.1:** *Loss in the CO_2 capture capacity during the first 20 cycles as observed*

Figure I.2.2: *Loss in the CO₂ capture capacity during the first 20 cycles after refinement.*

```matlab
close all
clear
clc
data1 = xlsread('masterTGA.xlsx','AZ42-take2');
data2 = xlsread('masterTGA.xlsx','AZ42-take1');
data3 = xlsread('masterTGA.xlsx','AZ42-take3');
% AZ42-take1
time1        = data1(57:19080,1);
T1           = data1(57:19080,2);
weight1      = data1(57:19080,3);
% AZ42-take2
time2        = data2(57:19080,1);
T2           = data2(57:19080,2);
weight2      = data2(57:19080,3);
% AZ42-take3
time3        = data3(57:19115,1);
T3           = data3(57:19115,2);
weight3      = data3(57:19115,3);
weight3      = weight3-min(weight3);
% Combining data-sets
TIME2 = time2 + time3(length(time3));
TIME3 = time1+TIME2(length(TIME2));
TIME     = [time3;TIME2;TIME3]; % don't be confused.
WEIGHT   = [weight3;weight2;weight1];
plot(TIME,WEIGHT)
hold on
[pn,ln] = findpeaks(-WEIGHT,'MinPeakHeight',-0.5);
% [pn,ln] = findpeaks(-CAPACITY,'MinPeakHeight',-0.5,'
    MinPeakDistance',...
%     20,'Threshold',1e-7, 'MinPeakProminence',1);
```

```matlab
30 plot(TIME(ln),-pn,'ko','MarkerFaceColor','r','MarkerSize',7);
31 hold off % some unwanted peaks are also shown here.
32 %% Refined plot
33 % minimum points for each cycle from 1 through to 21st
34 pn=-pn;                                % size(-pn) = 21 1
35 format long g
36 originalweight = 16.5;  % in mg
37 N              = 150;   % total umber of cycles N
38 t=TIME(ln);
39 for i = 1:N-1
40 cycletime = (t(i+1)-t(i))';
41 end
42 Cap(1:ln(1)) = ((WEIGHT(1:ln(1))-pn(1))/originalweight).*100;
43 for j = 1:N-1
44  Cap(ln(j)+1:ln(j+1)) = ...
45  ((WEIGHT(ln(j)+1:ln(j+1))-pn(j+1))/originalweight).*100;
46 end
47 Cap = Cap';
48 Capacity_time = TIME(1:ln(N));
49 figure(2)
50 plot(Capacity_time,Cap,'b-')
51 hold on
52 plot([0 12050],[0 0],'k--')
53 ylim([-0.5 18]);
54 xlim([0 max(Capacity_time)]);
55 xlabel('Time (min)','FontName','TimesNewRoman','FontSize',30);
56 ylabel({'CO_2 Capture Capacity';'(gCO_2/g-sorb)'},'FontName',...
57         'TimesNewRoman','FontSize',40)
58 set(gca, 'XTick', 0:2000:12050, 'YTick', 0:5:16,'FontSize',30);
59 annotation('textbox',[0.22,0.8,0.1,0.1],'String','Run #1','FontSize
       ',...
60            30,'EdgeColor','none')
61 annotation('textbox',[0.46,0.8,0.1,0.1],'String','Run #2','FontSize
       ',...
62            30,'EdgeColor','none')
63 annotation('textbox',[0.74,0.8,0.1,0.1],'String','Run #3','FontSize
       ',...
64            30,'EdgeColor','none')
```

I.3 Conversion Calculation

An example of a script used in the calculation of the actual conversion of, for example, undoped dolomite from the TGA data after 63 cycles.

```matlab
1 close all
2 clear
3 clc
4 data = xlsread('masterTGA.xlsx','longdolomite');  sample1 = 21.7;
5 time          = data(56:19110,1);
6 T             = data(56:19110,2);
```

```matlab
7  weight         = data(56:19110,3);
8  plot(time,weight)
9  hold on
10 [pn,ln] = findpeaks(-weight,'MinPeakHeight',4.5);
11 plot(time(ln),-pn,'ko','MarkerFaceColor','r','MarkerSize',7);
12 hold off %
13 %% Refined plot
14 % minimum points for each cycle from 1 through to 67th
15 pn=-pn;                              % size(-pn) = 21 1
16 format long g
17 originalweight = 21.7;
18 N              = 67;                 % total umber of cycles N
19 t=time(ln);
20 for i = 1:N-1
21 cycletime = (t(i+1)-t(i))';
22 end
23 Wt(1:ln(1)) = weight(1:ln(1))-pn(1);
24 for j = 1:N-1
25  Wt(ln(j)+1:ln(j+1)) = weight(ln(j)+1:ln(j+1))-pn(j+1);
26 end
27 Wt = Wt';
28 Conversion = Wt./(originalweight*0.4583);
29 Wt_time = time(1:ln(N));
30 figure(2)
31 plot(Wt_time,Conversion,'b-')
32 [pts,npts] = findpeaks(Conversion,'MinPeakWidth',100,...
33         'MinPeakDistance',150);
34 plot(pts)
```